THE UNIVERSITY OF ALBERTA

HIGH PRECISION MEASUREMENTS OF X-RAY DIFFRACTION INTENSITIES

A Thesis

Submitted to the Faculty of Graduate Studies
In Partial Fulfilment of the Requirements
for the Degree of Doctor of Philosophy

DEPARTMENT OF MINING AND METALLURGY

by

JOHN ALBERT GOLDAK

EDMONTON, ALBERTA

MARCH, 1964

UNIVERSITY OF ALBERTA

FACULTY OF GRADUATE STUDIES

The undersigned certify that they have read and recommend to the Faculty of Graduate Studies for acceptance, a thesis titled

HIGH PRECISION MEASUREMENTS OF

X-RAY DIFFRACTION INTENSITIES

submitted by JOHN ALBERT GOLDAK

in partial fulfilment of the requirements for the degree of Doctor of Philosophy.

ABSTRACT

The design, construction and performance of an x-ray diffraction system capable of measuring intensities with a precision of 0.1 percent, and lattice parameters with an accuracy of 0.0001A and higher precision is described. The complete x-ray optical system is contained in a high vacuum (E-6 mm of Hg) chamber. The specimen temperature can be varied from 77K to 700K. The operation of the system is automatic; data are recorded on IBM cards and processed by a computer.

The slope and ratio methods of measuring the Debye temperature of nickel are compared, and the ratio method is considered superior. The Debye temperature of nickel obtained from twenty-eight determinations by the ratio method is 423.±4K. It is not believed to be possible to determine the change in the Debye temperature in cold worked nickel because of the difficulty in separating the Bragg scattering from the background.

ACKNOWLEDGEMENTS

This work was carried out under the able supervision of Professor J. Gordon Parr. His understanding, guidance and encouragement are deeply appreciated. Discussions with Dr. A. B. Bahtia, Dr. J. Sample and Dr. F. D. Manchester were most helpful. Mr. W. Corfield and Mr. J. Brugman made a major contribution to the electronics design and construction. The cooperation and assistance of Mr. A. Heyworth greatly expedited the computing work. Mr. J. McMurray assisted in many ways. I wish to thank my wife who showed great patience in typing this thesis.

The financial support of the National Research Council of Canada (NRCA-1277) who contributed substantially and the Defence Research Board of Canada (DRB-9535-16) is gratefully acknowledged. A scholarship from the National Research Council provided financial support.

CONTENTS

APPENDICES

LIST OF FIGURES

LIST OF TABLES

INTRODUCTION

INTRODUCTION

Fifty years have passed since x-ray diffraction was a scientific centre of attention, and its power has been to some extent forgotten with the advent of new, intriguing, techniques: therefore it is worthwhile to recall some important advantages of x-ray diffraction methods.

Statistical parameters such as the root mean square amplitude of thermal vibration of atoms in a crystal, and the average size and shape of small crystals which are impossible, or at least difficult and tedious, to obtain by direct image microscopy may be obtained directly by diffraction methods. The resolution of diffraction methods is higher than direct image methods. Since the momentum of x-ray photons and phonons is comparable, it is possible to investigate elastic constants, interatomic force constants and the spectrum of lattice vibrations. The importance of x-ray diffraction in the analysis of the structure of matter (gas, liquid and solid) is well known.

Before meaningful physical results can be obtained by x-ray diffraction methods three conditions must be observed: (1) the intensity of scattering must be measured over the necessary volumes of reciprocal space; (2) the type of scattering studied must be isolated from the total scattered intensity; (3) the isolated intensity must be analysed to obtain the pertinent data.

The experimenter is responsible for the first requirement, the

theoretician for the third; the second condition is the meeting ground of the theoretician and experimenter. As x-ray diffraction methods advance, it will become increasingly difficult for one person to cope with all three aspects.

The intimate relationship between the resolution and precision of experimental apparatus and the information the apparatus yields is emphasized in a diffraction theory recently developed by Hosemann and Bagchi (1962). This theory begins with the realization that measured values do not correspond to functions in the classical mathematical sense (i.e. a one to one mapping of two or more sets.) For example, the intensity of x-ray scattering referred to reciprocal space is not measured at a point ($x_1\, x_2\, x_3 = x_i$) but over a small volume, say x_i to $x_i + \Delta x_i$. The value of Δx_i, which is a measure of the resolution, depends only on the apparatus. Clearly, structure finer than Δx_i cannot be resolved at all. Further, the measured intensity does not represent a mathematical point but, because of errors, actually represents a range of probable values. Finally the experiments are performed not from time minus infinity to plus infinity but over a restricted time -- usually a very short time -- which again limits the value of the experimental data available.

Thus, the theory is designed to extract all the useful, or real, information from experimental data without becoming enmeshed in details that cannot be observed. To obtain data containing more

information, the precision, or the resolution, of the apparatus must be improved. The main object of the work described in this thesis is the design, construction, and operation of an x-ray diffraction apparatus (XRAS) to provide the best data possible within the imposed limits of time, financial resources, and technological facilities.

Experiment has shown that when a well collimated beam of x-rays encounters a collection of atoms in the gaseous, liquid or solid state, secondary x-rays are emitted in all directions. In general the intensity of the secondary x-rays is weak compared to the incident beam: it is usually less than 0.01percent. The secondary radiation, although emitted in all directions, is not uniformly distributed; it does not have a uniform wavelength; it is not uniformly polarized. It is produced by a number of processes, and to investigate any one of these processes it is necessary to select for examination only that part of the secondary radiation which will give the pertinent information. The remainder must be eliminated, but before it can be safely eliminated it must be recognized, and possibly analysed.

This problem, which comprises the second objective of this project, has not been satisfactorily solved. Laue or Bragg scattering is particularly important because it is used in some way in virtually all x-ray diffraction work. Yet in this work the precision of measuring Bragg scattering is limited not by the experimental data but by the method of isolating the Bragg scattering from the total scattering.

The importance of this problem has not been emphasized in the past, presumably because it was not obvious with less precise data.

The third problem, the analysis of a specific type of scattering to obtain desired physical results, encompasses a large field. However, some aspects are of general significance. For example, those studies which view the ion as the elementary structural unit, require a knowledge of the scattering by a single, isolated ion. The structure of the ion is relatively insensitive to the presence of other ions and therefore the total intensity scattered by a collection of ions can be obtained by adding the scattering from each ion. Scattering from an ion with spherical symmetry depends only on the x-ray wavelength and scattering angle and is described by a function called the scattering factor. Theoretical calculations of the scattering factor by methods of Hartree-Fock and Thomas-Fermi have been published for most atoms and ions. The precision of experimentally determined scattering factors is worse than 1 percent and often as poor as 5 percent, and it will not be substantially improved until the problem of uniquely separating Bragg scattering from the background is solved. This problem affects all x-ray diffraction analyses.

Measurements in x-ray diffraction that are made over periods that are long compared to the period of the x-rays (E-18 seconds)*

---

* The notation E-18 = 10^{-18} follows the format used in the common computer language Fortran.

or thermal motion (E-12 seconds), are generally related to a static model that represents the structure averaged over time. The effect of thermal motion in reducing the amplitude of the electron density distribution must be considered: this is accomplished to a first approximation by a Debye temperature factor, -2M, which is related to the absolute temperature and the Debye temperature of the specimen. Theoretical calculations of a correct temperature factor are not satisfactory because the problem of thermal motion of atoms, even for the simplest crystal, has not been satisfactorily solved.

The vibrational properties of a crystal that control the Debye temperature also exert a major influence on the strength, rigidity, hardness, melting point, and thermodynamic properties. Thus most of the characteristics of materials that interest a metallurgist could be related to a single unified theory of lattice vibrations. Theoretical approaches such as Born and Huang's work 'Dynamical Theory of Crystal Lattices', are far ahead of experimental results. The careful study of the Debye temperature of nickel from x-ray diffraction data, which is the second objective of this thesis, is a modest contribution to the experimental data needed to develop the theory of lattice dynamics.

It is hoped that the introduction has shown that the usefulness of x-ray diffraction to science depends on the production of high quality data, and equally upon an appreciation of the difficulties that exist in relating x-ray diffraction theory to experiment.

APPARATUS

APPARATUS

1. THE SELECTION OF AN X-RAY DIFFRACTION SYSTEM

The general design of the x-ray diffraction system (XRAS) and the reasons for the design are briefly outlined to provide an overall view before discussing the individual parts of the system.

Those systems which record data on film or strip charts are rejected because the precision is limited to worse than 1 percent by the recording medium. A system capable of high precision measurements must detect, count and record digitally the x-ray photons. Bragg-Brentano focusing (James, 1958 p. 334) is the only arrangement which has sucessfully employed photon counters. (Baun and Renton (1963) briefly described a diffractometer based on Seeman-Bohlin geometry). The Bragg-Brentano method, which is used on all commercial diffractometers, maintains a specimen surface at angle theta and detector at angle two theta to the incident beam. A horizontal circle diffractometer simplifies cryostat design.

Continuous scanning techniques used on most commercial diffractometers are unsuitable for high precision studies because of the difficulty in relating the time at which a photon is detected to the scattering angle. Therefore a step scanning procedure has been adopted for XRAS in which the apparatus is stationary during each measurement. To preserve precision the data must be recorded in

a digital form on a medium such as printed paper, perforated paper tape, I.B.M. (International Business Machine) cards, digital magnetic tape, etc. The initial choice of perforated paper tape was quickly discarded and I.B.M. cards are now used for data recording. For practical considerations the operation of the apparatus is almost entirely automatic; for versatility the optical system is placed in a high vacuum chamber, and the specimen holder may be used over a temperature range of 70 K to 800 K.

2. ERRORS INTRINSIC TO THE X-RAY DIFFRACTION APPARATUS

An effective design of an x-ray diffraction system depends upon an initial appreciation of the sources of error, for an x-ray diffraction system is complex, and involves many components that can cause significant errors in the data. These components and the errors they cause are discussed below.

(a) The Stability of the X-ray Beam

The intensity, direction and spatial position of the incident beam are assumed constant with respect to time. Changes in direction and spatial position of the beam are due primarily to changes in the shape and position of the focal spot, which in turn are presumably due to changes in the position of the x-ray tube filament. Operating the filament at a low temperature should minimize such changes. Further, such changes can be detected by repeating a measurement.

The intensity of the spectral K line is given empirically by the equation:

$$I = Bi(V - V_k)^n \tag{1}$$

I - intensity of the K line

B - empirical constant

i - tube current

V - tube voltage

V_k - excitation voltage of the K line

n - empirical constant approximately equal to 1.5

The relative change in I with i and V is given by

$$dI/I = B(V - V_k)^n di/(Bi(V - V_k)^n) + nBi(V - V_k)^{n-1} dV/(Bi(V - V_k)^n) \tag{2}$$

$$dI/I = di/i + ndV/(V - V_k) \tag{3}$$

Hence the intensity I varies linearly with tube current and to a higher power with tube voltage. For example, consider a molybdenum target operated at 48kv and $V_k = 16$kv and $n = 1.5$

$$dI/I = di/i + 2.3dV/V \tag{4}$$

If the tube is operated at 32kv, the relative change in I is given by

$$dI/I = di/i + 3dV/V \tag{5}$$

In this case the intensity varies as the third power of the tube voltage, which illustrates the importance of a highly stable voltage source.

In XRAS the voltage source is stable to 0.01 percent: this can contribute an error in beam intensity as large as 0.04 percent. The tube current is said to be stable to 0.01 percent. The variations in tube voltage and current combined may produce an error as large as 0.05 percent. The author would be pleasantly surprised if beam intensity were stable to 0.1 percent over long periods of time, because aging effects and temperature variations cause an unknown error. However a 0.1 percent error is usually much less than the statistical error, and is therefore tolerable.

(b) Statistical Errors in Measured Intensities

The x-ray photons in the incident beam are randomly spaced in time because they are related to electrons ejected thermally, and therefore randomly, from the x-ray tube filament. The average number of x-ray photons per unit time is called the intensity. It is assumed that if measurements were made over an infinite (sufficiently long) period of time the 'true' value of the intensity would be determined. The probable error (i.e. the error which is as likely to be exceeded as not) caused by counting only N photons is $0.67N^{-\frac{1}{2}}$. This error can be made as small as one's patience allows.

The ripple in the high voltage supply to the x-ray tube causes a pulsation in the incident beam intensity with a frequency of 120 cycles per second (full wave rectified). If the high voltage supply were 'smooth' the probability of emitting a photon would be constant with time.

(c) Noise or Non - X- Ray Background

The non - x-ray background is caused by background radiation (e.g. cosmic rays) and "noise" in the electronics. The signal pulse (voltage) height is directly proportional to the energy of the photon detected. Wavelengths longer than 5Å cannot normally be detected with scintillation detectors because the signal is smaller than the electronic noise (see page 27). In XRAS the non - x-ray background is presumably due to background radiation that cannot be distinguished from the K radiation. If this is the case, it cannot be further reduced with present techniques. Many modern x-ray diffraction systems report non - x-ray backgrounds as high as 1.5 counts per second -- a value which affects experiments involving weak intensities, such as diffuse scattering or weak Bragg reflections. In XRAS the total non-x-ray background is 0.1 counts per second.

The relative probable error, $\Delta I/I$, in an intensity measurement of I counts in the presence of a background of B counts is

$$\Delta I/I = 0.67(I+B)^{0.5}/(I-B) \tag{6}$$

Hence it is desirable to make $I \gg B$. In XRAS B/I is probably always less than 0.02.

The effect of statistical errors on precision is dependent upon the incident beam intensity available and one's patience. In XRAS, Philips x-ray tubes are operated at 600 watts. It is physically

possible to construct rotating anode tubes with a power of 300,000 watts. (The strength and thermal conductivity of the anode limit the maximum heat dissipation). With such a tube, experimental time could be reduced by a factor of 500 or even more if the intensity of diffracted radiation is weak.

(d) Time Interval Measurement

An intensity measurement involves counting a number of photons in a specified time interval. The error in the time interval (±3E -7 seconds in 10 seconds is specified by the manufacturer) in XRAS may be reasonably neglected.

(e) Specimen Temperature

Although a 1 K error in specimen temperature is significant in some x-ray diffraction experiments, such as precision lattice parameter and Debye temperature studies, it is probably not practical to measure temperature over a 800 K range in a routine manner with higher precision. In XRAS the temperature is measured with a chromel-alumel thermocouple, ice junction and 4725 Rubicon Potentiometer, which is readable to 1 microvolt. The observed temperatures are believed accurate to ± 1.0 K.

(f) Optical Alignment

The optical alignment of the x-ray source, specimen, detectors and collimators affects the intensity. The basic difficulty is that one

hopes the alignment is 'good', but does not know the amount of misalignment: otherwise one would correct it. Measurements of relative intensity are not as sensitive to alignment as are absolute measurements.

Approximately three months were spent aligning XRAS using alignment jigs based on a design by Parrish and Lowitzsch (1959). It is believed that most adjustments are within 0.001 inches or 1 minute of arc. In addition, a set of electromagnets was arranged to move the specimen through an arc of 10 minutes (2:1 adjustment) and a displacement of 0.010 inches (specimen eccentricity). Surprisingly, the peak intensity was not increased by more than 3 percent by the finest adjustments possible (estimated at 30 seconds of arc and 0.0001 inches displacement). However, the 331 peak from nickel with MoK radiation was displaced as much as 0.03° theta by displacements of the order 0.010 inches. The data were not plotted to observe the change in line profile, which could affect the integrated intensity.

These results suggest that the intensity is not particularly sensitive to misalignments less than 0.001 inches. This is understandable when one considers that x-rays are scattered not by the specimen surface but by a finite thickness. With a nickel specimen and MoK radiation at 50° Bragg angle, 1 percent of the intensity is scattered from depths below 0.004 inches, 10 percent from below 0.0004 inches and 60 percent from below 0.00004 inches. Thus misalignment errors smaller than the effective thickness of the specimen surface, which is

of the order of 0.0001 inches, are not expected to greatly affect the intensity.

The above argument is not intended to condone careless alignment, but it is a situation in which one can only do one's best. The error in this work caused by misalignment seems impossible to evaluate, but great care was taken to minimize the error.

(g) Summary

The statistical error due to the finite number of photons counted is usually the largest error, and it depends substantially on the intensity of x-rays and the time available. The instability of the incident x-ray beam probably limits the precision in XRAS to about 0.1 percent. The alignment error cannot be evaluated but appears to be small. In relative intensity measurements at least, the alignment error should be negligible. Errors originating in the other components of XRAS (detector, amplifier, pulse height analyzer and counter) probably do not total 0.1 percent. Given sufficient time and x-ray power, intensity measurements with a precision approaching 0.1 percent appear to be practical.

3. THE X-RAY DIFFRACTION SYSTEM - XRAS

This description of the x-ray diffraction system, called XRAS, roughly follows the flow of energy and information from the x-ray generator to the IBM card punch. Figure 1, a schematic block diagram illustrates the organization; figure 2 provides an overall view of the

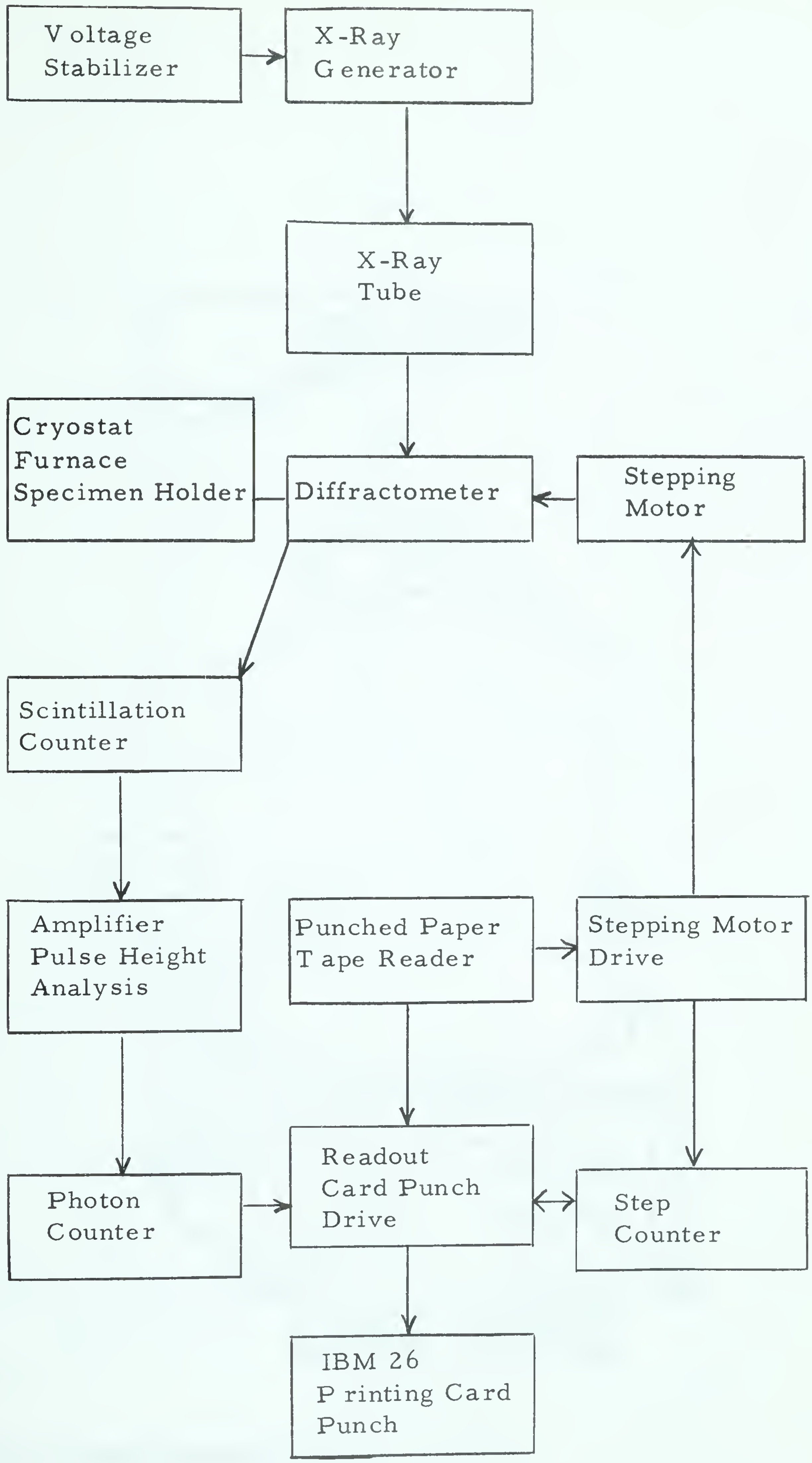

Figure 1. Arrangement of Circuits in XRAS

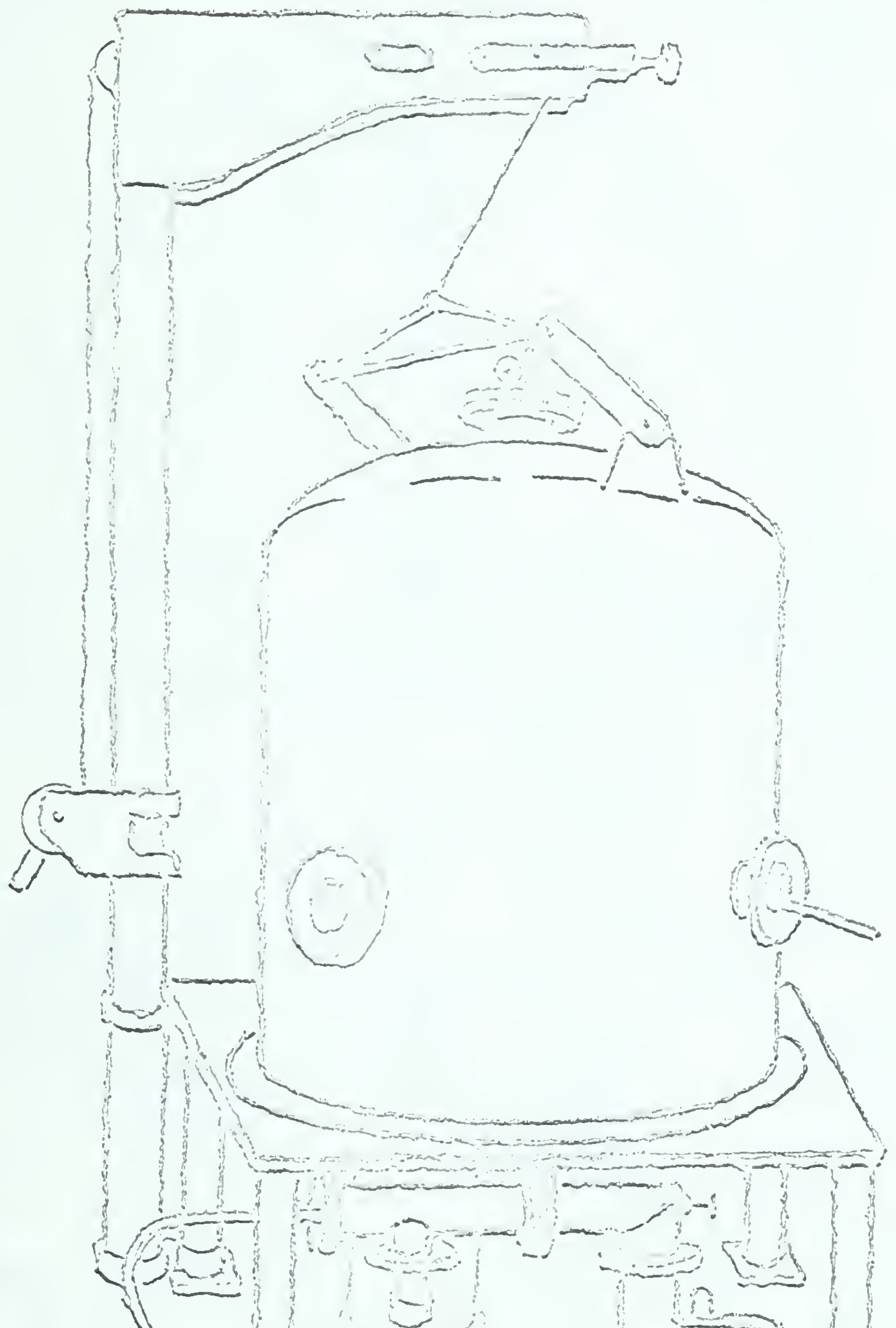

Figure 2. The Vacuum System

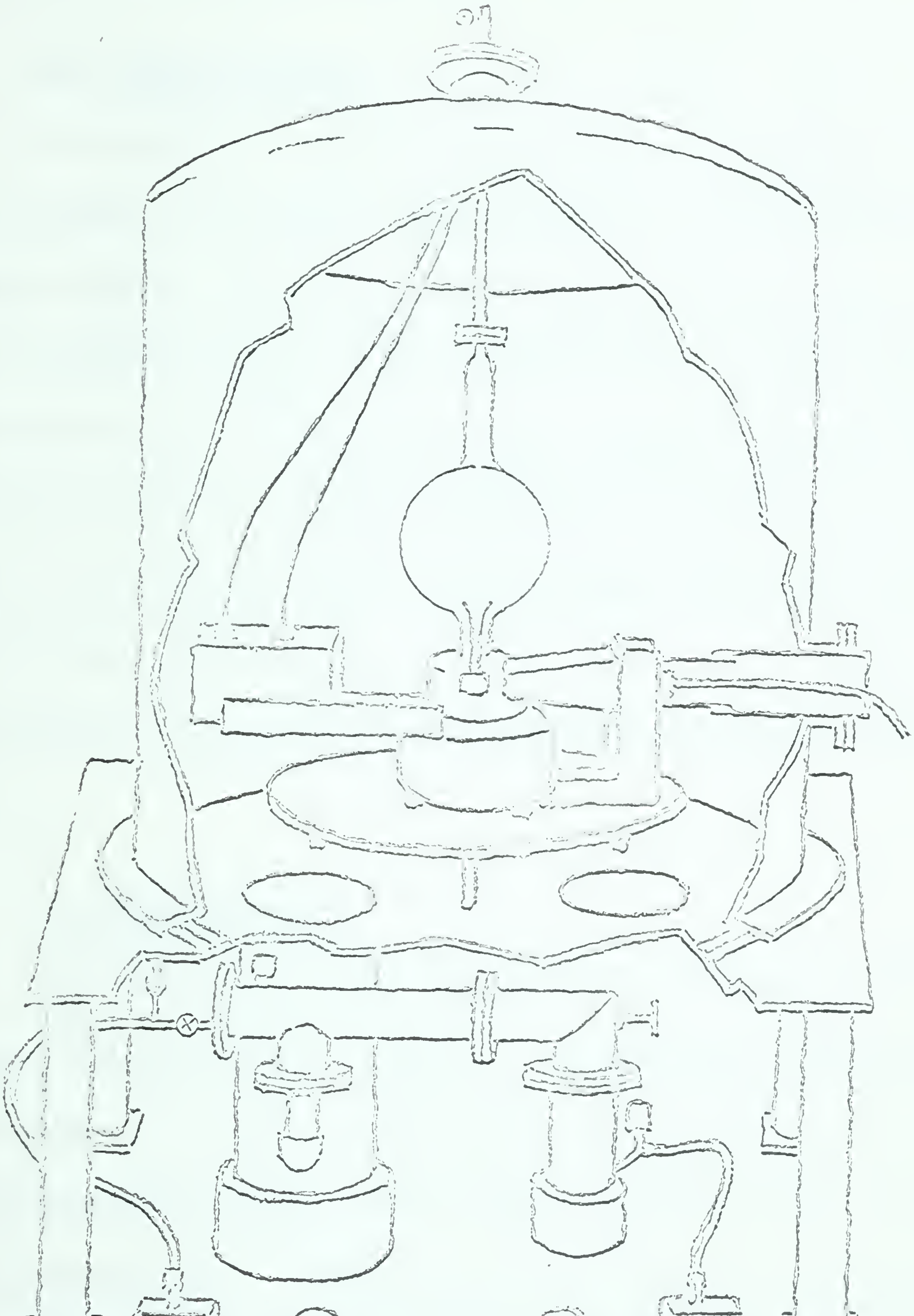

Figure 3. Cutaway View of Vacuum System

vacuum system which houses the x-ray optical system; figure 3 is a cut-away view of the optical system.

(a) X-ray Generator

A model D3-F, made by Rigaku-Denki, provides up to 40 ma at 60 kv of full-wave-rectified unfiltered power. A model 2501 Sorenson voltage regulator maintains the input voltage constant within 0.01 percent, with a response time of 1 cycle and less than 5 percent distortion. The x-ray tube current is stabilized so that a change from 20kv to 40 kv causes less than 0.3 ma change. Considering that the input voltage is stable to 0.01 percent, only a 4 volt variation from 40kv is expected, and this could alter the tube current by about 1 part in 25,000. Clearly, any variation in tube current is largely due to temperature changes and aging.

(b) Diffractometer

The SG-II Rigaku Denki horizontal circle diffractometer is well suited for operation with a cryostat. The precision is specified at 7 seconds of arc. The standard synchronous motor was replaced by a slo-syn stepping motor, which is driven at 100 steps per revolution of the diffractometer. The motor can be driven asynchronously up to 100 steps per second, which corresponds to 30° theta per minute. An eight channel perforated paper tape reader permits 'programmed'

scanning by driving the motor either forward or reverse, and either continuously or at one step per reading. The paper tape advances one character after the motor takes thirty two steps. The paper tape code is defined as follows:

Table I. Paper Tape Format

Type of Scan	Paper Tape Channel									
	1	2	3	4	5	6	7	8	9	0
Motor steps once forward after each reading	x*		x							
Motor steps once backwards after each reading		x	x							
Motor driven forward at up to 100 steps per second. No readings are taken.	x			x						
Motor driven backwards at up to 100 steps per second. No readings are taken		x		x						

* The 'x' indicates a hole is punched in the paper tape.

For unambiguous operation only two holes can be punched in one character. Programmed scanning permits the operator to obtain the

maximum information in the experimental time available.

(c) Angle Readout

At the beginning of a scan the angle is observed and a transistorized binary-coded decimal counter is set to zero. This counter records the number of steps taken which, together with the starting angle, defines the angle at any later time. With each reading the number of steps accumulated in the counter is recorded on IBM cards. This method encounters difficulties if the motor direction is reversed, because the counter is unable to subtract and the angle recorded continues to increase. A shaft encoder, which reads the angle directly, would not only avoid this problem but would also eliminate the error in reading the starting angle.

(d) X-ray Detector, Amplifier and Counter

A Norelco scintillation detector using a beryllium window, sodium iodide crystal, Dumond photomultiplier tube and preamplifer, was selected in preference to a proportional counter because of higher detection efficiency and virtually unlimited life, even though the noise is higher and the energy resolution poorer. High voltage for the detector is supplied from a John Fluke 502A with a range of 500 to 5000 volts, which may be set to 1 volt and with 0.005 percent regulation. The ripple, which is specified at less than 5 millivolts, is further reduced by a factor of 0.0001 by a filter built from two 15 uf capacitiors and two 45 henry chokes.

The noise in the high voltage supply is probably due to pick-up and thermal fluctuations. A noise level of the order of 1 millivolt originates in the Norelco detector.

The pulse from the detector is amplified 10-fold by a Franklin 349A preamplifier before entering a Franklin model 349 double delay line linear pulse amplifier and pulse height analyzer, which further amplifies the pulse and passes only those pulses with height less than a set maximum and greater than a set minimum. As the pulse height is proportional to the energy of the photon which caused the pulse, a degree of monochromatization is obtained. The pulses are accumulated in a six digit Beckman 7061 counter in which the time base is accurate to 3 E-7 seconds and may be preset within 1 millisecond from 1 milli second to 10 seconds. The counter has a 1-2-2-4 binary coded decimal output of 12 volts at 5 megohms. Utilizing this output the number of counts accumulated in the counter during the preset time interval is recorded on IBM cards with an IBM 26 printing card punch.

The readout system, paper tape reader, angle counter, IBM card punch drive, and the control system were designed and built at this university by the author and the Electronics Division (headed by Mr. W. Corfield) of Technical Services.

(e) Detector Performance

XRAS is a general purpose system and requires a versatile x-ray

detector. The sodium iodide scintillation detector was selected for several reasons. The quantum counting efficiency, that is the percentage of incident photons absorbed in the detector, neglecting the absorption in the 0.005 inch beryllium window, is virtually 100 percent in the x-ray region. In comparison, the quantum counting efficiency of the Norelco xenon-filled proportional counter is only of the order of 20 percent for MoK x-rays. The life of the scintillation detector is virtually unlimited. However, proportional counters contain a quench gas such as methane, which is decomposed by about E+10 photons, and this limits its useful life to a few days in intense reflections or near the direct beam. These two reasons led to the rejection of the xenon-filled proportional counter for XRAS.

The resolving time of the scintillation detector, preamplifier, amplifier and counter is one microsecond. This can only be improved by using faster scintillators such as anthracene and equally fast electronics. (No detector used at present for x-ray diffraction provides higher resolving times although solid state detectors show considerable promise.) Except in the most intense reflections dead time losses are negligible or easily corrected by:

$$N_t = N/(1 - NT). \qquad (7)$$

N_t - true intensity in counts per second

N - measured intensity

T - dead time — 1.2 E-6 seconds for integral pulse height analysis.

— 4 E-6 seconds for differential pulse height analysis.

This equation does not apply exactly, because the photons from an unfiltered full-wave rectified x-ray generator are not perfectly random with time.

In the scintillation detector the absorbed photon causes a fluorescence with intensity proportional to the energy of the photon. This fluorescence in turn causes photoelectrons to be ejected from the dynodes of the photomultiplier tube. The photoelectrons from the last dynode form the pulse which will be amplified linearly for pulse height analysis. This pulse, which is characterized by its voltage or pulse height, is not exactly proportional to the energy of the x-ray photon because the fluorescence in the sodium iodide crystal and the ejection of photoelectrons in the photomultiplier tube involve statistical factors.

There are two methods used for pulse height analysis. The integral method consists of measuring the number of pulses per unit time which are greater than a set value. In the differential method, the number of pulses per unit time whose heights lie between two set values are measured. The lower value is called the base line and the difference between the two values is called the window. The pulse height analysis obtained with the detector set on the peak of the 731,553 reflection of

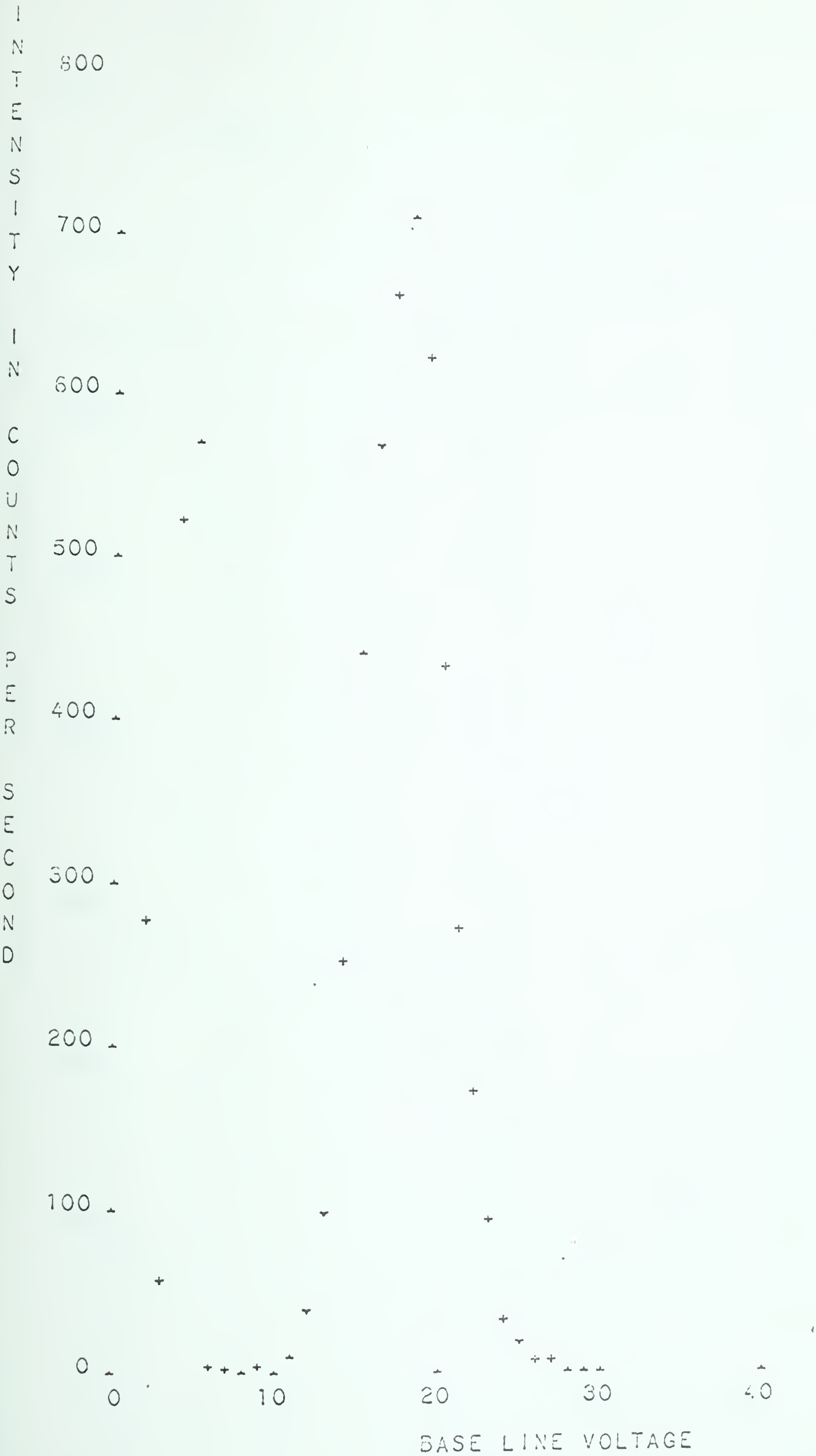

Figure 4. Differential Pulse Height Analysis of MoK Radiation

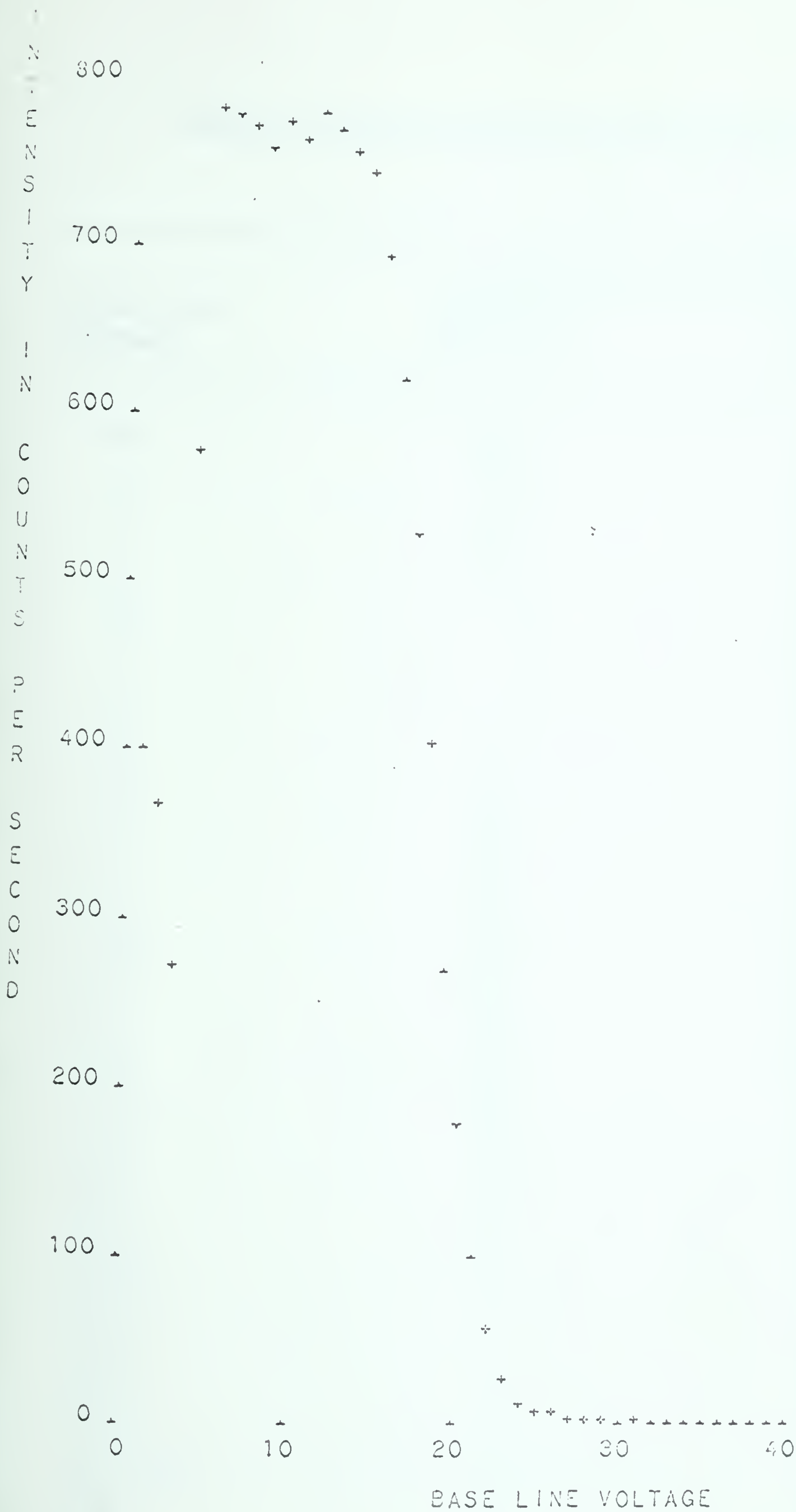

Figure 5. Integral Pulse Height Analysis of MoK Radiation

Table 2. Data for Differential and Integral Pulse Height Analysis

Base Line Voltage	Intensity (Counts per Second) Differential Method	Integral Method
0	2449	5019
1	397	4587
2	80	3406
3	747	7216
4	817	9781
5	6	9746
6	3	9657
7	2	9490
8	7	9691
9	12	9585
10	17	9770
11	56	9636
12	141	9459
13	361	9306
14	631	8677
15	813	7773
16	947	6601
17	1016	5052
18	890	3381
19	619	2238
20	389	1272
21	246	720
22	137	329
23	46	166
24	27	86
25	11	30
26	11	37
27	1	37
28	0	30
29	1	16
30	0	30
31	0	9
32	0	17
33	0	17
34	0	11
35	0	8
36	0	10

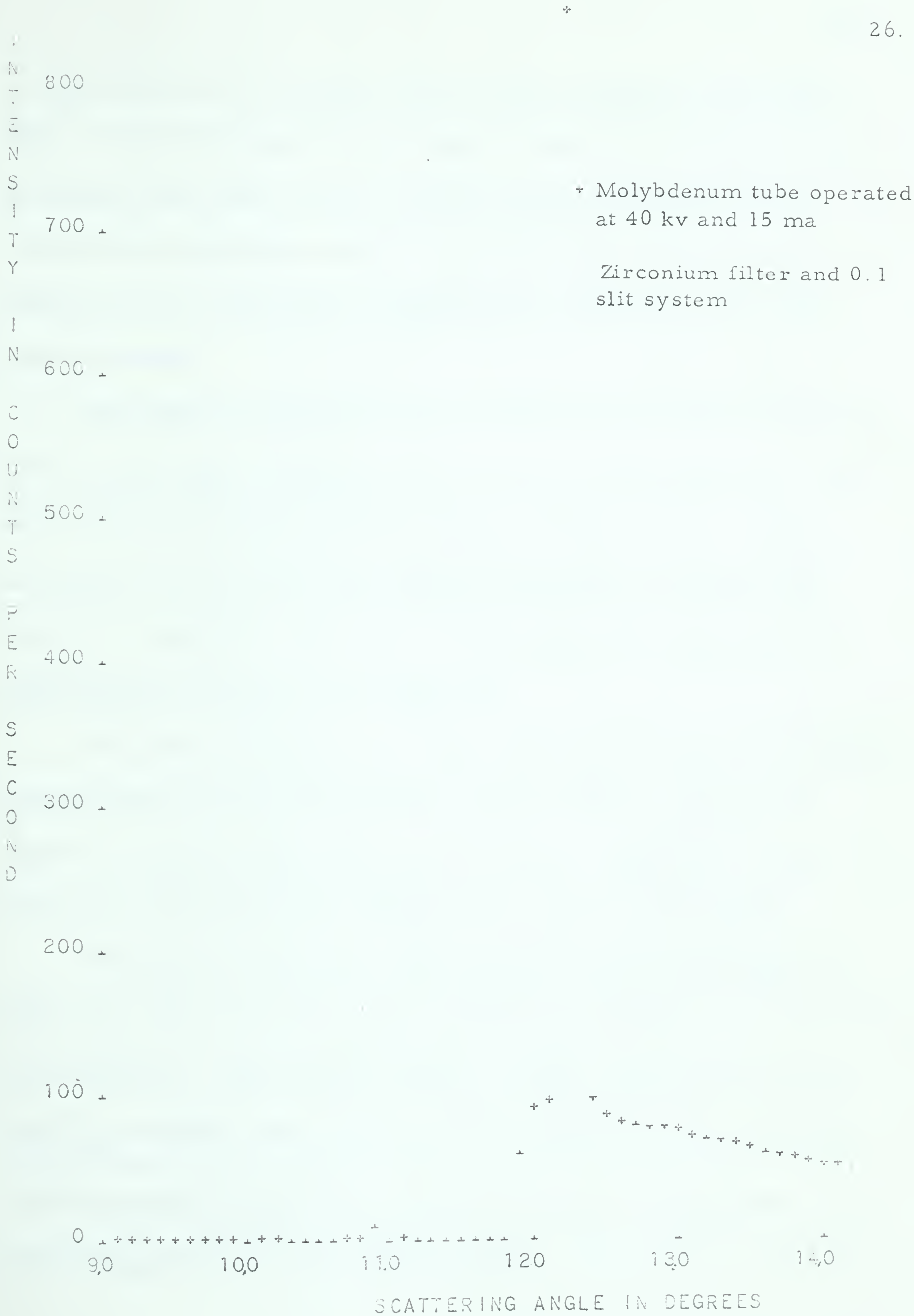

Figure 6. The $10\bar{1}1$ Reflection of MoK from a Quartz Single Crystal

a $Cu_{80}Ni_{20}$* specimen with MoK x-rays is shown in figures 4 and 5 and table 1. The bell-shaped curve of figure 4 clearly shows the statistical fluctuation in the pulse heights. In this case the differential method contains more information than the integral method. The very low intensity at 5, 7, and 8 volts is masked by the statistical error in the integral method.

Normally the baseline is set at 12 volts and the window at 10 volts, which accepts approximately ninety percent of the MoK radiation. The pulses from 0 to 5 volts are largely due to electronic noise. However the number of electronic noise pulses greater than the normal 12 volt base line is negligible. Therefore electronic noise does not contribute significantly to the non-x-ray background.

The noise and ripple in the high voltage supply to the photomultiplier tube contribute to the width of the bell curve in figure 4. This is the reason for using the highly stable 0.005 percent regulation low ripple (less than 5 microvolts) high voltage power supply for the detector.

The very low intensity on either side of the MoK peak (figure 4) shows that in this case the x-rays received by the detector are essentially monochromatic. There are two reasons for this: the filter effectively absorbs x-rays with lower energy; and the scattering factor, a function

---

* The notation $Cu_{80}Ni_{20}$ is used to describe an alloy containing 80 atomic percent copper and 20 atomic percent nickel.

of theta, approaches zero for higher energy x-rays at the high angle (49° theta in this case). Apparently it would be undesirable to use a crystal monochromator because the increased monochromatisation would not offset the error due to the reduced intensity. However, in figure 6 the $10\bar{1}1$ reflection from a quartz single crystal clearly shows a high intensity of white radiation above the zirconium absorption edge at 11° two theta. Apparently a crystal monochromator would be useful here.

4. THE VACUUM SYSTEM

The usual design (Forrester, 1961) of high or low temperature x-ray diffraction apparatus incorporates one to three windows each of which is crossed twice by x-rays. In addition to the problems of constructing such windows and the intensity loss they cause, the possibility of non-uniform absorption exists. This may arise through segregated impurities of high atomic number or Bragg reflection occurring at some parts of the window. Further, windows greatly reduce the space available for devices such as furnaces and cryostats, and hence complicate the design. All of these problems are avoided in XRAS by placing the entire x-ray optical system in a high-vacuum chamber.

The system described here was designed to reach a vacuum of E-6 mm of Hg. Not the least significant reason for this figure is the difficulty of attaining much better vacua. At this pressure, liquid nitrogen consumption is less than 2 litres per 24 hours -- which is reasonable; and

with minor modifications liquid helium operation should be possible. Further, at E-6 mm of Hg many materials remain sensibly uncontaminated at elevated temperatures.

Figure 7 shows the pressure vs. time curve for pumping down the system. To 4E-6 mm of Hg, the pressure falls by a factor of ten every two minutes. If pumps could be kept hot by a suitable valve arrangement, the system could be pumped down to 4.5E-6 mm of Hg in about twenty minutes. However, because of diffusion pump warm-up time, and to avoid decomposing the pump oil, approximately 90 minutes are required to evacuate the system. Without the aid of refrigerants, getters, adsorption agents or baking, the ultimate vacuum measured with a VEECO RG 21A ionization gauge is 8E-7 mm of Hg. If a leak detector were available, it is felt that the ultimate vacuum could be lowered to E-7 mm of Hg by reducing the leak rate.

(a) The Vacuum Chamber

The vacuum chamber is welded from A7 hot rolled steel with a hand-polished inside surface. The diameter is 42 inches and the height is 58 inches. The performance of this system indicates that stainless steel is not necessary for operation at E-6 mm of Hg. Most metal joints in the system are welded but a few are soldered. Almost all demountable seals are made with neoprene 'O' rings.

The steel bell jar can be raised about 38 inches above the table

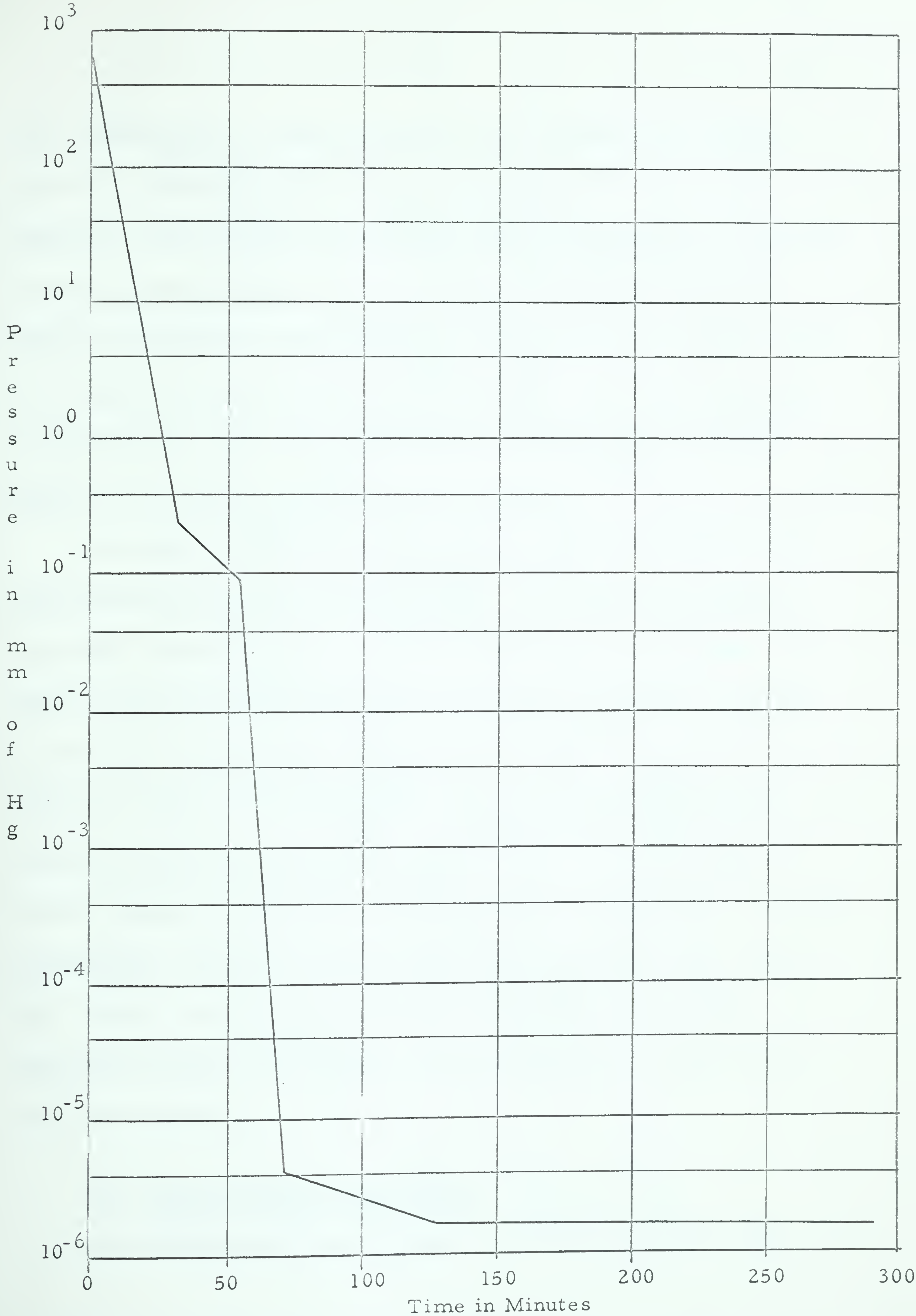

Figure 7. Pressure vs. Time for Pumping Down Vacuum System

top. With the bell jar raised, the entire x-ray optical system can be placed in or taken from the chamber as a single unit. For minor operations such as changing specimens, slits, x-ray tubes, etc., access is usually gained through a 14 inch porthole in the table. (A 15 inch porthole would call for less dexterity.) The available floor space (9 feet x 13 feet) dictated the use of a vertical chamber: however a horizontal vacuum chamber using, say, 6 foot diameter hemispheres would be cheaper, more flexible, versatile and convenient.

A number of difficulties arose with the large diameter (42 inch) seal between the bell jar and the table top. 'O' rings of this diameter are made, at least by one manufacturer, by vulcanizing 'O' rings cord. However, the tolerances on both the cord and the vulcanized joint were so poor that no measureable vacuum was obtained. The problem was solved by cutting a 0.375 inches wide strip from 0.375 inches thick neoprene sheet and vulcanizing the joint. These 'O' rings (which are actually gaskets) are adequate at pressures of E-6 mm of Hg. Two seals are used, and a space between the rings can be evacuated to E-2 mm of Hg. However, evacuating between these seals does not affect the measured vacuum in the chamber, which indicates that the seals have a very slow leak rate.

(b) Cryostat and Furnace Design

The cryostat and furnace design are shown in figure 8. The

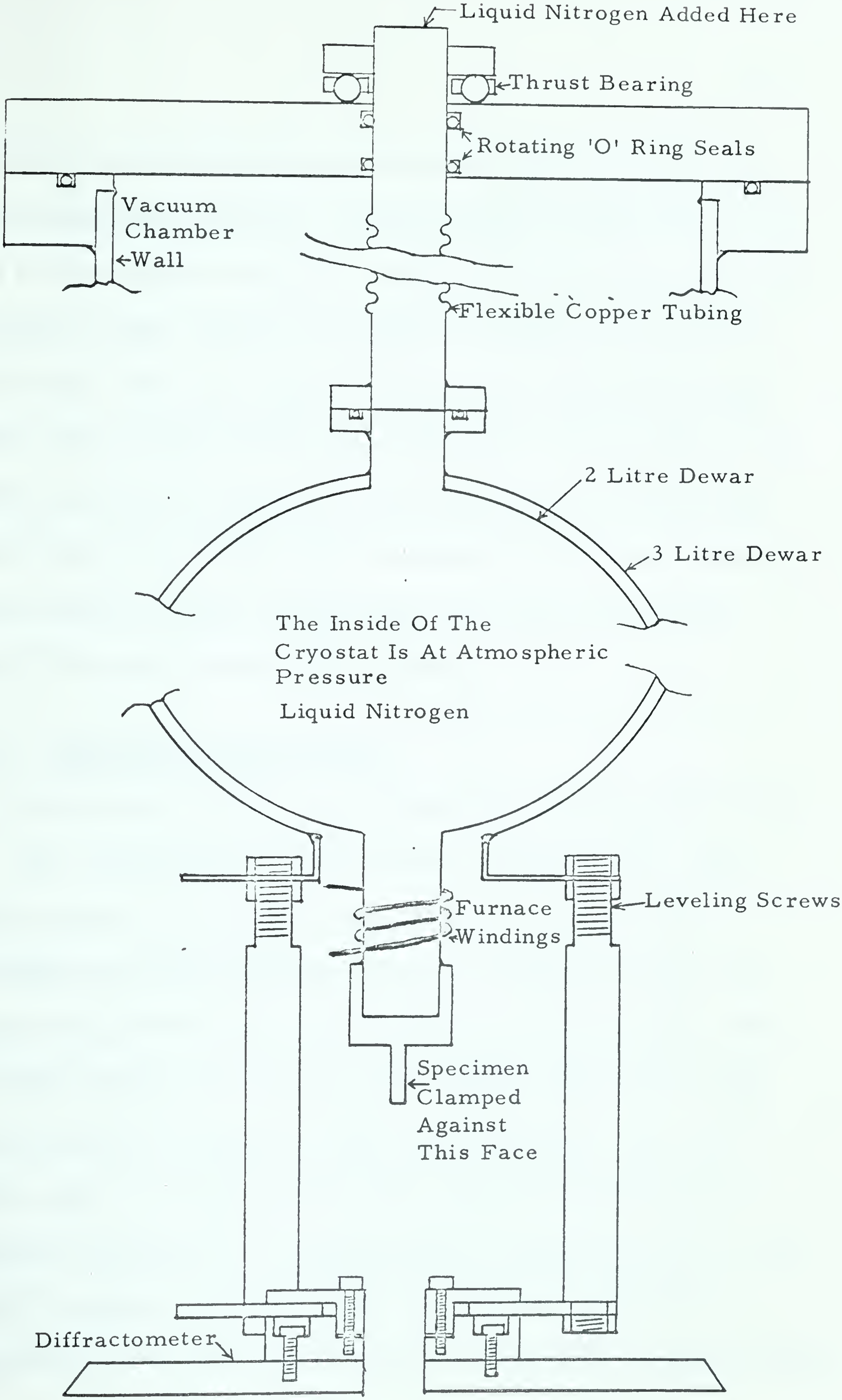

Figure 8. Cryostat and Furnace Design

outside of the assembly is under vacuum and the inside of the two litre flask is at atmospheric pressure. Liquid nitrogen is added from the top, through 1 inch stainless steel pipe. A double 'O' ring rotating seal allows the cryostat to rotate relative to the vacuum chamber as the scattering angle is varied. However, the axis of this rotation must pass through the centre of the rotating 'O' ring seal if stresses on the cryostat, which could alter the specimen alignment, are to be avoided. Therefore the complete x-ray optical system must be aligned with the vacuum chamber. A section of flexible copper tubing between the 2 litre flask and the rotating 'O' ring seal permits some variation.

(c) Alignment of Diffractometer

The alignment procedure was adopted from Parrish and Lowitzsch (1959). The method utilizes a set of precisely machined jigs. First, the diffractometer is set in a slide with the desired take-off angle (5^{o} in XRAS) at the correct distance (185 mm in XRAS) from the x-ray tube. This slide permits the x-ray tube focal spot, the divergence slit and the diffractometer axis to be precisely aligned, while the take-off angle and focal spot to specimen distance are maintained. The 0.00^{o} scattering angle is set at the position where the maximum intensity is measured by the detector. It is doubtful that this setting is more accurate than 0.01^{o} two theta. The error limits the accuracy of all angular measurements, and is in no way avoided by the usual extrapolation methods.

Three leveling screws, which support the cryostat, are used to adjust the specimen support to the desired height, and place the specimen mounting surface parallel to the diffractometer axis. The latter axis is adjusted with the aid of a machine square.

The 2:1 angular relationship between specimen and detector, and specimen eccentricity adjustments are made with a jig that just touches the outside of both slit assemblies when the detector is set to 0.00° two theta. In making this adjustment the cryostat is moved relative to the diffractometer. The lock screws are set so that the movement is firm but avoids the 'stick and slip' condition. When the desired position is obtained, the lock screws are tightened. In tightening the lock screws no stresses occur which could alter the alignment.

When the vacuum chamber is evacuated, the 1 inch thick steel table top is deflected upwards about 0.1 inches by atmospheric pressure. If the x-ray tube and diffractometer were mounted directly on the table top, this deflection would destroy the alignment of the x-ray tube relative to the diffractometer. The problem is overcome by mounting the complete x-ray optical system on a 24 inch diameter 1 inch thick steel plate supported by three legs (figure 3). The deflection moves the entire optical system but does not disturb its alignment. The rotating 'O' ring seal and the flexible copper tubing (figure 8) permit some movement between the optical system and the vacuum chamber.

(d) Scintillation Counter

If the scintillation counter is operated in vacuum the preamplifier tube (6U8A) fails in approximately three hours because of inadequate cooling. Therefore, the detector assembly is mounted in a steel box (figure 9) through which compressed air is blown to provide the necessary cooling. Flexible copper tubing, which carries the compressed air and electrical leads to the detector, is connected to rotating 'O' ring seals in the top flange of the vacuum chamber to permit the detector to rotate with the scan. X-rays are admitted to the detector through a 0.005 inch beryllium window sealed to the box with an 'O' ring. With this arrangement, the non-x-ray background is about 5 counts per minute with the differential pulse height analyzer set to pass 90 percent of CuK or MoK x-rays. It is believed that thermoelectric cooling would reduce detector noise and permit the detector to be used for much longer wavelengths.

(e) High Voltage Lead to the X-ray Tube

The most difficult problem encountered in operating the entire x-ray optical system in vacuum was caused by the high potential applied to the x-ray tube. At pressures less than atmospheric but greater than E-5 mm of Hg. arcing activated protective circuits that turned off the x-ray generator. In addition to the inconvenience, this is a serious disadvantage because it is very difficult to reset the x-ray generator to its previous intensity.

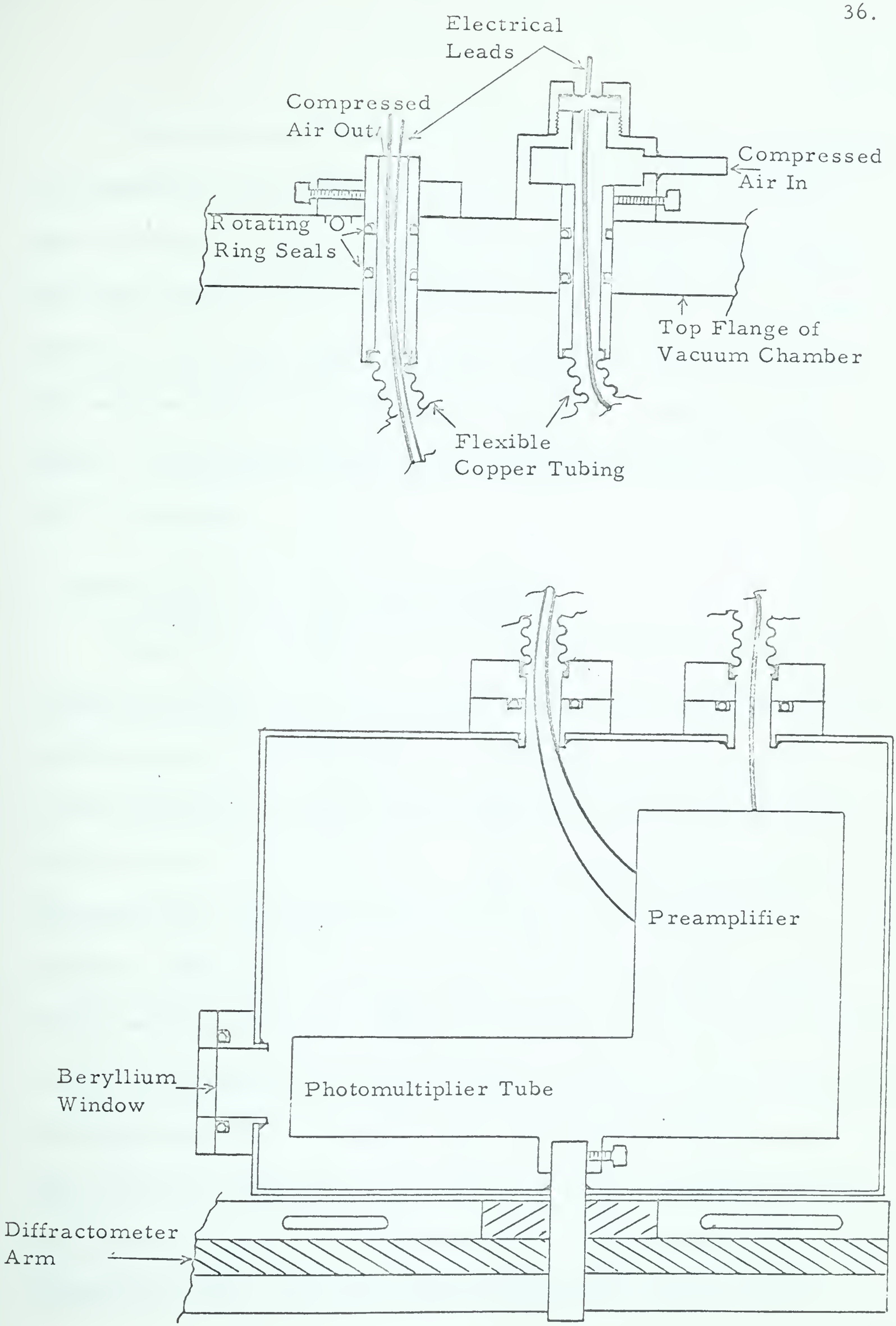

Figure 9. Detector Housing Design

The problem was solved by making the high voltage connection in air outside the vacuum (figures 1 and 10). This seal can be extended about 12 inches and deflected about 20° in any direction. This permits the optical system to be aligned with the top rotating 'O' ring seal independently of the high voltage connection. Because of air pressure the seal must be clamped in position after the optical system has been aligned. Compressed air blown into the connection cools the x-ray tube and 'O' ring seals.

5. AUTOMATIC STEP SCANNING SYSTEM

Manual step scanning has been used for several years for precision intensity measurements in x-ray diffraction. In this method the operator sets the desired scattering angle and time interval. At the end of the set time interval, the angle and the number of counts accumulated are written in a note book. The cycle is then repeated for a new angle. The monotonous character of this tedious task encourages operator mistakes; and the numerical analysis of the recorded data is equally tedious and time-consuming. Many advantages are gained by performing the step scanning operation automatically: the angle is set more precisely; the accumulated count is recorded faster and with much greater reliability. Once the equipment is started an operator is no longer needed, and therefore 24 hours per day operation is possible instead of the usual five hours per day. The most important advantage is the convenience

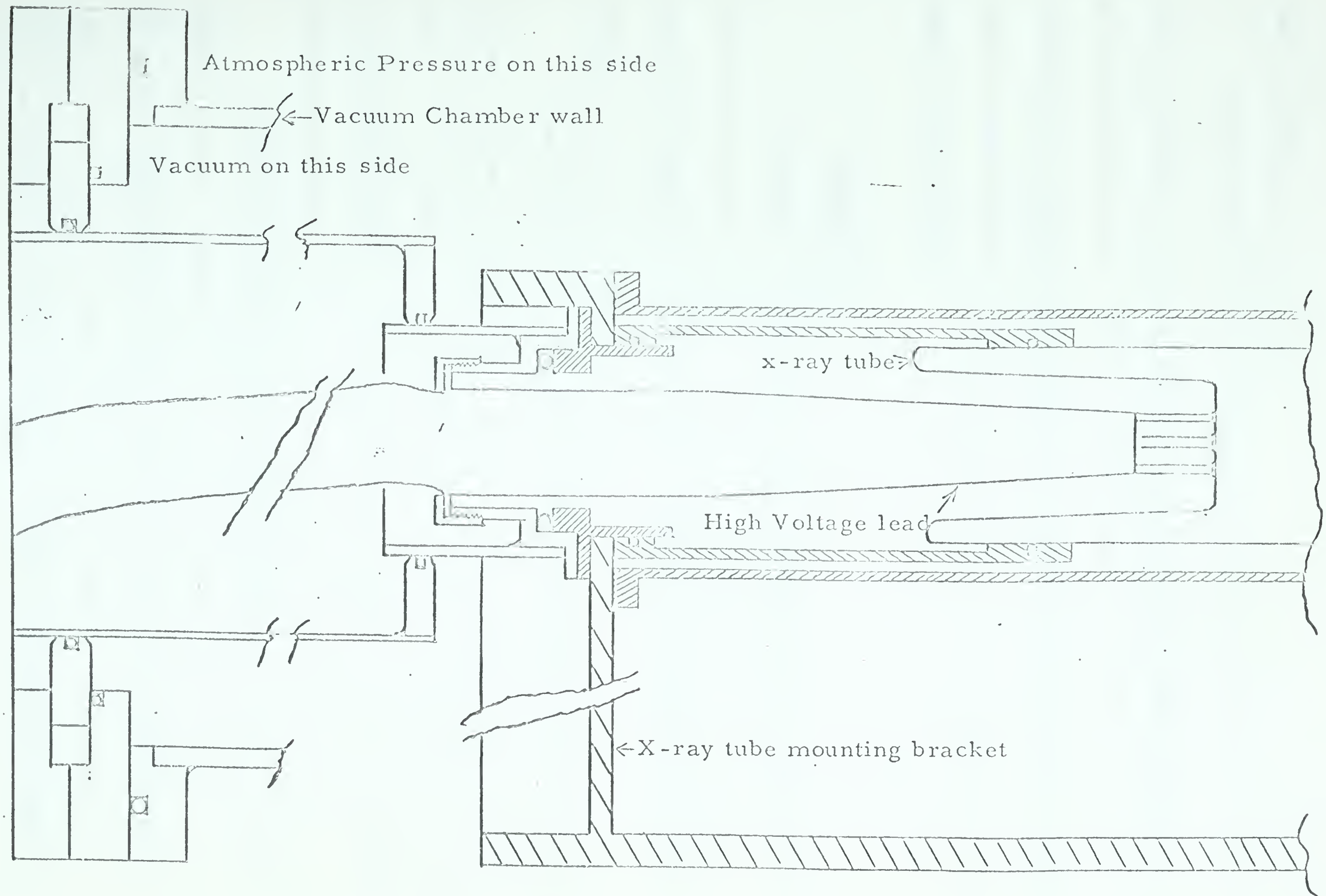

Figure 10. High Voltage Connection to X-ray Tube

that encourages precision work.

With commercially available equipment step scanning is used as a last resort, but with the equipment described here step scanning is used as a matter of routine. Data recorded directly on IBM cards are quickly processed by computer (IBM 1620) with high precision and few mistakes; and the experimenter has time to concentrate on the design and interpretation of experiments.

(a) Design Basis

The design of an automatic step-scanning system must start with the selection of the counter, the diffractometer drive motor, and the recording medium (e.g. IBM cards). Then these components must be integrated to form a complete system.

When XRAS was designed in 1960, the Beckman 7061 was one of the few counters available with readout. This counter uses electronic tubes and provides a 1-2-2-4 BCD (binary coded decimal) high impedance (5 megohms) readout. The transistorized counters currently available with low impedance (10k) readout would permit a simpler design.

A Slo-Syn stepping motor (American Superior Electric Model SS250) driven at 100 steps per revolution was selected because it is basically a digital device and compatible with the rest of the system. Further, the author is not familiar with the design and operation of servomechanisms. Various ratchet or indent mechanisms appear to

be unreliable and slow; Geneva gear systems show promise, but it was felt that their development would take too long.

The original recording medium, perforated paper tape (PPT), was selected because of its low cost and common usage. However PPT has all the disadvantages of old parchment: it is awkward to read, store and modify. In addition it is not compatible with many modern computers and is intolerably slow. IBM cards are similar to books: they are easy to read, store and modify. XRAS is the first x-ray diffraction system to record data directly on IBM cards and all x-ray diffraction systems described in the literature use PPT (Abrahams 1962).

The years of intensive research and development in computers can be used to advantage in designing a digital system such as XRAS. It is not necessary to understand in detail the operation of circuits such as flip-flops, gates, diodes matrices, etc., but only their function and input-output characteristics. Thus it is not necessary to be an electronics expert to design large digital systems — a fact recognized by computer manufacturers.

The incredible reliability of components necessary for operation of a large system is not generally appreciated. For example, a system with E+6 components each of which has a failure rate of one in E+6 would probably never perform ten consecutive operations without a failure. Therefore marginal operation cannot be tolerated in a large digital system. In XRAS the signal to noise ratio in digital circuits is usually

100:1 ; that is, if a signal pulse is 10 volts, noise pulses are 0.1 volts or less. After one year and some E+7 operations only three transistors have failed out of a total of 200 transistors and 1000 diodes. This demonstrates the high reliability of the system.

(b) Counter Readout

This is the problem of transferring the counter reading (the number of counts accumulated in a fixed time) to a recording medium such as IBM cards. The 7061 counter used in XRAS has a 1-2-2-4 BCD; for each decimal digit there are four output wires which possess levels of -15 volts or more negative to signify a binary zero, and levels of 0 volts or positive to signify a binary 'one'. The code is shown in detail in table 3 and the pin numbers on the output plug of the 7061 are shown in table 4. This code is not convenient to drive an IBM card punch nor does it have sufficient power.

At this point it is necessary to select a 'code' to be used for recording. The choice is not arbitrary; typewriters, card punches and printers use a decimal code; perforated paper tape punches, digital magnetic tape, and ferrite core storage usually use a BCD 1-2-4-8 code. A pure binary code which is used in many large computers (IBM 7040, 7070, and 7090) is difficult to convert to any decimal code and vice versa. However, any code based on the decimal system can easily be obtained from a pure decimal code by a simple diode circuit, which can be quickly

built for a few dollars. Circuits to convert, for example, BCD to most other decimal based codes involve months of work and hundreds of dollars. Considering the rapid obsolesence of digital equipment, the flexibility of a decimal code is an important advantage.

Table 3. Four-Line Binary Code

In the tabulation, a '0' represents a negative potential of 15 volts or more with respect to ground; a '1' represents a potential at ground level or positive with respect to ground.

Decimal digit registered	First binary stage	Second binary stage	Third binary stage	Fourth binary stage
0	0	0	0	0
1	1	0	0	0
2	0	1	0	0
3	1	1	0	0
4	0	1	1	0
5	1	1	1	0
6	0	0	1	1
7	1	0	1	1
8	0	1	1	1
9	1	1	1	1

Table 4. Identification of Pin Numbers on Digital Recorder Socket

Table 4 gives the pin numbers on the Digital Recorder socket for the four binary lines of each decimal digit position.

Order of digit read		First binary stage	Second binary stage	Third binary stage	Fourth binary stage
Highest	10^5	Pin 4	Pin 3	Pin 2	Pin 1
Second	10^4	8	7	6	5
Third	10^3	12	11	10	9
Fourth	10^2	16	15	14	13
Fifth	10^1	20	19	18	17
Sixth	10^0	24	23	22	21

NOTE: Pin 39 carries a control signal from the counter. This pin is negative during the display period and positive from reset until the end of the next counting period.

Pin 40 is the 'inhibit reset' line. When this pin is grounded the counter cannot reset.

The circuits developed to convert the 1-2-2-4 BCD 7061 output to a decimal code are shown in figure 11. Each 7061 BCD output is fed to a binary gate with two outputs. These outputs have two configurations 0 and +12 or +12 and 0 volts. Using the notation $\bar{1}$ to mean 'not 1', one can imagine the BCD code is now in the form $1-\bar{1}-2-\bar{2}-2-\bar{2}-4-\bar{4}$. The decimal conversion of this code is given in table 5. The code is simply converted to a decimal code by the 8 x 10 diode matrix shown in figure 11.

Table 5. Matrix for 1-1-2-2-2-2-4-4 to Decimal Conversion

8 Line Binary Code	Decimal Digit Represented									
	1	2	3	4	5	6	7	8	9	0
1	+		+		+		+		+	
$\overline{1}$		+		+		+		+		+
2		+	+	+	+			+	+	
$\overline{2}$	+					+	+			+
2				+	+	+	+	+	+	
$\overline{2}$	+	+	+							+
4						+	+	+	+	
$\overline{4}$	+	+	+	+	+					+

In the matrix, diodes are placed exactly as the '+' in table 6. The operation of the matrix can be understood by the following example; when the decimal 1 is input the 1, $\overline{2}$, $\overline{2}$, $\overline{4}$ condition lines are held at + 12 volts (1k) and the $\overline{1}$, 2, 2, 4 condition lines are held nearly at ground potential (22 ohms). The interrogating pulse comes in on the 10 load lines through a 22k resistors. On the '1' load lines, the diodes are held at +12 volts by the binary gates and allow the interrogating pulse to pass without reducing its pulse height. However on the '2' load line with diodes at $\overline{1}$, 2, $\overline{2}$, $\overline{4}$ the $\overline{1}$ and 2 diodes are held near ground potential. Thus the 22k load resistor and 22 ohm grounding resistor in the binary gate act as a voltage divider and a pulse of some 10 millivolts appears on the '2' load line. A similar situation occurs on the remaining 8 load lines. Thus, when the gates are in the BCD

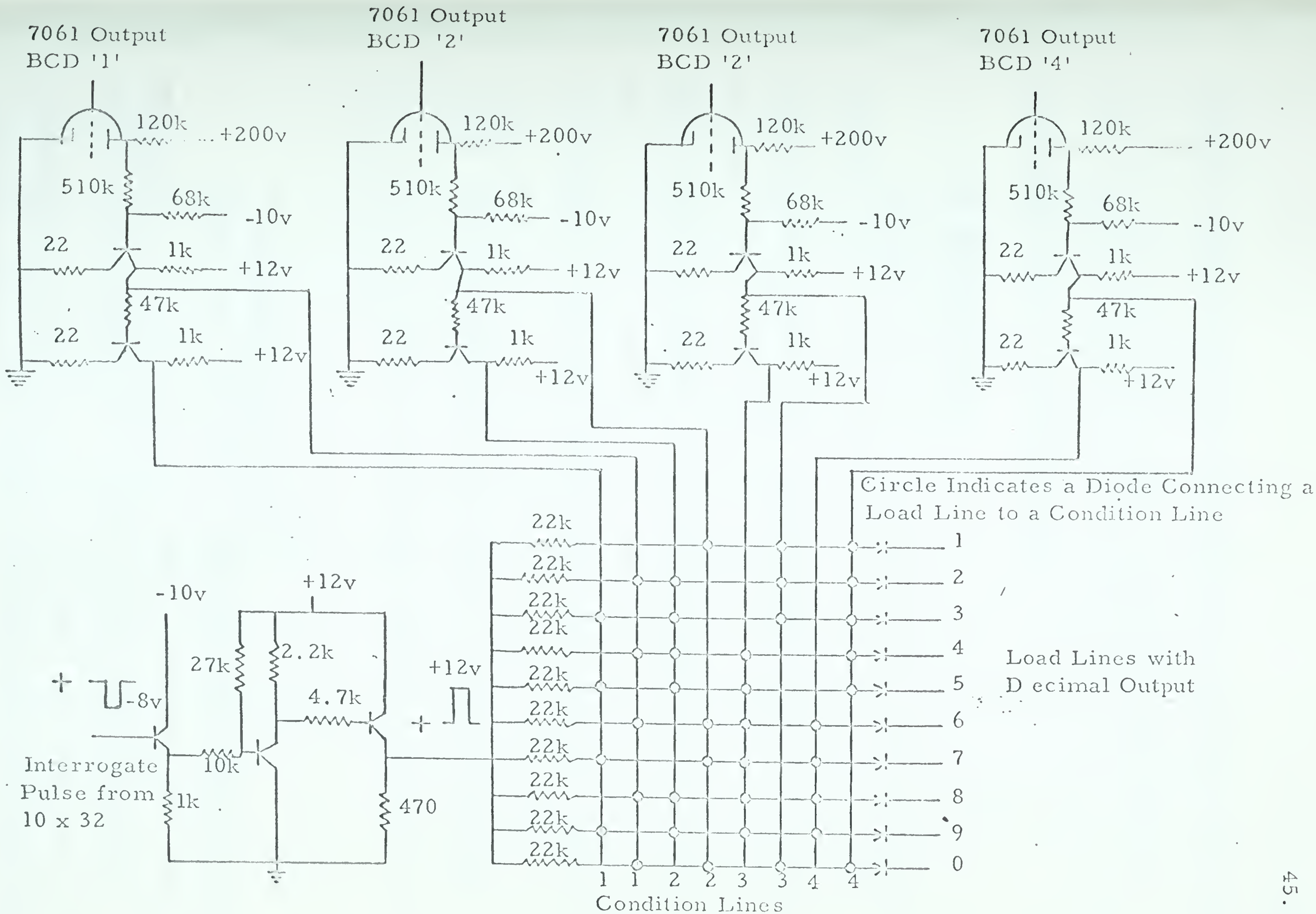

Figure 11. BCD to Decimal Converter Circuit

$1-\overline{2}-\overline{2}-\overline{4}$ configuration, the interrogating pulse is transmitted only by the '1' line. In this way the BCD code is converted to a decimal code. All timing problems with exception of the interrogating pulse are avoided because the system is essentially static.

(c) <u>IBM Punch Drive</u>

The pulses from the 8 x 10 diode matrices are fed to 10 Schmitt triggers, one for each decimal number, which output only when their input exceeds +6 volts. These circuits amplify and shape the pulse and eliminate any noise that might have developed. Each Schmitt drives a three-transistor amplifier (1 amp 40 volts output), called a solenoid driver. The solenoids, which are mounted in a frame over the keyboard of the IBM 26 card punch, mechanically activate the keys. The card punch can be used in the normal manner by simply lifting off the solenoid frame. The high reliability of the solenoids is perhaps surprising. In three months of continuous operation one malfunction occurred and this was caused by dirt.

(d) <u>Timing the Readout Cycle</u>

At this stage, the problem is reduced to one of timing the interrogating pulses (starting, stopping, and pulse distribution). The timing sequence for a readout cycle in XRAS is shown in figure 12 by the waveforms at a number of points in the circuit. The readout cycle is started by a signal from the 7061 on pin 39 when the preset time interval

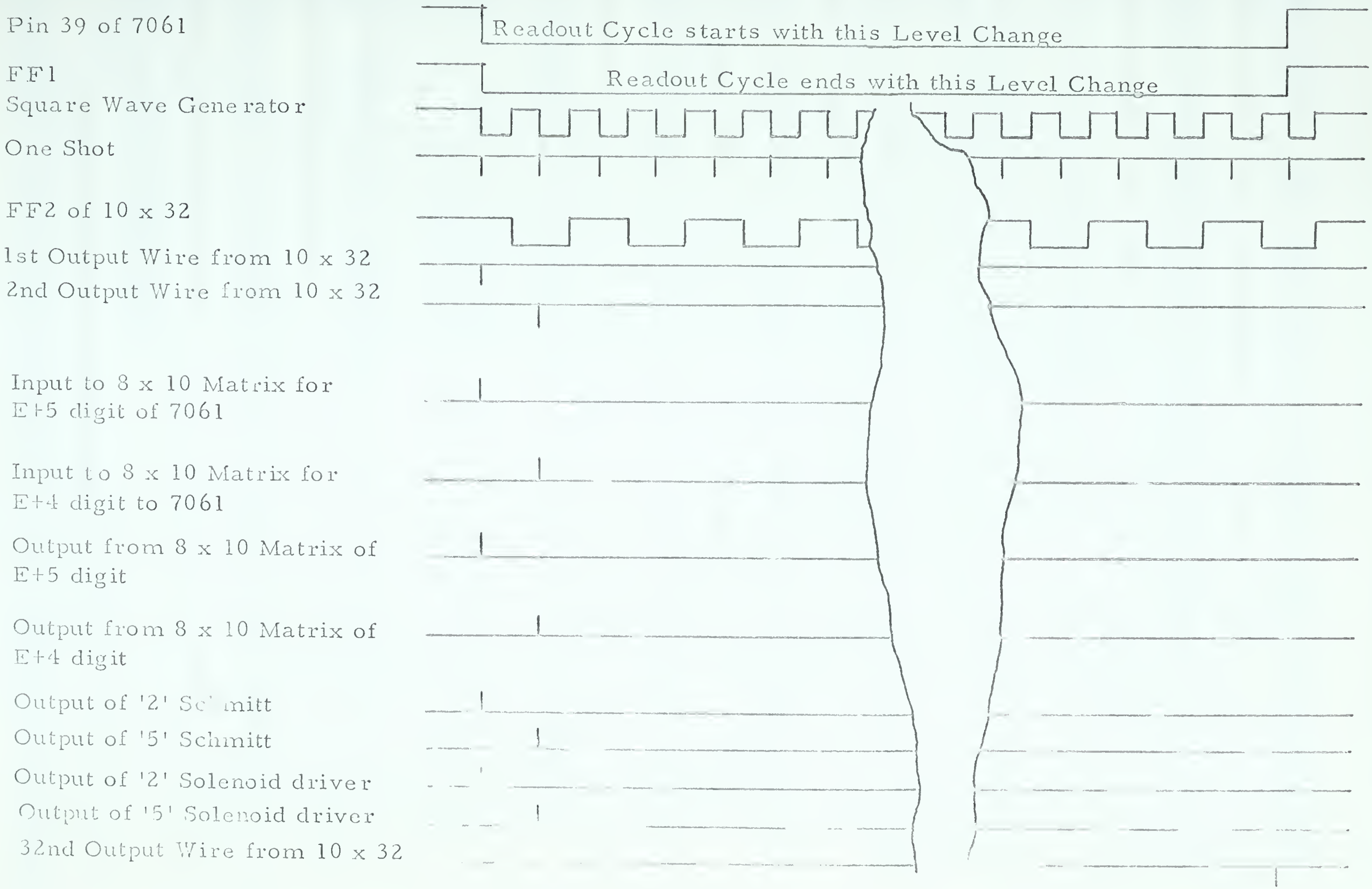

Figure 12. Waveforms from the Readout Circuits (7061 Reading 250000)

has elapsed. The signal turns 'on' flip-flop 1(FF1) which grounds pin 40 of the 7061 in order to inhibit the counter until the readout is complete, and at the same time turns on a square wave generator which provides the 'timing' of the readout cycle. The negative-going edge of the square wave fires a 'one shot' (5 millisecond pulse width when used with a card punch) which forms the interrogating pulses. The positive-going edge of the square wave sets the flip-flops which condition the 10 x 32 matrix. Thus the pulses from the one shot appear sequentially on the 32 output wires of the 10 x 32. The first output pulse from the 10 x 32 is P1, the second P2, etc. Pulse P1 interrogates the 8 x 10 matrix for the 10^5 digit of 7061. Pulses P2 to P6 interrogate the 10^4 to 10^0 digits. Pulse P7 is not used, but its period is used by the punch to skip one column and separate the 7061 reading from the angle counter reading on the IBM card (see figure 14). Pulses P8 to P12 interrogate the angle counter 8 x 10 matrices. Pulse P13 punches a zero, for convenience; pulse P16 advances the angle counter by one count; pulse P17 advances the stepping motor one step. Pulse P32 turns off FF1, which stops the square wave generator and releases pin 40 of the 7061 from ground. This enables the 7061 to begin the next observation. The output pulses from the 10 x 32 that are not used at present are available for equipment modifications.

The layout of the timing and pulse distribution circuits is shown in figure 13. The schematics for the flip-flops, square wave generator,

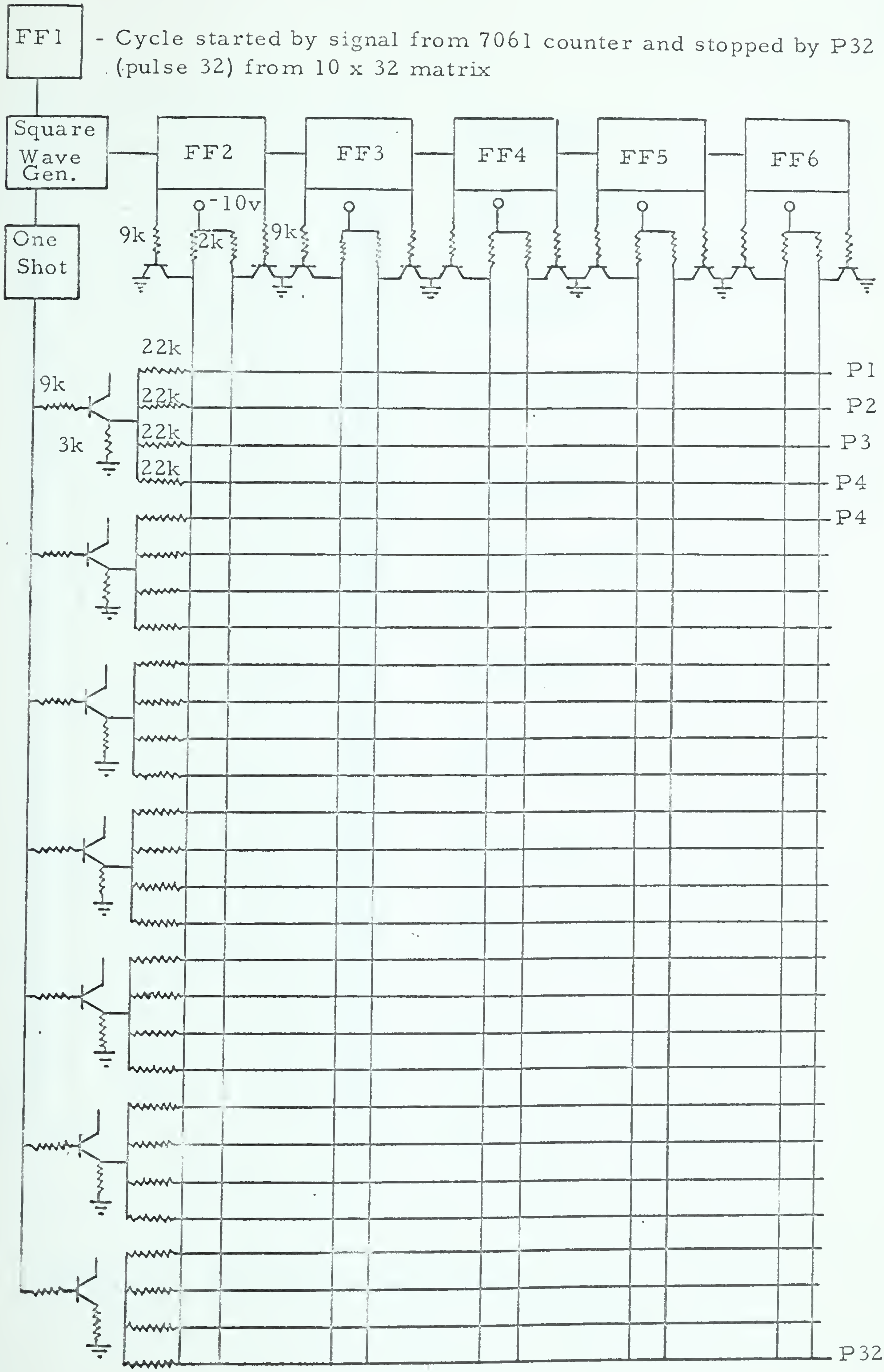

Figure 13. Schematic of Pulse Timing and Distribution Circuit.

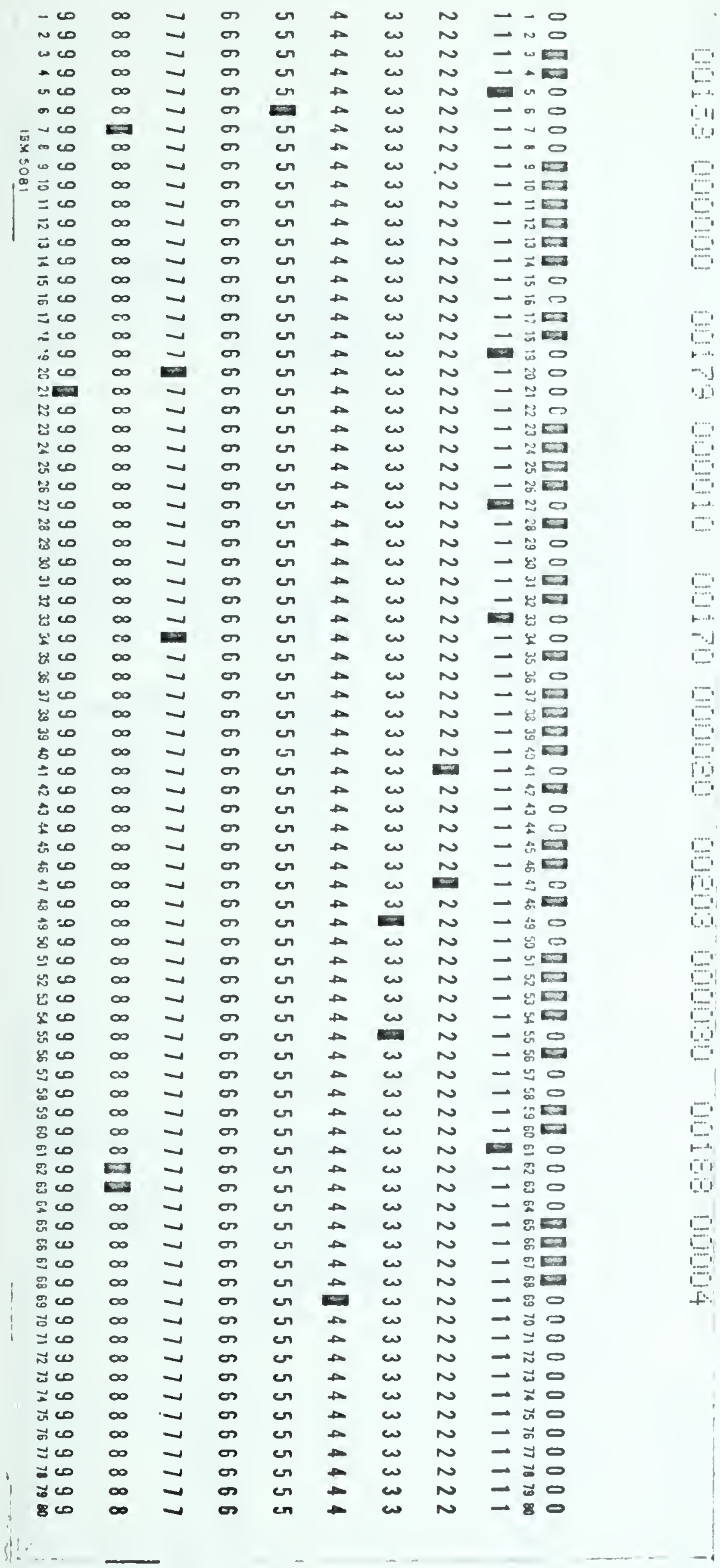

Figure 14. Example of a Data Card

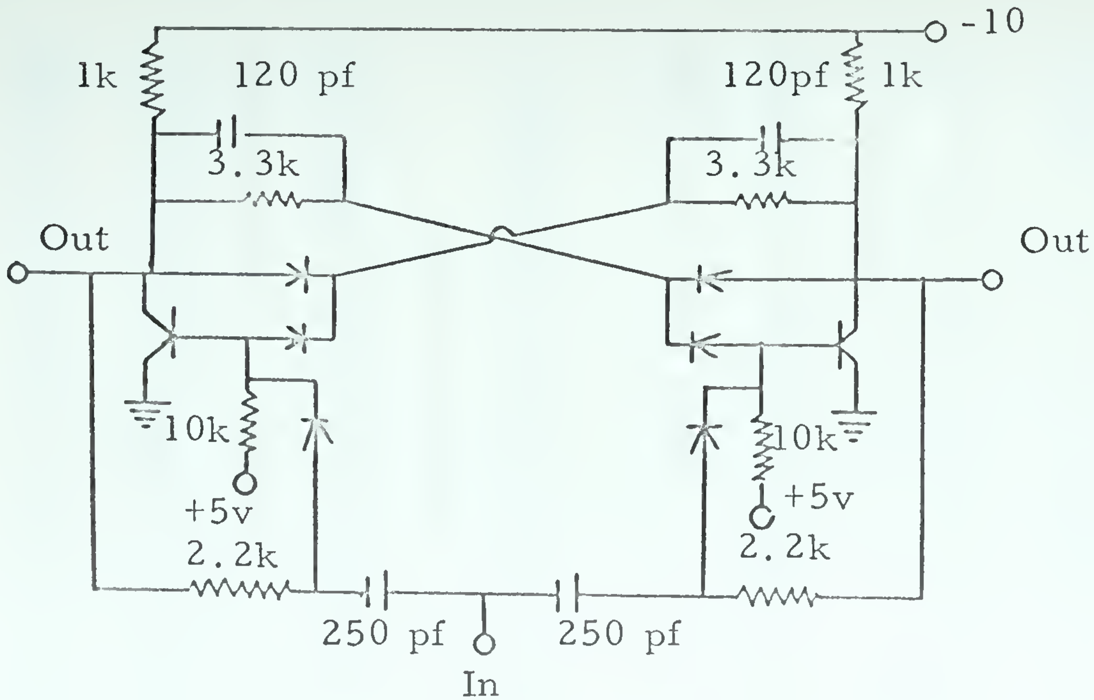

FLIP-FLOP

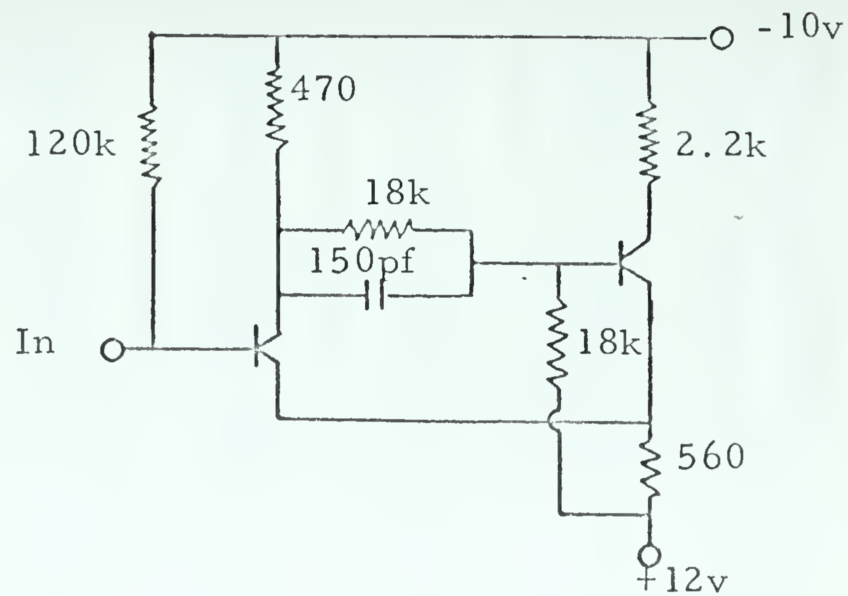

SCHMITT TRIGGER

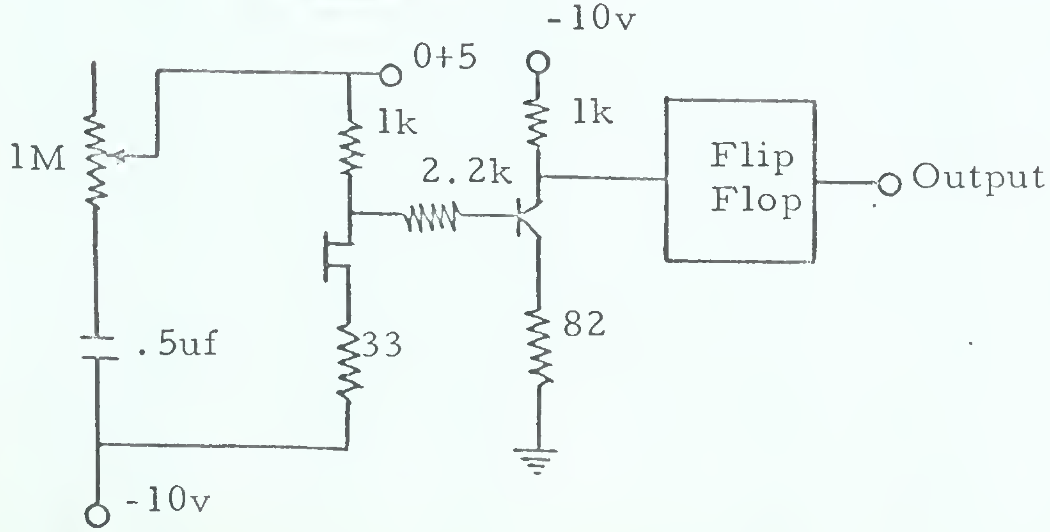

Square Wave Generator

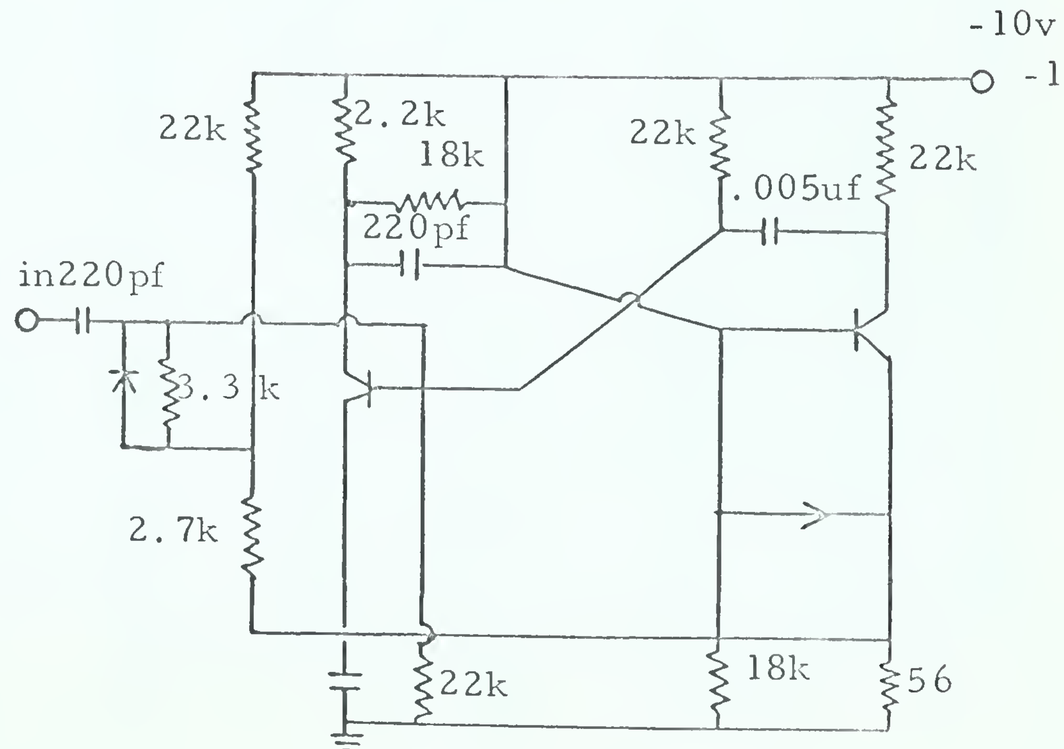

One Shot

Figure 15. Schematic Circuit Diagrams for Flip-Flop, Square Wave Generator, One Shot, and Schmitt

one shot and emitter followers is given in figure 15. The emitter followers designed by the author have useful characteristics. The emitter followers that condition the matrix have a very low resistance (about 10 ohms) when 'on'. This heavily grounds signals through the diodes where necessary and provides a high signal-to-noise ratio on the output from the 10 x 32 matrix. The emitter followers that amplify the interrogating pulse provide a very low impedance pulse (20 ohms) to the load line with a low current drain (3.3k) in the standby state.

One of the important advantages of this readout system is the ease with which the readout rate (characters per second) can be varied. By simply varying the frequency of the square wave generator the readout rate can be varied from 0.5 to 50,000 characters per second. The pulse width of the one shot must be adjusted for each application by changing one capacitor. Thus the system can drive, with few modifications, almost any digital output device, such as a typewriter, perforated paper tape punch, card punch, and digital magnetic tape recorder.

6. EVALUATION OF THE PERFORMANCE OF XRAS

An x-ray diffraction system measures the diffracted intensity of a small volume of reciprocal space. The performance of such a system can be evaluated by considering the accuracy and precision of measuring the location of this volume in reciprocal space and the intensity. In XRAS the volume is located by specifing the scattering angle.

The accuracy and precision of the scattering angle measurement were determined by a lattice parameter measurement of nickel; and the accuracy of intensity measurements was assessed by an analysis of the 731-553 reflection from nickel.

(a) Lattice Parameter of Nickel

The results of six determinations of the lattice parameter of nickel are listed in table 6. The specimen used in run 42 was a powder compact prepared by compressing Sherritt Gordon nickel powder (99.9 percent nickel) to 30,000 psi and annealing at 550 C. The specimen was mounted in a split clamp, and both clamp and specimen were polished on a diamond lap to a mirror finish. The surface was etched slightly with a solution containing 50 percent nitric acid and 50 percent acetic acid by volume. The specimen used in runs 112 and 113 was made by cold-worked Inco electrolytic nickel (99.5 percent nickel) by hammering. The surface was again polished and etched. In runs 127 and 130 this specimen was annealed at E-7 mm of Hg in a high-frequency furnace at approximately 650 C and repolished. In runs 134 and 135 the specimen from runs 127 and 130 was reduced in thickness by 20 percent by rolling, and then repolished. The surface roughness of the specimens appears to be of the order of micro-inches.

The locations of the peak intensities of the molybdenum $K_{\alpha 1}$ and $K_{\alpha 2}$ Bragg reflections in the range 25° to 55° theta were taken as

the Bragg angles. This is done very quickly with digital data and is not arbitrary. The lattice parameter is determined by a Nelson-Riley extrapolation, performed by the Fortran program shown with the input data on page 56; and the output data is shown on page 57. The extrapolated value is found by a least square analysis that is carried out with the Fortran program shown on page 119. The output from run 42 shown on page 57 yields a lattice parameter of 3.5235658Å, with standard deviation of 0.0000018Å. The slope of the extrapolation is 0.0023Å.

The lattice parameter of the annealed specimens determined from runs 42 and 127 is 3.5236Å at 298 K ± 1K. The difference between the lattice parameters from the two runs is only 0.00004Å. The correction for refraction would increase the lattice parameter to 3.5237Å. This is in good agreement with Pearson's (1958) value, 3.5237Å, which indicates that the accuracy of angular measurements in XRAS is high. The precision of the results is emphasized by the small value of the standard deviation. If higher angle reflections were used the standard deviation would presumably be even smaller.

Table 6. Lattice Parameter Results

Slope (Å)	Run	Temp.	Parameter	Std. Dev.	Condition
0.002	42	300	3.5235658	2 E-6	Annealed
0.0008	127	300	3.5236057	5 E-6	Annealed
0.0002	130	77	3.5149968	9 E-7	Annealed
Thermal expansion			0.0087089		
0.0004	112	300	3.5248818	7 E-8	Cold Worked
0.0004	113	77	3.51177674	2 E-6	Cold Worked
Thermal expansion			0.0071144		
0.0005	134	300	3.5247801	1 E-7	Cold Worked
0.0013	135	77	3.5169277	2 E-7	Cold Worked
Thermal expansion			0.0078524		

The lattice parameter of the cold worked specimens is about 0.03 percent larger than the lattice parameter of the annealed specimens. If the effect is real, it implies that the presence of vacancies and dislocations has increased the lattice parameter. However a change in the profile of the reflection caused by cold work could shift the location of the peak intensity without shifting the centroid of the reflection. Then it could be argued that the effect is not real. However the fact that the linear thermal expansion is different for the cold worked specimens suggests that the effect is real.

The accuracy of the results is limited by the accuracy in setting

```
..I J.GOLDAK LATTICE PARAMETER EXTRAPOLATION 922102 SAVE CARDS
..LOAD FORTRAN EXECUTE DUMP
 10    FORMAT(4I2,2XF7.3)
 12    FORMAT(2F20.10)
 1     READ 10,I,J,K,L,S
       WL1=0.70926
       WL2=0.713543
       S1=3.14159265*S/360.
       S=SIN(S1)
       C=COS(S1)
       X=J*J+K*K+L*L
       SS=S*S
       SX=SS/X
       IF(I)2,2,3
 2     WL=WL2
       GO TO 4
 3     WL=WL1
  7    FORMAT(3F20.10)
  4    D=0.25*WL*WL/SX
       D=SQRT(D)
       R=0.5*C*C*(1.0/S+1.0/S1)
       PUNCH 12,R,D
       GO TO 1
       END
 1 4 0 0    47.40
   4 0 0    47.70
 1 3 3 1    52.00
   3 3 1    52.33
 1 4 2 0    53.44
   4 2 0    53.77
 1 4 2 2    59.03
   4 2 2    59.41
 1 3 3 3    62.98
   3 3 3    63.44
 1 4 4 0    69.38
   4 4 0    69.85
 1 5 3 1    73.03
   5 3 1    73.54
 1 6 0 0    74.25
   6 0 0    74.74
 1 6 2 0    78.98
   6 2 0    79.62
 1 5 3 3    82.53
   5 3 3    83.16
 1 6 2 2    83.70
   6 2 2    84.35
 1 4 4 4    88.34
   4 4 4    89.05
 1 5 5 1    91.86
   5 5 1    92.55
 1 6 4 0    92.97
   6 4 0    93.80
 1 6 4 2    97.69
   6 4 2    98.49
 1 5 5 3   101.21
   5 5 3   102.05
```

```
..I J.GOLDAK LATTICE PARAMETER EXTRAPOLATION 922102 SAVE CARDS
..LOAD FORTRAN EXECUTE
   32
```

NELSON-RILEY FACTOR	LATTICE PARAMETER
2.05644900	3.52911540
2.03918610	3.52938970
1.81150220	3.52622740
1.79541530	3.52671270
1.74260500	3.52723530
1.72727890	3.52836430
1.50363700	3.52647950
1.48884150	3.52713380
1.35756040	3.52773520
1.34159360	3.52596010
1.15228420	3.52479940
1.13852210	3.52522520
1.04954210	3.52588620
1.03590840	3.52601700
1.01720570	3.52540650
1.00448310	3.52680520
.90032008	3.52684940
.88546702	3.52431560
.82057893	3.52587450
.80707857	3.52513200
.79565578	3.52579450
.78208525	3.52481970
.70286735	3.52609820
.68947187	3.52497650
.63840042	3.52484070
.62631793	3.52563900
.61904898	3.52632920
.60487177	3.52348520
.54161651	3.52463160
.52923280	3.52449540
.48863939	3.52484930
.47656102	3.52500860

```
I J.GOLDAK LEAST SQUARES ANALYSIS 922102E  SAVE CARDS
LOAD CARDS
  .34170216E+02   .43596926E+02
  .11283159E+03   .39784298E+03
  .12049986E+03   .43956430E-02
LEAST SQUARES ANALYSIS
   A=    .35235658E+01(+OR-    .17783270E-05)
   B=    .22668330E-02(+OR-    .13052861E-05)
 Y=B*X+A
```

the zero scattering angle. This is at least as great as the errors in machining the gear drive -- 7 seconds of arc. The accuracy is further limited by the error in reading the starting angle of each scan and in measuring the specimen temperature. A temperature change of 1K causes a change of 0.000044Å in the lattice parameter of nickel at 300K.

The standard deviation suggests that the precision of the data is somewhat greater than the accuracy. Therefore relative measurements of higher precision are conceivably useful. The runs at 77K and 300K permit a calculation of the linear thermal expansion of nickel. The average expansion for runs 112-113, 127-130, and 134-135 is 0.0079 per K, which is in good agreement with the value of 0.0077 obtained by Nix and McNair (1941) by a dilatometric method. None of the three values differs by more than 10 percent from Nix and McNair's value. This, combined with the fact that the slope of the extrapolation does not change greatly, suggests that the alignment is not seriously altered by cooling the specimen to liquid nitrogen temperatures. Further, the small value of the standard deviation suggests that the extrapolation has not neglected angle-dependent factors.

It is necessary to emphasize that neither XRAS nor the experimental technique used to determine the lattice parameter of nickel was designed specifically for precise lattice parameter determinations. The precision obtained is entirely a by-product of the care taken to obtain precision intensity measurements.

(b) The Precision of Intensity Measurements

The intensities, corrected for Lorentz-polarization and the variation in scattering factor with angle, from eight scans of the nickel 731-553 reflection at 300K are listed in table 7. The values are taken from data from runs 100 to 103 and from 108 to 111 given in appendix II. The average value and the standard deviation associated with each intensity are included. The scans were completed within a three day interval.

Table 7. Intensities Associated with the 731-553 Reflection

Run number	Total integrated intensity	Intensity at 49.62° theta	Background at 49.875° theta	Background at 52.87° theta
100	512.516	33.555	32.418	29.406
101	510.660	32.852	31.800	29.951
102	509.614	32.564	30.963	29.055
103	510.014	33.242	32.953	29.365
108	514.711	32.666	32.053	29.772
109	513.856	32.962	32.703	29.147
110	509.299	31.929	30.992	28.830
111	520.030	32.437	32.868	30.651
Average	510.093	33.136	31.979	29.374
Std. Dev.	2.2	0.040	0.16	0.088
Percent Std. Dev.	0.43	0.12	0.5	0.3

The first value in table 7 is the integrated intensity for 49.750° to 52.999° theta. The second value is the intensity from 49.500° to 49.749° theta. The third and fourth values are the background intensities measured between 49.750° and 49.999° and between 52.750° and 52.999° theta

respectively.

The standard deviations range from 0.12 percent to 0.50 percent with an average value of 0.34 percent. Considering that the statistical error caused by the finite number of photons counted has not been eliminated, these results verify the original estimate that intensity measurements with a precision approaching 0.1 percent are possible.

(c) Summary

Lattice parameters can be measured from data from XRAS with accuracy of the order of 0.0001Å and probably some what greater precision. The precision of intensity measurements approaches 0.1 percent. Further, such high precision measurements can be made more conveniently with XRAS than routine measurements with commercially available apparatus. Except , possibly, for the lack of a crystal monochromator, it is believed that in XRAS the main object of this thesis 'the design, construction and operation of an x-ray diffraction system (XRAS) to provide the best data possible within the imposed limits of time, financial resources, and technological facilities', has been accomplished.

PROCESSES OF X-RAY SCATTERING

PROCESSES OF X-RAY SCATTERING

The processes of x-ray scattering of interest in x-ray diffraction are:

1. Fluorescent scattering
2. Compton scattering
3. Coherent scattering

In order to isolate one effect it is necessary to be able to identify and eliminate the others. This is the most uncertain part of this study. In the following paragraphs the characteristics of the various types of scattering are discussed.

1. FLUORESCENT RADIATION

If the incident x-ray beam contains photons of sufficient energy to excite atoms in the specimen, characteristic (K, L, M, etc.) radiation can be emitted from the atoms as they return to their normal state. Such radiation is unpolarized and uniformly distributed in all directions. The fluorescence yield (the ratio of the number of atoms which emit Q radiation to the number of atoms from which Q electrons have been ejected) increases with atomic number, and approaches unity. Rescattered fluorescent radiation is related to crystal orientation (James 1958 p.439).

In XRAS, the effect of fluorescent radiation when MoK radiation and nickel specimens are used is negligible. As only NiK radiation

has significant energy compared to MoK, L and M radiation need not be considered. The ratio of MoK to NiK transmitted by the zirconium filter is about 2000. Further, the pulse height analyzer rejects most NiK pulses. The above contention was verified by using a copper x-ray tube, nickel specimen, and zirconium filter. The pulse height analyzer was set to pass 90 percent of the MoK intensity. The intensity observed was of the order of 1 count per second for the Ni 111 reflection using CuK radiation which, with a nickel filter and the pulse height analyzer set for CuK, would be about 5000 counts per second. The one count per second is probably white radiation and not CuK. The intensity of NiK, which has lower energy than CuK, would be even smaller. Therefore, the effect of fluorescent radiation in this work is entirely negligible.

2. COMPTON SCATTERING

An acceptable theory of Compton scattering must account for, (a) the wavelength and (b) the intensity of the scattered wave. The wavelength problem, which is relatively simple, is discussed in some detail. However the intensity aspect is enormously complex and to date only rough approximations are available. For example, only a free atom model is considered: yet, with x-rays in the one angstrom range, the Compton recoil electron receives energy in the range 0 to 600 eV. It is exactly in this energy range that the electron states of an atom are most sensitive to the crystal structure in which the atom is located.

The assumption of total incoherence of Compton scattering, which all theories use, is a second approximation. In the limit of long waves or small angles the change in wavelength approaches zero; and then the assumption of total incoherence is certainly questionable. These contentions are supported by C. B. Walker's (1956) measurements of the Compton scattering from the (100) plane of aluminum single crystals at 5 K, which do not agree with the suggested formula. In view of these questions and the complexity of the derivation a qualitative approach to the intensity of Compton scattering derived from the suggested formula must suffice.

(a) Wavelength

The wavelength of a photon scattered at an angle two theta by the Compton process is found by applying the principle of conservation of energy and momentum. Let an incoming photon with frequency v_o , energy hv_o , wave vector K_o , and momentum $\hbar K_o$, collide with a free electron at rest with mass m, energy mc^2 , and zero momentum. The scattered photon possesses energy hv and momentum $\hbar K$, and the recoil electron has momentum P and energy $c\sqrt{m^2 c^2 + P^2}$.

h - Planck's constant

$\hbar = h/2\pi$

c - speed of light

The conservation of energy requires

$$h\nu_o + mc^2 = h\nu + c\sqrt{m^2c^2 + P^2} \tag{8}$$

The conservation of momentum requires

$$\hbar K_o = \hbar K + P \tag{9}$$

where K_o, K, and P are vectors as shown in figure 16.

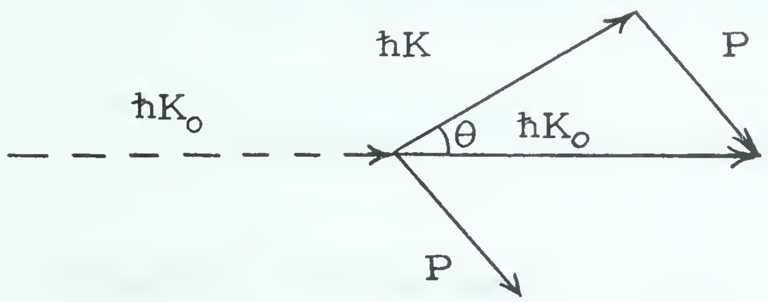

Figure 16. Momentum Diagram for Compton Scattering -- A photon with momentum $\hbar K_o$, on striking an electron at rest, is scattered through an angle theta and left with momentum $\hbar K$. The electron has acquired a recoil momentum P.

P is expressed in terms of $\hbar K_o$, $\hbar K$ and theta.

$$P^2 = \hbar^2 K_o^2 + \hbar^2 K^2 - 2\hbar^2 |K_o||K| \cos\theta \tag{10}$$

This value of P is placed in equation 8 after it has been squared

$$h^2(v_o - v)^2 + 2hmc^2(v_o - v) = m^2c^4 + c^2P^2 - m^2c^4 \qquad (11)$$

$$h^2(v_o - v)^2 + 2hmc^2(v_o - v) = (c\hbar K)^2 + (c\hbar K_o)^2 - 2c^2\hbar^2 K_o K\cos\theta \qquad (12)$$

The relationship $hv = (h/2\pi)(2\pi/W)c = c\hbar K$, where W is the wavelength, is used to simplify equation 12.

$$(hv_o)^2 + (hv)^2 - 2h^2 v_o v + 2hmc^2(v_o - v) = (hv_o)^2 + (hv)^2 - 2h^2 v_o v\cos\theta \qquad (13)$$

$$(v_o - v)/v_o v = (h/mc^2)(1-\cos\theta) \qquad (14)$$

$$1/v - 1/v_o = (h/mc^2)(1-\cos\theta) \qquad (15)$$

$$W - W_o = \Delta W = 0.0243\,(1-\cos\theta) \qquad (16)$$

Clearly, the wavelength of the Compton scattered photon increases with scattering angle by an amount which varies from zero to 0.0486Å. This difference with MoK radiation is not sufficient to permit the pulse height analyzer to eliminate the Compton scattering from the coherent scattering at any angle.

(b) Intensity

The intensity of Compton or modified scattering, I_{mod}, is given by Compton and Allison (1935 p.254).

$$I_{mod} = I_e R\,(Z - \sum f_{kk}^2 - \sum_{k \neq l}\sum f_{kl} + ZI_m) \qquad (17)$$

I_e is the scattering from one electron by an incident wave of electric intensity E. In the approximation used I_e is independent

of the binding energy of the electron in the atom and corresponds to the scattering from a free electron at rest.

$$I_e = c\sin^2\theta\ \ddot{M}^2/(8\pi r^2 c^4) \tag{18}$$

c - speed of light

θ - Bragg angle

r - distance from the electron to the observation point

$$\ddot{M} = e^2 E_0 \cos(2\pi v_0 t)/m \tag{19}$$

e - electron charge e.s.u.

m - electron mass

E_0 - electric vector of the incident wave

v_0 - frequency of the incident wave

R accounts for the reduced energy in the scattered wave

$$R = (v/v_0)^3 \tag{20}$$

v - frequency of the scattered wave

Z is the number of electrons in the scattering ion.

$$f_{kk} = \iiint \psi_k\ \ \psi_k^* \cos(k_1 a \cos\alpha)d\tau \tag{21}$$

f_{kk} the electronic structure factor in the approximation used is is equal to the atomic scattering factor. Many published values of f_{kk} are available. The term is equal to Z when theta equals zero, and it decreases as theta increases and as W, the wavelength, decreases.

ψ_k is the wave function of an electron in the k state.

ψ_k^* is the complex conjugate of ψ_k

$k_1 = 4\pi\sin\theta/W$, the modulus of the diffraction vector.

$a\cos\alpha$ = the distance from the origin perpendicular to the reflecting plane to the plane containing the scattering volume $d\tau$.

$$f_{kl} = \int\int\int \psi_k \quad \psi_l^* \cos(k_1 a \cos\alpha)\, d\tau \qquad (22)$$

The f_{kl} term, developed by Waller and Hartree (1929), considers that some of the transitions used in f_{kk} are forbidden by the Pauli excusion principle. This is the only term which is difficult to evaluate and from which very few values have been published. Compton and Allison (1935 p.254) state "ordinarily this correction is negligible, but may in an extreme case amount to 10 percent of the incoherent scattering".

$$I = 1 + \alpha^2(1-\cos 2\theta)/\left((1-\cos^2 2\theta)\,(1+\alpha(1-\cos 2\theta))\right) \qquad (23)$$

$$\alpha = hv/(mc^2) \qquad (24)$$

The term I_m was developed by Klein and Nishina (1929) by the application of Dirac's quantum mechanics, which are invariant with the Lorentz transformation. It is noteworthy that the term is significant only at relativistic velocities, and represent rays which are almost completely unpolarized. Compton and Allison (1935 p. 254) state, "this term is negligible for ordinary x-rays wavelengths".

If the last two terms, $\sum_{k \neq 1}\sum f_{kl}$ and ZI_m in equation 17, are neglected, it is readily seen that I_{mod} is zero at 0.0° theta and increases smoothly to 90° theta, because the atomic scattering factor, $\sum f_{kk}^2$, decreases and I_e increases with theta. Lonsdale (1942) has published detailed calculations from equation 17 for sylvine with MoK radiation. She states, "Compton and unmodified background scatterings are comparable at liquid air temperatures, the Compton scattering becoming of increasing importance as the scattering angle increases beyond 90° (two theta)". The Compton scattering is expected to be slightly less intense from nickel than from sylvine but is still expected to contribute significantly to the background scattering in this work.

It is interesting to compute the energy range of the recoil electron when one angstrom x-rays are used.

$$E \leq h\nu_0 - h\nu = hc\,(1/W_0 - 1/W) = hc\,(W - W_0)/(WW_0) \qquad (25)$$

$$W - W_0 \leq 0.0486\text{A} \qquad (26)$$

$$0 \leq E \leq (6.62E\text{-}27)\ (3E\text{-}10\ (0.0486E\text{-}8)/(1.0486) \qquad (27)$$

$$0 \leq E \leq 9.2E\text{-}10 \text{ ergs} = 600 \text{ eV} \qquad (28)$$

At 0K, the energy of the Fermi level is taken as zero. The state of the recoil electron must satisfy both the Pauli principle and Brillouin zone considerations. Therefore the intensity of Compton scattering from a perfect crystal at absolute zero cannot be a smooth function as equation 17 implies. However, beam divergence, crystal imperfections, and polycrystalline samples are expected to smooth the intensity of Compton scattering.

XRAS cannot resolve the Compton scattering from coherent scattering when MoK radiation is used with nickel specimens. If the intensity of Compton scattering varies only slowly, it causes no direct errors in this work except for the effect of increasing the background at high angles. This in turn makes it more difficult to isolate the Bragg scattering.

3. COHERENT SCATTERING

Waves that are scattered with the same phase angle as the incident wave and without change in wavelength are said to be coherently scattered. The validity of the assumptions (e.g. James 1958 chapter 1) usually made in developing a theory of coherent scattering of x-rays is

examined. The fact that the phase angle is always known permits the intensity scattered in any direction to be calculated by adding vectorially the amplitudes of the waves scattered in the desired direction. This procedure is commonly referred to as 'Huygens' construction'. It clearly cannot be applied to primary fluorescent radiation because there is usually no phase relationship between the absorbed and emitted radiation. Huygens' construction has not been applied to Compton scattering, where its validity is not known if, indeed, it is valid at all. In x-ray diffraction it is used sucessfully to describe Laue or Bragg scattering and diffuse scattering.

The remarkable aspect of Huygens' construction is that it usually provides the correct answer in x-ray scattering although the model is certainly a false one. For example, Huygens' construction assumes an infinitely long plane wave incident on a scatterer, and each point in the scatterer becomes the centre of a spherical wavelet. This implies that the incident energy and the scattered energy do not change with time. This is certainly untrue because photon detectors such as scintillation counters measure not the energy but the derivative of the energy with respect to time. In fact, the amplifier in XRAS uses the second derivative of the energy with respect to time to measure energy. Therefore the concept of a steady continuous incident plane wave in which the derivative is zero is unrealistic because the incident energy is quantized.

The life of an optical photon in matter is estimated at less than

E-9 seconds, from the response time of fast scintillators (anthracene). In XRAS Bragg reflection occurs with incident beam intensities of the order of E+5 photons per second, where the average time between photons is E-5 seconds. Because the incident photons are random in time, the possibility of two photons arriving 'at the same time' is one in E+10 photons. This is of the order of once per day.. However, Bragg reflection occurs approximately once in E+5 photons or once per second in this case. Therefore Bragg scattering must be a one photon process. In addition, wavelength measurements of Bragg scattered photons indicate the energy is not measurably (1 part in E+5) changed. Therefore if energy is conserved the photon must be either scattered or not scattered but it cannot be partially scattered as Huygens' construction suggests.*

On the other hand, Huygens' construction assumes that the incident wave passes through the scatterer and each scattering point becomes the centre of a spherical wavelet of scattered radiation. The total intensity of such wavelets computed or measured for MoK x-rays scattered from the 111 reflection of an aluminum single crystal is less than 0.1 percent of the incident intensity. If Huygens' construction is applied to a single incident photon, the wavelength of the Bragg scattered photon should be approximately one thousand times the wavelength of the incident photon, if energy is conserved. This conflicts with the previous paragraph which states that the wavelength of the scattered photon is not detectably changed. Therefore, as a physical model for x-ray diffraction

*the following argument is qualified by the note on Page 83.

Huygens' construction is not consistent with experimental data, even though it provides the correct answer in many cases.

The exact nature of the process of Bragg scattering offers some difficulty. The momentum of the coherently scattered photon is changed because the direction of the wave vector changes as much as 180°, but the modulus of the wave vector is unchanged. How then is it possible to conserve energy in the process? It has been suggested that the photon interacts with a large mass, which suffers a momentum change $M\Delta V$. The energy change $\frac{1}{2}M\Delta V^2$ is a second order infinitesimal compared to the momentum change $M\Delta V$.

These criticisms are not intended to reject Huygens' theory but only the suggestion that it provides a complete and final answer. Indeed, no other theory has been able to explain Laue or Bragg scattering, although Dr. J. Sample of the Physics Department of the University of Alberta has suggested that highly advanced modern theories avoid these difficulities.

The most general theory of diffraction developed to date (Hosemann and Baggchi, 1962) states ' The physical processes underlying all diffraction phenomena are described by Huygens' theory'. The theory of coherent scattering developed here follows that of Hosemann and Baggchi.

4. LAUE OR BRAGG SCATTERING

Equations describing Bragg scattering are developed from two standpoints; the Fourier transform method following Hosemann and

Bagchi (1962) is the more powerful; the consideration of path differences provides a better physical picture of Bragg scattering. The equations may be developed to include the effect of thermal vibration of the lattice points on the Bragg scattering; and this effect is related to the parameter known as the Debye temperature.

(a) The Intensity Function

The theory of coherent scattering developed here is based on Fraunhofer diffraction theory for which the necessary inequalities are well satisfied by XRAS. The inequalities are:

$$rK \gg 1 \qquad\qquad r = |X - Y| \gg Y \tag{29}$$

In XRAS, the specimen to detector distance r is 17 cm., and K, the wave vector for MoK, is 9E+8 cm .

$$rK \approx 1.5\ E+10 \gg 1$$

$$17 \gg 10E-4 \geqq Y$$

X is undefined.

The $|Y|$ is limited by the mosaic size of the crystals.

Intensity of coherent scattering J_c (B) in Fourier space at the point B is given by Hosemann and Baggchi (1962 p. 27). The following development follows their work.

$$J_c\ (B) = f_e^2\, f_\theta^2\, R(B) R^*(B) J_p / r^2 \tag{30}$$

J_e is the time average of the incident intensity. (30a)

r - the distance from the scatterer to the detector.

The factors f_e and f_θ depend on the experimental arrangement. For example, using x-rays with the Bragg-Brentano focussing method and a polycrystalline specimen,

$$f_\theta^2 = (1+\cos^2 2\theta)/(\sin^2\theta \cos\theta) \tag{31}$$

where θ - Bragg angle

$R(B)R^*(B)$ is the only factor in equation 30 which depends on the density distribution of scattering matter, i.e. the structure.

B - vector in reciprocal or Fourier space

X - vector in real space

$\rho(X)$ - the density of scattering matter at the point defined by X. In x-ray diffraction $\rho(X)$ is always the electron density, and

$$R(B) = \int \rho(X) \exp 2\pi i(B{\cdot}X) dv_x \tag{32}$$

where R(B) is the Fourier transform of $\rho(X)$, and $R^*(B)$ is defined as

$$R^*(B) = \int \rho(X) \exp(-2\pi i (B{\cdot}X)) dv_x \tag{33}$$

The factor $R(B)R^*(B)$ is the intensity function I(B). Hosemann and Bagchi's representation has the advantage that the observed intensity of coherent scattering can be quickly factored into useful parts. For example,

it is clear that if the intensity is measured at a point B at two temperatures then the ratio of the intensities depends only on the structure. It is therefore reasonable to suggest that the Debye temperature of a crystal can be determined from such measurements if there is no change in crystal structure.

$$Jc(B)_{T=T_1} / Jc(B)_{T=T_2} = R(B)R^*(B)_{T=T_1} / R(B)R^*(B)_{T=T_2} \qquad (34)$$

Equation 30 applies to gases, liquids, crystals and amorphous structures. The intensity of coherent scattering from a crystal, that is, the evaluation of I(B), is next considered after the establishment of some notation.

(b) <u>The Bravais and Reciprocal Lattices</u>

Let A_1, A_2, A_3 be fixed independent vectors and let n_1, n_2, n_3 take all positive and negative integral values including zero. Then the set of points $n_1A_1 + n_2A_2 + n_3A_3 = An$ maps out a translation lattice which in this work will be taken as the space lattice or Bravais lattics in real space. Because real crystals are finite, the values of n are limited. For a lattice parallelepiped with sides n_1A_1, n_2A_2 and n_3A_3 the value of n_i lies between zero and $N_i - 1$. The general vector in real space will be written as $p_1A_1 + p_2A_2 + p_3A_3 = Ap$ where p takes all real values.

There exists a set of vectors B_1, B_2, B_3 defined with respect to A_1, A_2, A_3, as follows:

$$A_i \cdot B_j = \delta_{ij} \qquad \begin{array}{l} \delta_{ij} = 1 \text{ if } i = j \\ \delta_{ij} = 0 \text{ if } i \neq j \end{array} \qquad (35)$$

The prescription for finding B_1 in terms of A_i is

$$B_1 = A_2 \times A_3 \; / \; (A_1 \cdot (A_2 \times A_3)) \tag{36}$$

The lattice defined by the collection of points

$$l_1 B_1 + l_2 B_2 + l_3 B_3 = lB$$

where l_1, l_2, l_3 take all positive and negative integral values including zero, is called the reciprocal lattice. The general vector in reciprocal space defined by B_1, B_2, B_3 is written

$$h_1 B_1 + h_2 B_2 + h_3 B_3 = hB$$

Where h_1, h_2, h_3 are elements of the set of real numbers.

(c) Evaluation of the Intensity Function for a Crystal

In order to evaluate I(B) for a crystal, it is necessary to evaluate R(B) which is defined by equation 30. The density function $\rho(X)$ for a space lattice can be defined as

$$\int \rho(X) dv_x = 1 \text{ if } X = An \text{ (i.e. if X is a lattice point)} \tag{37}$$
$$= 0 \text{ if } X \neq An$$

The Fourier integral

$$R(B) = \int \rho(X) \exp(2\pi i(B \cdot X)) dv_x \tag{38}$$

can now be replaced by a summation

$$R(B) = \sum_{n_1=0}^{N_1-1} \sum_{n_2=0}^{N_2-1} \sum_{n_3=0}^{N_3-1} (\exp(2\pi i(B\cdot An)) \qquad (39)$$

for a lattice parallelepiped with sides n_1A_1, n_2A_2, n_3A_3. This is a geometric series with the following sum.

$$R(B) = \prod_{i=1}^{3} (1-\exp(2\pi i N_i B\cdot A_i)/(1-\exp(2\pi i B_i\cdot A_i)) \qquad (40)$$

The intensity function for the lattice parallelepiped is now

$$I(B) = R(B)R\,(B) = \prod_{i=1}^{3} (1-\cos 2\pi N_i B\cdot A_i)/(1-\cos 2\pi B\cdot A_i) \qquad (41)$$

$$I(B) = \prod_{i=1}^{3} \sin\pi N_i B\cdot A_i/\sin\pi B\cdot A_i \qquad (42)$$

This intensity function has principal values when each of the factors $B\cdot A_i$ has an integral value; and this condition leads to the Laue equations.

$$A_i\cdot B = 1 \quad (i=1,2,3),\ (1=0,\pm1,\pm2,\pm3\ldots\ldots) \qquad (43)$$

Ewald's construction (James 1958, p.7), which shows that the principal maxima in equation 42 occur when B is a reciprocal lattice point, offers an alternative viewpoint.

(d) Coherent Scattering from a Lattice by a Consideration of Path Differences

Equation 42 may also be developed by considering the path differances between waves scattered from the lattice points. Let S_0 be a unit vector in the direction of the incident beam, S_1 a unit vector in the

direction of the scattered beam, and r the vector from the origin to the observation point.

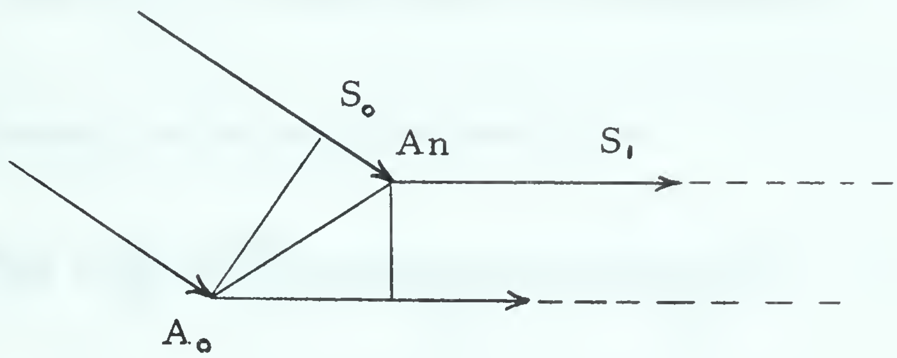

Figure 17. Path Difference on Scattering from Lattice Points

The path difference between wavelets scattered from the origin A_o and An, observed at a large distance r from A_o, is $An \cdot S_1 - S_o$ which is equivalent to a phase difference $(2\pi/W)\, An \cdot S_1 - S_o$. The vector S where

$$S = (S_1 - S_o)\,(2\pi/W) \tag{43a}$$

is called the diffraction vector. The amplitude of the wave scattered from An in the direction S_1 at a distance r is

$$Y = (\Phi/r)\exp(iwt + iAn \cdot S) \tag{44}$$

Φ is the amplitude such that the equation is correct when r = 1. If r is large compared to An, it may be taken as a constant. The total amplitude of the scattered wave in the direction S_1 by the lattice parallelepiped is

$$Y(S) = (\Phi/r)\exp(iwt)\sum_{n_1=0}^{N_1-1}\exp(iS \cdot A_1 n_1)\sum_{n_2=0}^{N_2-1}\exp(iS \cdot A_2 n_2)\sum_{n_3=0}^{N_3-1}\exp(iS \cdot A_3 n_3) \tag{45}$$

This again is a geometric series with the sum

$$Y(S) = (\Phi/r)\prod_{i=1}^{3}(1-\exp(iS\cdot A_i N_i) / (1-\exp(iS\cdot A_i)) \tag{46}$$

The intensity scattered in the direction S_1 is

$$Y(S)Y^{*}(S) = (\Phi/r)^2\prod_{i=1}^{3}(\sin(\underline{S\cdot A_i N_i}) / \sin(\underline{S\cdot A_i}))^2 \tag{47}$$
$$\qquad\qquad\qquad 2 \qquad\qquad\quad 2$$

Except for the constant factor $(\Phi/r)^2$ equation 47 is identical with equation 42 obtained from the Fourier transform of $\rho(X)$ if $S = 2\pi B$. From either of these equations, the Laue equations may be written in the following manner:

$$|S|\,|A_i|\cos\alpha_i = l_i \tag{48}$$

$$(2\sin\theta/W)(A_1\cos\alpha_1) = l_1 \tag{49}$$

$$(2\sin\theta/W)(A_2\cos\alpha_2) = l_2$$

$$(2\sin\theta/W)(A_3\cos\alpha_3) = l_3$$

where α_i are direction cosines, and l_i are integers.

A plane in real space with intercepts A_1/l_1, A_2/l_2, A_3/l_3 is described by Miller indices $(l_1 l_2 l_3)$ if $l_1\, l_2 l_3$ have no common factor. The second term in the above Laue equations is the modulus of the vector normal to the $(l_1 l_2 l_3)$ lattice plane and is equal to the distance d_{hkl} between the planes $(l_1 l_2 l_3)$. This interpretation leads to the Bragg equation

$$n W = 2d_{l_1 l_2 l_3} \sin\theta \tag{50}$$

If the integers $l_1 l_2 l_3$ have a common factor, n, the reflection is considered to be of order n. The order of the reflection does not arise in Laue's or Ewald's interpretation.

A closer examination of the intensity function of the lattice yields a relationship between the width of the principal maximum (Bragg reflection) and the number of lattice points. The principal maximum falls to zero when $A_i^{*} \cdot B$ changes by $\pm 1/N_i$. Thus the width of a reflection increases as the crystal size decreases, because $N_i A_i$ is a measure of the size of the crystal.

(e) <u>The Effect of Thermal Motion on the Intensity Function</u>

The effect of small lattice disturbances, such as thermal motion, can be described in the following manner starting from equation 39 and taking $S = 2\pi B$.

$$I(S) = R(S)R^{*}(S) = \sum_{n=0}^{N-1} \sum_{m=0}^{M-1} \exp(iS \cdot A'n - A'm) \tag{51}$$

where $A'n$ and $A'm$ represent the disturbed position of the lattice points An and Am.

The vectors Un and Um represent the displacement of lattice points n and m from their equilibrium or ideal positions given by An and Am.

Equation 51 can be rewritten as:

$$I(S) = \sum_{m_i=0}^{M_i-1} \sum_{n_i=0}^{N_i-1} \exp(iS\cdot An - Am)\exp(iS\cdot Un - Um) \tag{52}$$

This expression becomes more precise as the period of the radiation becomes small compared to the period of the lattice disturbance. The first term does not vary with time. The second term in equation 52 must be averaged with respect to time. The following definition is convenient:

$$p_{mn} = (S\cdot Un - U.m) \tag{53}$$

The average value of $\exp(ip_{mn})$ written as $\exp(i\overline{p}_{mn})$ is sought. The function $\exp(-\overline{p}^2_{mn}/2)$ is a close approximation to $\exp(i\overline{p}_{mn})$ if p is small.

$$\exp(-\overline{p^2}/2) = 1 - \overline{p^2}/2 + \overline{p^4}/8 \tag{54}$$

Equation 53 can be averaged by substituting the value of the modulus of $S = (4\pi/W)\sin\theta$ and designating the projection of Um on S as Un_s.

$$p^2_{mn}/2 = (4\pi/W)^2 \sin^2\theta\,(Un_s - Um_s)^2/2 \tag{55}$$

Debye assumed the lattice points vibrate independently of each other (i.e. no interaction). This assumption leads to

$$\overline{(Un_s - Um_s)^2} = \overline{Un_s^2} + \overline{Um_s^2} - 2\overline{Un_sUm_s} \tag{56}$$

$$\overline{Un_s^2} = \overline{Um_s^2} = \overline{U_s^2} \qquad \overline{Un_sUm_s} = 0 \tag{57}$$

$$\overline{(Un_s - Um_s)^2} = 2\overline{U_s^2} \tag{58}$$

Equation 55 can now be written as

$$\overline{p^2_{mn}}/2 = (4\pi/W)^2 \sin^2\theta \overline{U_s^2} = 2M \tag{59}$$

This the well known temperature factor suggested by Debye (1913).

The temperature factor can be applied to equation 52

$$I(S) = N + \exp(-2M)\sum_{n'=0}^{N-1}\sum_{m'=0}^{M-1}\exp(iS\cdot An - Am) \tag{60}$$

The first factor arises from the N terms where n = m. In the second factor the primes indicate that the summation is only over pairs of different points (i.e. $n \neq m$).

Taking the summation in equation 60 over all pairs of points leads to

$$I(S) = N(1 - \exp(-2M)) + \exp(-2M)\prod_{i=1}^{3}(\sin(\frac{S\cdot A_i N_i}{2}) / (\sin(\frac{S\cdot A_i}{2})) \tag{61}$$

The first term N(1-exp(-2M)) represents general scattering, which increases from zero when $\theta = 0$, to a maximum when $\theta = 90°$. However, the scattering power of the atom decreases as the angle of scattering increases. Therefore this term represents a broad maximum at moderate angles. If the vibration of each lattice point is not assumed to be independent, this general scattering, or temperature diffuse scattering, will show broad maxima at the reciprocal lattice points.

A comparison of the second term of equation 61 with equation 42 shows that this term represents the Laue scattering given by equation 42 reduced by the factor exp(-2M). Therefore the effect of lattice

vibrations on the Bragg reflections may formally be treated by considering a lattice at rest with reduced scattering power. Hence the definition of the density function of the space lattice $\rho(X)$ given by equation 37 can be modified to include the effect of thermal vibration

$$\int \rho(X)\, dv_x = \exp(-2M) \quad \text{if } X = An \qquad (62)$$
$$= 0 \quad \text{if } X \neq An$$

The peak intensity of the Bragg reflection is proportional to N

$$\lim_{S\cdot A_i N_i \to k\pi} (\sin(S\cdot A_i N_i/2) \,/\, (\sin(S\cdot A_i/2)) = N^2 \qquad (63)$$

where $\quad k = \pm 1, \pm 2, \pm 3, \ldots$

However, the width of the Bragg reflection varies as 1/N, and thus the integrated intensity of a Bragg reflection varies as N. Therefore, the intensity difference between the general scattering and the Bragg reflections is not as great as might be anticipated from equation 63.

Note:

Dr. Bagchi has explained that the criticism of Huygens' construction is not valid. The difficulty in accounting for the energy in the scattered wave arises if the incident beam is assumed to be an infinite, plane, monochromatic, electromagnetic wave. In fact it consists of photons or packets of polychromatic waves. Huygens' construction should be applied to the wave packets rather than to the idealized infinite incident wave.

LATTICE VIBRATIONS

LATTICE VIBRATIONS

Vibrations possess three common characteristics: an equilibrium position (i.e. a postion where vibration is not necessary); a restoring force, which opposes motion of the body away from its equilibrium position; an inertia force which opposes acceleration. The restoring force in crystals controls the elastic properties, and in most crystals is related to the force necessary to move a dislocation. This suggests that a detailed study of lattice vibrations in metals would provide a deeper understanding of the most important properties of metals, their strength and workability.

The simple evaluation of $\overline{(S\cdot Un-Um)^2}$ in the previous section provides the correct answer to the effect of thermal vibration of the lattice points on the intensity of Bragg scattering. However, a more detailed analysis of lattice vibrations is necessary to relate the Debye temperature to the temperature factor. This section briefly outlines the analysis presented by James (1958 chapter V).

(a) Normal Coordinates and the Phase Lattice

Small displacements of the lattice points can be explained by assuming that the lattice is traversed by a set of plane waves.

$$U_n(K) = a_k \cos(w_k t - K\cdot An - \delta_k) \qquad (64)$$

U_n (K) is the displacement of the lattice point n at time t caused by the

plane wave with wave vector K.

$$|K| = 2\pi/W$$

W - is the wavelength

w - is the circular frequency

δ_K - is the phase angle

K·An is a phase difference and (n_1, n_2, n_3) are integers. Therefore the vector components

$$(K\cdot A_1, K\cdot A_2, K\cdot A_3) = (g_1, g_2, g_3) = g_i \tag{65}$$

must also define the phase difference. The set of ordered triples (n_1, n_2, n_3) can be used to define a lattice in a new space called H space. Then the ordered set of triples (g_1, g_2, g_3) defines another space called P, or phase space, which is reciprocal to H space. These spaces are dimensionless.

Physically, g_i is the phase difference for the K wave between two lattice points separated by the vector A_i. Then n·g is the phase difference for the K wave between lattice points separated by the vector A n. Any phase difference is single-valued only in an interval of length 2π. It is convenient to select the interval.

$$-\pi \leq g_i \leq \pi \tag{66}$$

This in turn implies the following inequalities:

$$-\pi \leq K \cdot A_i \leq \pi \tag{67}$$

$$-\pi/A_i \leq K \leq \pi/A \tag{68}$$

$$-1/2A_i \leq 1/W \leq 1/2A_i \tag{69}$$

$$2A_i \leq W \leq \infty \tag{70}$$

Inequality 70 states that wavelengths shorter than the translations $2A_1$, $2A_2$, $2A_3$ are excluded, not because they are impossible, but because they would duplicate waves in the chosen range.

The above discussion assumes an infinite lattice: the case of a finite lattice is introduced most simply by M. Born's cyclic boundary conditions. In referring to these conditions L. Brillouin (1953) states, 'For an ideal isotropic continuum, there is a boundary condition which avoids these complications -- a perfect, smooth, rigid boundary -- but it does not work for crystal lattices.' To apply Born's conditions a rectangular parallelepiped with edges N_1A_1, N_2A_2, N_3A_3 is selected from the infinite space lattice. For sufficently large values of N_1, N_2, N_3 the intensive properties are independent of $N = N_1N_2N_3$, i.e. the effect of surface may be neglected. It is assumed that all motions are periodic in distances N_1A_1, N_2A_2 and N_3A_3 parallel to A_1, A_2 and A_3 respectively. Then the inequalities of equations 66 to 70 are restricted

further to

$$2A_i \leq W \leq 2N_i A_i \tag{71}$$

$$\pi/A_i \geq |K| \geq \pi/N_i A_i \tag{72}$$

$$\pi \geq g_i \geq \pi/N_i \tag{73}$$

Further, the possible phases of the waves must satisfy

$$N_i g_i = 2\pi m_i \tag{74}$$

or

$$g_i = 2\pi m_i/N_i \qquad (m_i = 0 \pm 1 \pm 2 \ldots \pm N_i/2) \tag{75}$$

because of the periodicity assumed.

The ordered set of triples $(m_1, m_2, m_3) = m_i$ defines a lattice called the phase lattice in phase space with translations $2\pi/N_1$, $2\pi/N_2$, $2\pi/N_3$. The vector defined by any ordered triple m_i gives a possible vector g_i in phase space which defines a lattice wave, and the total number of phase lattice points is $N = N_1 N_2 N_3$. There are N waves vectors with 3 polarizations for a total of 3N waves. The density of points in the phase lattice is $N/(2\pi)^3$.

(b) The Calculation of $(\overline{S \cdot Un - Um})^2$ in Terms of Normal Coordinates

The displacement Un of the lattice point An is obtained by summing the displacements due to all the lattice waves.

$$U_n = \sum_{gj} a_{gj}\, e_{gj} \cos(w_{gj} t - n\cdot g - \delta_{gj}) \tag{76}$$

e_{gj} - polarization vector - i. e. a unit vector in one of the three independent direction of of vibration of the lattice (j=1, 2, 3) associated with the waveg.

a_{gj} - amplitude of the gj wave.

δ_{gj} - phase angle

w - circular frequency, radians per second

$|K| = 2\pi/W$ when W is the wavelength of the wave.

Each wave is stopped and started again many times in the interval required for an observation; and on each occasion the wave starts the phase angle, δ_{gj}, is independent of its previous value. Therefore the average value of a sine or cosine term containing δ_{gj}, will be zero.

The displacements Un from equation 76 are used to evaluate equation 55, which may be written

$$\tfrac{1}{2}\overline{P^2_{mn}} = \tfrac{1}{2}\overline{(S\cdot U_n - U_m)^2} \tag{77}$$

Substituting Un from equation 76, we have

$$\tfrac{1}{2}\overline{P^2_{mn}} = \tfrac{1}{2}\sum_{gj} (S\cdot e_{gj})^2 a^2_{gj}\, \overline{(\cos(w_{gj} t - n\cdot g - \delta_{gj}) - \cos(w_{gj} t - m\cdot g - \delta_{gj}))^2} \tag{78}$$

In averaging the left side, any term which contains different values of δ_{gj} will vanish because δ_{gj} is an even function. For terms with the same

value of gj the average value of each cosine squared is $\frac{1}{2}$. The cross products give two terms: the cosine of the sum (which vanishes on averaging because it contains a term $2\delta_{gj}$) and the cosine of the difference (in which the δ_{gj} terms cancel each other). The result is

$$\tfrac{1}{2}\overline{p_{mn}^2} = \tfrac{1}{2}\sum_{gj} \overline{(S\cdot e_{gj})^2 a_{gj}^2} \ (1-\cos(g.n-m)) \tag{79}$$

The first term

$$\tfrac{1}{2}\sum_{gj} \overline{(S\cdot e_{gj})^2 a_{gj}^2} = 8\pi^2(\sin\theta/W)^2 \sum_{gj} \overline{(a_{gj})^2} \tag{80}$$

where $\sum \overline{(a_{gj})^2}$ is the component of the amplitude in the direction S. Twice the mean square displacement $\overline{U_S^2}$ is the mean square amplitude. Therefore this term, $16\pi^2(\sin\theta/W)^2\,\overline{U_S^2} = 2M$, is the Debye temperature factor of equation 59. Hence

$$2M = \tfrac{1}{2}\sum_{gj} (S\cdot e_{gj})^2\,\overline{a_{gj}^2} \tag{80a}$$

The second term of equation 79, which describes the effect of coupling the lattice points, results in broad maxima at the reciprocal lattice points of diffuse scattering. This term is of no further interest in this work.

(c) Relationship between the Mean Square Amplitude of Vibration and Temperature

The kinetic energy E_k of lattice points is

$$E_k = \tfrac{1}{2}\sum_{n} m\dot{U}_n^2 \tag{81}$$

where the summation is taken over all lattice points. From equation 76

$$\dot{U}n = -\sum_{gj} e_{gj}\, w_{gj}\, a_{gj}\, \sin(w_{gj}\, t - ng - \delta_{gj}) \tag{82}$$

The above value of $\dot{U}n$ is substituted into equation 81, which is then averaged. The average value of the square of the sine is $\frac{1}{2}$, since terms with different values of gj contain δ_{gj} terms and vanish.

$$\overline{\dot{U}_n^2} = \frac{1}{2}\sum_{gj} w_{gj}^2\, \overline{a_{gj}^2} \tag{83}$$

$$E_k = \frac{1}{4}\sum_{n} m \sum_{gj} w_{gj}^2\, \overline{a_{gj}^2} \tag{84}$$

The total energy $\overline{E}$ is half the kinetic energy

$$\overline{E} = \frac{1}{2} mN \sum_{gj} w_{gj}^2\, \overline{a_{gj}^2} \tag{85}$$

E_{gj} is defined as the energy associated with the wave defined by gj

$$\overline{E} = \sum_{gj} E_{gj} \tag{86}$$

From quantum theory the energy associated with a harmonic oscillator is

$$E_{gj} = (\overline{n}_{gj} + \tfrac{1}{2})\hbar w_{gj} \tag{87}$$

where $\hbar$ is Planck's constant.

$$\overline{n}_{gj} = 1/(\exp(\hbar w_{gj}/kT) - 1) \tag{88}$$

comparing equations 85, 86 and 87 leads to

$$\tfrac{1}{2}m\, w_{gj}^2\, \overline{a_{gj}^2} = (\overline{n}_{gj} + \tfrac{1}{2})\hbar w_{gj} \tag{89}$$

$$\overline{a_{gj}^2} = (2\hbar/mN)\,(\overline{n}_{gj} + \tfrac{1}{2})/w_{gj} \tag{90}$$

This value of $\overline{a_{gj}^2}$ can now be substituted into equation 80a to give

$$2M = \sum_{gj} (S\cdot e_{gj})^2 (\hbar/mN)\,(\overline{n}_{gj} + \tfrac{1}{2})/w_{gj} \tag{91}$$

If we define G_{gj} as

$$G_{gj} = (\hbar/mN)\,(S\cdot e_{gj})^2 (\overline{n}_{gj} + \tfrac{1}{2})/w_{gj} \tag{92}$$

Then $$2M = \sum_{gj} G_{gj} \tag{93}$$

At this point it is evident that an accurate summation over gj requires the frequency distribution function, which, with rare exceptions, is unavailable. However, Debye assumed a frequency distribution, and this offers useful results.

(d) The Numerical Evaluation of the Temperature Factor -2M for a Cubic Crystal by Debye's Method

Debye (1913) developed a method of evaluating an approximation of $\sum_{gj} G_{gj}$. In Einstein's (1905) theory of specific heats, where w_{gj} was a constant, the summation is simple. Debye's method, which is a better approximation, assumes the lattice is an isotropic elastic continuum, in which all waves with a specified polarization travel with the same phase velocity independently of wavelength and direction.

This leads to a frequency distribution function f(v) dv proportional to v^2, which permits $\sum_{gj} G_{gj}$ to be approximated with an integral.

The number of waves with polarization j in an isotropic solid having a $|g|$ less than a given maximum g_m is given by the number of phase lattice points in a sphere of radius g_m. Further, this number is equal to N if g_m is the maximum value permitted by the lattice. Recalling that the density of phase lattice points is $N/(2\pi)^3$

$$(4\pi/3)g_m^3 N/(2\pi)^3 = N \tag{94}$$

Using the relationship $|g| = Aw_j / V_j$, where A is the modulus of the translation vector for a cubic lattice and w_j is the circular frequency for waves of polarization j, and V is the phase velocity for waves with polarization j (V_j is a constant), enables equation 94 to be written

$$w_{m_j}^3 = (3/4\pi)(2\pi)^3 (V_j / A)^3 \tag{95}$$

Debye assumed a mean frequency w_m given by

$$w_m^3 (1/V_l^3 + 2/V_t^3) = (9/4\pi)(2\pi/A)^3 \tag{96}$$

where V_l and V_t are the phase velocities of longitudinal and transverse waves.

The summation in equation 91 can be replaced by an integration over the phase lattice. The frequency distribution function f(g) dg for the phase lattice is the number of phase lattice points lying in a thin

spherical shell between $|g|$ and $|g| + |dg|$.

$$f(g)\,dg = 4\pi|g|^2|dg|\,N/(2\pi)^3 \tag{97}$$

This is used as the elemental volume of integration. It is convenient to change the variable in equation 97 to w_j, using $|g| = w_j A/V_j$, and hence

$$f(w_j)\,dw_j + 4\pi(A/V_j)^3 w_j^2\,dw_j\,N/(2\pi)^3 \tag{98}$$

Then, substituting into equation 91 and integrating from zero to w_m, we have

$$2M = (\hbar/mN)\sum_j \int_0^{w_m} (S\cdot e_{gj})^2(\overline{n}_{gj} + \tfrac{1}{2})(4\pi(N/(2\pi)^3)(A/V_j)^3)w\,dw \tag{99}$$

Now $(S\cdot e_{gj})^2$ is S^2 times the square of the projection of the unit vector, e, on S. For a given polarization j, e takes all values with equal probability and therefore

$$\sum_{gj}(S\cdot e_{gj}) = S^2/3 \tag{100}$$

Equation 99 simplifies to

$$2M = (\hbar S^2/m)\sum_j (1/((3/4\pi)(2\pi)^3(V_j/A)^3)\int_0^{w_{mj}} (\overline{n}_{gj} + \tfrac{1}{2})w\,dw \tag{101}$$

If the value of w_m from equations 95 and 96 is placed in equation 101 we have

$$2M = (3\hbar S^2/mw_m^3)\int_0^{w_m} (\overline{n}_{gj} + \tfrac{1}{2})w\,dw \tag{102}$$

Recalling equation 88, equation 102 can be written

$$2M = (3\hbar S^2 / m w_m^3) \int_0^{w_m} (1/(\exp(\hbar w/kT) - 1) + \tfrac{1}{2}) w\,dw \tag{103}$$

The following two definitions are convenient

$$z = \hbar w/kT \tag{104}$$

$$x = \hbar w_m/kT \tag{105}$$

Equation 103 can be written

$$2M = (3\hbar S^3 / m w_m) (kT/\hbar w_m)^2 \int_0^{x} (1/(\exp z - 1) + \tfrac{1}{2}) z\,dz \tag{106}$$

$$2M = (3\hbar S^2 / m w_m) (1/x^2) \left(\int_0^{x} (1/(\exp z - 1) z\,dz) + x^2/4 \right) \tag{107}$$

Defining D(x) as

$$D(x) = (1/x^2) \left(\int_0^{x} 1/(\exp z - 1) z\,dz + x^2/4 \right) \tag{108}$$

Equations 107 becomes

$$2M = (3\hbar S^2 / m w_m) D(x) \tag{109}$$

The Debye temperature, θ_D , is defined as

$$\theta_D = \hbar w_m/k \tag{110}$$

Introducing θ_D into equation 109

$$2M = (3\hbar^2 S^2 / m k \theta_D) D(x) \tag{111}$$

if $\hbar$ is replaced by $h/2\pi$ and S by $4\pi \sin\theta/W$

$$2M = (12h^2/mk\theta_D)D(x)\sin^2\theta/W^2 \qquad (112)$$

From values of 2M experimentally determined at known temperatures, θ_D can be computed by an iterative numerical method. The equation cannot be solved analytically. There are two methods for measuring 2M: the slope method and the ratio method. These methods are now discussed in detail.

(e) <u>The Slope Method</u>

The slope method utilizes the variation of 2M with scattering angle theta. Recalling equation 62, the scattering power of a lattice point is equal to exp(-2M). This is a function of $\sin\theta/W$ (i.e. the scattering angle). Measured values of the scattering power, I_m, of a lattice point can be determined for several values of θ. For each value of $I_m(\theta)$ the following equation holds

$$I_m(\theta) = \exp(-2M) \qquad (113)$$

or

$$\ln(I_m(\theta)) = -2M \qquad (114)$$

Combining equations 112 and 114

$$\ln(I_m(\theta)) = -(12h^2/mk\theta_D)D(x)\sin^2\theta/W^2 \qquad (115)$$

This equation has the form y = bx

where $\qquad b = (-12h^2/mk\theta_0)D(x) \qquad (116)$

Therefore, from the slope b of a graph of $\ln(I_m)$ vs. $\sin^2\theta/W^2$, the Debye temperature can be calculated. The above analysis assumes the scattering power of a stationary lattice point is unity; and for simple structures (such as nickel) the lattice point is taken as the equilibrium position of an atom. Precise theoretical values of the scattering power (i.e. the atomic scattering factor f) which are generally accepted as accurate, have been published (Freeman, Watson 1961), and may be used instead of the value of unity.

In the case of simple structures such as nickel, the relative scattering factor is obtained by dividing the integrated intensity of a Bragg reflection by f_θ^2 (see equations 30 and 31) and the multiplicity factor P. The factor f_θ^2 accounts for the variation in intensity with angle due to geometrical factors. The powder method assumes that the crystallites are randomly oriented; but because there are six permutations of h00 and 48 of hkl, and hkl reflection is 48/6 times as probable as an h00 reflection. The multiplicity factors for the h00 and hkl are hence equal to 6 and 48 respectively.

(f) The Ratio Method

The ratio method exploits the temperature dependence of 2M. The scattering factor f is determined at two temperatures T1 and T2 at the same scattering angle (neglecting, for the moment, thermal

expansion). Equation 113 can be written

$$I_m(T1) = \exp(-2M(T1)) \tag{117}$$

$$I_m(T2) = \exp(-2M(T2)) \tag{118}$$

taking logarithms and subtracting 118 from 117.

$$r = \ln(I_m(T1)/I_m(T2)) = 2M(T2) - 2M(T1) \tag{119}$$

Substituting values of 2M from equation 112 we have

$$r = (12h^2/mk\theta_D)\,(D(\theta_D/T2) - D(\theta_D/T1))\,\sin^2\theta/W^2 \tag{120}$$

This is an implicit equation in θ_D which can only be solved numerically.

In the ratio method, the ratio of the integrated intensity of a Bragg reflection measured at two known temperatures can be used in equation 120, because all other factors are multiplicative and cancel.

The slight variation in intensity and scattering factor with the change in scattering angle caused by thermal expansion causes a small error. However, this can be eliminated by dividing the observed intensity by f_θ^2 (the Lorentz-polarization factor) and the theoretical scattering factor squared, f^2 . The angular shift experienced in the work described in this thesis due to thermal expansion is less than 0.15° theta. The uncertainty in the values of f_θ and f^2 will introduce no significant error over this small range.

(g) Summary

The section on coherent scattering develops an equation for the intensity of Bragg scattering which includes the effect of thermal motion of the lattice points. The section on 'Lattice Vibrations' relates the effect of thermal motion on the Bragg scattering to the Debye temperature, which is related to the elastic properties of the lattice. Finally, two methods -- the slope and the ratio method -- for experimentally determining the Debye temperature are discussed.

THE DETERMINATION OF THE DEBYE TEMPERATURE

THE DETERMINATION OF THE DEBYE TEMPERATURE

The slope and ratio methods for determining the Debye temperature depend on measurements of the relative scattering power of a lattice point (i.e. the atomic scattering factor) from measured values of the integrated intensity of Bragg scattering. It is now necessary to consider in detail the measurement of Bragg scattering.

1. THE INTEGRATED INTENSITY OF BRAGG REFLECTIONS

The Laue scattering in XRAS is called a Bragg reflection or Bragg scattering because the experimental arrangement is due to Bragg; indeed, methods of structural analysis by x-ray diffraction can be said to rest upon the Bragg reflection. This is true of the experimental determination of the scattering factor, temperature factor, and crystal structure; and virtually all the more sophisticated x-ray techniques, such as small angle scattering and diffuse scattering, utilize data obtained from the integrated intensity of Bragg reflections. Therefore, the problem of measuring the integrated intensity of Bragg reflections deserves serious consideration.

Basically there are two aspects to the precision measurement of Bragg intensities; very precise intensity measurements, and a precise method of separating Bragg scattering from the other kinds of scattering, which henceforth are called the 'background'. The first problem has been discussed in detail on pages 7 to 13. The second

problem is discussed below.

An examination of figures 6 and 18 emphasizes the difficulties in separating Bragg scattering from the background. These graphs were obtained by processing data cards from XRAS with an IBM 1620 computer and plotting the output with an IBM 807 plotter. Figures 6 and 18 show the $10\bar{1}1$ reflection from a quartz single crystal and 731-553 reflection from a nickel powder specimen respectively. In both cases a molybdenum x-ray tube was operated at 40 kv and 15 ma. A one degree slit system and a zirconium filter were used. The only human judgement or evaluation involved in these graphs was the decision where to start and stop the scan, and the plotting scale to be used. Each point, which is the average of 50 readings from XRAS is plotted with a precision of ±0.02 inches, according to IBM specifications. The structure of the Bragg reflection in figure 6 is lost in averaging the 50 readings. Actually, the $K_{\alpha 1}$-$K_{\alpha 2}$ peaks are well resolved. The program used for this plot is shown on page 101. The output from this program controls the typewriter on the 807 which makes the graph.

The quartz $10\bar{1}1$ reflection (figure 6) illustrates the non-linear nature of the background obtained with an absorption filter. Yet the methods generally used for separating the background from a reflection assume a linear background. This aspect of the problem is less serious at high scattering angles where the background is more uniform.

The background associated with the quartz $10\bar{1}1$ reflection, shown

```
..IDENT J.GOLDAK  4AUTOPLOT X-RAY DATA
..I   1 READING /STEP-0.1 DEGREES 2THETA/READING
..LOAD FORTRAN EXECUTE DUMP
      REWIND 1
      DIMENSION RHM( 20),THETA( 20),IRHM( 20),IETA( 20)
  4   FORMAT (1X5(F6.0,F6.2,2X))
 49   FORMAT(1XI4,1XI4,3F10.5)
100   FORMAT(7I5)
110   FORMAT(50H
  1   READ 49,K,K1,TAX,THET,TH
      ITHET=THET*10.0
      IWIDE=1100
      ISCAL=99
      I2=-45
      I3=-20
      JTHET=0
      IK11=JTHET
      IK1=JTHET+100
      IK2 =JTHET+200
      IK3 =JTHET-20
      IK4 =JTHET+400
      IK5=-70
      IK6=JTHET+600
      IUP=450
      IOVER=240
      WRITE OUTPUT TAPE 1,100,1,IWIDE,1500,IOVER,IUP,JTHET,0
      WRITE OUTPUT TAPE 1,100,2,1,0
      DO 103 J=1,K
      RN=0.0
      READ 4,(RHM(I),THETA(I),I=1,5)
      IF(RHM(1))104,104,6
  6   CONTINUE
      DO 50 I=1,5
      IRHM(I)=RHM(I)*TAX
      RN=RN+RHM(I)*TAX
      RN=RN*0.2
      IRN=RN
      ITA=(5*(J-1)+I)
      IRN=IRHM(I)
      WRITE OUTPUT TAPE 1,100,3,ITA,IRN
 50   CONTINUE
103   CONTINUE
104   CONTINUE
      WRITE OUTPUT TAPE 1,100,2,1,0
      IY=0
      IX=0
      DO 60 L1=1,50
      WRITE OUTPUT TAPE 1,100,3,IX,IY
      IX=IX+100
 60   CONTINUE
      IX=0
      DO 70 L1=1,8
      WRITE OUTPUT TAPE 1,100,3,IX,IY
      IY=IY+100
 70   CONTINUF
      WRITE OUTPUT TAPE 1,100,4,IK11,I2,0
```

```
READ 110
WRITE OUTPUT TAPE 1,110
WRITE OUTPUT TAPE 1,100,4,IK5,850,10
READ 110
WRITE OUTPUT TAPE 1,110
WRITE OUTPUT TAPE 1,100,4,IK1,850,0
READ 110
WRITE OUTPUT TAPE 1,110
WRITE OUTPUT TAPE 1,100,4,IK1,825,0
READ 110
WRITE OUTPUT TAPE 1,110
WRITE OUTPUT TAPE 1,100,4,IK1,800,0
READ 110
WRITE OUTPUT TAPE 1,110
WRITE OUTPUT TAPE 1,100,4,IK1,775,0
READ 110
WRITE OUTPUT TAPE 1,110
WRITE OUTPUT TAPE 1,100,5,JTHET,I3,ISCAL,ITHET,10,0
WRITE OUTPUT TAPE 1,100,5,IK3, 0,9,0,100,10
WRITE OUTPUT TAPE 1,100,6
CALL EXIT
END
```

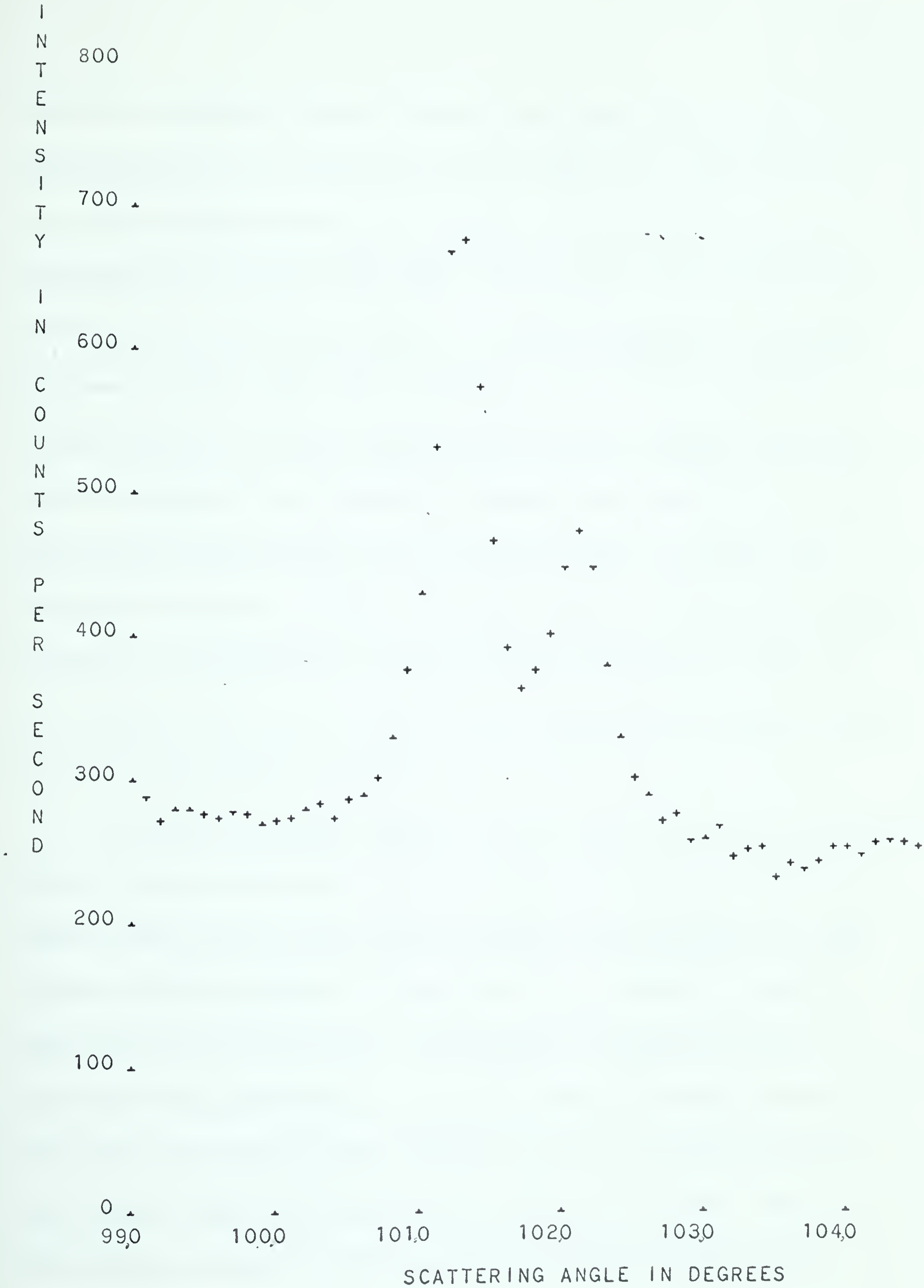

Figure 18. The 731-553 Reflection from Nickel

in figure 6, appears to be better defined then the background associated with the nickel 731-553 reflection shown in figure 18. As the ratio of the peak to background intensity increases and the reflection narrows, the relative error in the Bragg reflection caused by error in estimating the background intensity decreases. In simpler language, it is easier to measure a large effect than a small one. The obvious implication is that intensities should be measured from single crystals, which provide the strongest Bragg scattering. However the problems of growing, orienting and cutting single crystals are appreciable. Further, the intensity from single crystals can be quite sensitive to alignment because the width of reflections from perfect crystals is only of the order of a few seconds of arc. Nevertheless, single crystals will be used in XRAS as soon as they become available.

A simpler technique suggested by the author and recently developed by Mr. Timbres of this department utilizes a preferred recrystallization texture (cube texture) in face-centred cubic metals to simulate a single crystal. With this method the Bragg scattering can be increased by a factor of ten for h00 reflections, which allows a considerable improvement in the precision of isolating the Bragg scattering. However, the problem of measuring weak reflections cannot be avoided in every case, and all reflections must be used in structure analysis. The measurement of atomic scattering factors and Debye temperatures requires high angle reflections where the background is highest and

the scattering factor smallest; and hence the intensity of Bragg reflections is usually weak.

In this work, where only the customary types of powder and polycrystalline specimens are used, the estimation of background intensity is the most difficult step. To the author's knowledge, no unique method of estimating the background has been published. Many papers include statements such as "It is possible that the tails of broadened reflections from deformed samples were not included completely in the peak area measurements, despite efforts made here to avoid this source of error". (Herbstein, Smuts, 1963). This is simply an admission of the possibility of erroneously estimating the background intensity.

Several schemes for improving the background estimate were considered. Sections on either side of the reflection could be taken as 'background' and a least square analysis performed to obtain a linear value. However, the initial choice of the background sections is as arbitrary as choosing a background directly, and the method has little advantage. The possibility of describing the reflection profile with a polynomial or Fourier series was considered: perhaps "background" could be defined in terms of a certain slope. However such a large number of terms would be required that an improved position in unlikely. Another possibility is to assume a line shape -- say a Gaussian or Poisson distribution -- and subtract this from the observed intensity. But all the above methods are artificial, and hence they are arbitrary in nature.

This point of view is emphasized by Ilyina (1962). He investigated x-ray reflections from deformed metals, and stated;

> "Our investigations thus lead us to the conclusion that deformation does not cause a loss of integral intensity if account is taken of the tails which are characteristic for deformed metals. However, the problem of the cause of these tails still remains unanswered. Are they to do with the principal maximum or do they represent diffusion scattering, the intensity of which varies non-monotonically with the angle and has peaks in the sites of reciprocal lattice? If the tails belong to the selective maxima then they can be attributed to second order distortions, i.e. to the presence of non-homogeneous elastic deformation of considerable magnitude in microsectors. The total volume of these sectors should not be very high.
>
> If the tails belong to the diffusion background due to atom displacement (third order distortions), then the existence of the background peaks must indicate some law in the distribution of displacements, similar to that which obtains in the propagation of

elastic waves in the case of thermal movement.

Theoretical and experimental investigations are necessary to clarify this problem".

A method devised by Keating (1959) to calculate the intensity due to one component of the $K_{\alpha 1}$ or $K_{\alpha 2}$ from the observed intensity would in effect reduce the width of the Bragg reflection by $\frac{1}{2}$ and hence reduce the error in the integrated intensity due to the error in estimating the background. The method requires a knowledge of the ratio of the intensity of the $K_{\alpha 1}$ to the $K_{\alpha 2}$ component, and some error in this ratio must be anticipated. This method was not used here because of the amount of programming it requires; and it would not solve the problem, although it might reduce it.

In this work, the background is taken as the minimum intensity on either side of a reflection. The average of the two values is used -- which is equivalent to assuming the background varies linearly. However, the angular interval over which the intensity is averaged must still be selected. XRAS measures the intensity with increments of 0.005° theta, but the computer can sum readings to provide any larger increment desired. As the increment is increased, the statistical error in each increment decreases; but obviously, the increment cannot be increased indefinitely. An increment of 0.25° theta (i.e. the sum of 50 readings) was found to possess a reasonable probable error (≈ 1 percent) without excessively distorting the observed intensity. The

method is not considered to be very satisfactory, but no better alternative is known.

2. NUMERICAL ANALYSIS

(a) Analysis of Data from XRAS

The data from each experiment or scan are contained in a set of IBM cards (figure 14) with the specimen temperature, specimen description, operating conditions and starting angle. The latter data are written on the back of the first data card of each set. It is desirable to reduce the measured intensity to the corrected intensity by dividing by f_θ^2 and f^2 , the Lorentz-polarization factor and the theoretical atomic scattering factor squared respectively. Then the integrated intensity of a Bragg reflection obtained from the corrected intensity can be used directly for the ratio method and need only be divided by the multiplicity factor -- an integer between 6 and 72 -- for the slope method.

This correction is performed by IBM 1620 computer with the Fortran program shown on page 109. This program sums a specified number of readings (usually 50 in this thesis) to give the total intensity (total number of counts) over a specified angular increment (usually 0.25° theta). Then the relative standard deviation, q, in the intensity is calculated from

$$q = N^{-\frac{1}{2}} \qquad (121)$$

```
..I J. GOLDAK X-DATA L.P.AND F**2 CORRECTION      922102 SAVE CARDS
..I 1 CARD IS NO OF DATA CARDS AND ANGLE THETA
..I FOLLOWED BY DATA CARDS. END WITH BLANK CARD
..LOAD FORTRAN EXECUTE DUMP
  10  FORMAT(1XI4,F20.8)
      DIMENSION FNI(31)
      FNI( 1)=28.00
      FNI( 2)=27.55
      FNI( 3)=26.34
      FNI( 4)=24.63
      FNI( 5)=22.70
      FNI( 6)=20.74
      FNI( 7)=18.86
      FNI( 8)=17.11
      FNI( 9)=15.51
      FNI(10)=14.08
      FNI(11)=12.82
      FNI(12)=11.80
      FNI(13)=10.78
      FNI(14)=10.04
      FNI(15)=9.29
      FNI(16)=8.76
      FNI(17)=8.23
      FNI(18)=7.85
      FNI(19)=7.47
      FNI(20)=7.18
      FNI(21)=6.91
      FNI(22)=6.685
      FNI(23)=6.46
      FNI(24)=6.27
      FNI(25)=6.08
      FNI(26)=5.905
      FNI(27)=5.73
      FNI(28)=5.565
      FNI(29)=5.40
      FNI(30)=5.24
      FNI(31)=5.08
      READ 10,N,A
      DIMENSION RHM(10),THETA(10)
 4    FORMAT(1X5(F6.0,F6.2,2X))
 5    FORMAT(1XF9.3,4F10.3,F16.2)
      PUNCH 30
      PUNCH 31
30    FORMAT(55H0  THETA INTEGRATED INTENSITY RATE OF    PROBABLE
31    FORMAT(55H           INTENSITY             CHANGE      ERROR
      A=A*3.1415926535/180.
      A=A*0.5
      RHU2=0.0
      RHU4=0.0
12    CONTINUE
      DO 40 L=1,10
      RHU1=RHU2
      RHU3=RHU4
      DO 20 J=1,2
      READ 4,(RHM(I),THETA(I),I=1,5)
      IF(RHM(1))8,8,7
```

```
 7    CONTINUE
      DO 21 I=1,5
21    RHU4=RHU4+RHM(I)
20    CONTINUE
      SSD=1./SQRTF(RHU4)
      A=A+3.14159265/3600.
      WL=0.7107
      S=SINF(A)
      C=COSF(A)
      POL=S*S*C/(2.+4.*C*C*(C*C-1.))
      SWL=S/WL
      G=20.*SWL+1.
      I=G
      G1=I
      F=FNI(I)+(FNI(I)-FNI(I+1))*(G1-G)
      FF=F*F
      RHU4=RHU4*POL/FF
      RHU5=(RHU4-RHU3)/RHU4
      RAT  =RHU5/SSD
      A1=A*180.0/3.14159265
      RHU2=RHU2+RHU4
      PUNCH 5,A1 ,RHU2,RHU4,RHU5,SSD,RAT
40    CONTINUE
      PUNCH 41
41    FORMAT(1H0)
      GO TO 12
 8    CALL EXIT
      END
```

```
I  100 2803  99.00 300
BRANCH 0040R
```

THETA	INTEGRATED INTENSITY	INTENSITY	RATE OF CHANGE	PROBABLE ERROR	
49.749	33.555	33.555	1.000	.015	62.94
49.999	65.974	32.418	-.035	.016	-2.16
50.249	99.231	33.256	.025	.016	1.57
50.499	139.333	40.101	.170	.014	11.66
50.749	203.513	64.180	.375	.011	32.37
50.999	251.592	48.079	-.334	.013	-24.96
51.249	297.973	46.381	-.036	.013	-2.67
51.499	331.530	33.556	-.382	.016	-23.72
51.749	362.945	31.415	-.068	.016	-4.08
51.999	393.730	30.784	-.020	.016	-1.21
52.249	424.404	30.674	-.003	.016	-.21
52.499	453.552	29.148	-.052	.017	-3.01
52.749	483.109	29.557	.013	.017	.80
52.999	512.516	29.406	-.005	.017	-.29

where N is the total number of counts. The probable error is $2q/3$. The intensity is divided by the Lorentz-polarization factor and the value of the theoretical atomic scattering factor squared f^2 which is interpolated from the values of Freeman and Watson (1961). For each angular increment the computer punches one line of output containing the scattering angle, the integrated intensity, the intensity of the increment, the difference, d, between the intensity of the increment and the previous increment, the relative standard deviation, q, and the ratio d/q. The sum of the intensities from the beginning of the scan to the current increment is the integrated intensity. The ratio d/q is a measure of the significance of the change in intensity. It is unlikely that d/q will exceed 4 as a result of statistical fluctuations. The output from experiment number 100 is shown on page 110. For convenience a two line space separates each ten lines of output data. The corrected intensity from all experiments used in this thesis is listed in appendix II.

(b) Calculation of the Background Intensity

The background and integrated intensities of a Bragg reflection are calculated from the corrected intensities from experiment 100 on page 110 in the following manner. The underlined values in the third column are taken as the background values on either side of the 731-553 Bragg reflection. The total background intensity is

$$(32.418+29.406)13/2 = 401.856 \qquad (122)$$

The reflection is 13 increments (3.25° theta) wide. The total intensity of the reflection is found by subtracting the underlined values of the integrated intensity (the second column).

$$512.516 - 33.555 = 478.961 \tag{123}$$

The integrated Bragg intensity is the difference between the total intensity (equation 123) and the background intensity. (equation 122).

$$478.961 - 401.856 = 77.105 \tag{124}$$

This value is directly proportional to the atomic scattering factor squared, f^2, times the multiplicity factor, P. In the ratio method the presence or absence of P is immaterial. However, the integrated Bragg intensity must be divided by P for the slope method.

(c) Numerical Solution for Ratio Method

The ratio method requires the solution of equation 120 for θ_D. Henceforth θ_D will be written as D to follow the notation used in the Fortran programs. Equation 120 written in full is

$$\ln(I(T1)/I(T2)) = (12h^2/mkD^3W^2)(T2^2\sin^2\theta 2(\int_0^{x_2} z/(\exp z-1)dz + x2^2/4) - T1^2\sin^2\theta 1(\int_0^{x_1} z/(\exp z-1)dz + x1^2/4)) \tag{125}$$

The Fortran program shown on page 115 solves the equation by an iterative method. The following notation is used in the program:

R1 - observed value of ln (I(T1)/I(T2)) (126)

R2 - computed value of ln (I(T1)/I(T2)) (127)

D - first estimate of the Debye temperature

D1 - second estimate of the Debye temperature

Equation 125 is written as $R2 = Z/D^3$ (128)

where

$$Z = (12h^2/mkW^2)(T2^2 \sin^2 \theta 2(\int_0^{x_2} z/(\exp z-1)dz + x2^2/4) - T1^2 \sin^2 \theta 1(\int_0^{x_1} z/(\exp z-1)dz + x1^2/4)) \qquad (129)$$

The goal is to find D such that y = 0 in the equation

$$y = R1 - R2 \qquad (130)$$

or $$y = R1 - Z/D^3 \qquad (131)$$

$$y' = dy/dD \qquad (132)$$

$$y' = 3Z/D^4 \qquad (133)$$

Applying Newton's method

$$D1 = D - y(D)/y'(D) \qquad (134)$$

or $$D1 = D - (R1 - Z/D^3)D^4/(3Z) \qquad (135)$$

This simplifies to

$$D1 = D(4 - R1D^3/Z)/3 \tag{136}$$

Substituting R2 from equation 128 yields (137)

$$D1 = D(4 - R1/R2)/3 \tag{138}$$

By this equation the original guess of the Debye temperature is improved. The method can be repeated to obtain any desired degree of accuracy. When the difference between two estimates is less than 0.01 percent, the equation is considered solved.

Newton's method would apply exactly if the value of the integrals was constant. However, it is usually possible to compute the Debye temperature with five digit precision in six iterations, which requires approximately 4 minutes of computer time. The initial estimate of the Debye temperature usually can be made with considerable precision from published results or Lindemann's (1910) melting point formula. However, the minute of computer time that might be saved does not justify the effort.

An example of the output from this program is shown on page 116. The initial estimate is 450 K and the final solution 424.90 K. The second estimate 428.80 K is very good, but thereafter the convergence is slower.

```
..I   J.GOLDAK DEBYE TEMP FROM X-RAY DATA 922103 SAVE CARDS
..LOAD FORTRAN EXECUTE DUMP
 100   FORMAT(F15.7,F13.9,F9.5,F13.6)
 101   FORMAT(3F13.4)
  1    READ 100,RHU1,RHU2,T1,T2
       PUNCH 99
       PUNCH 98
 99    FORMAT(1H1)
 98    FORMAT(1H5)
       PUNCH 100,RHU1,RHU2,T1,T2
       READ 101,ANG1,ANG2,D
       PUNCH 101,ANG1,ANG2,D
       READ  102,WL,A
       PUNCH 102,WL,A
 102   FORMAT(F12.8,E14.8)
       PUNCH 80
  80   FORMAT(1H5,10HDEBYE TEMP,11X14HINTENSITY RATO,7X14H(OBS-COMP)/OBS1
       PUNCH 81
  81   FORMAT(3X42HOLD    NEW     OBSERVED     COMPUTED          ,///)
       WL=1.0E+16/(WL*WL)
  2    R1=LOGF(RHU1/RHU2)
       R=0.17453292E-01
       ANG1=R*ANG1*0.5
       ANG2=R*ANG2*0.5
   3    S1=SINF(ANG1)
       S1=S1*S1*WL
  4    S2=SINF(ANG2)
       S2=S2*S2*WL
       AS1=A*S1
       AS2=A*S2
       T1T1=T1*T1
       T2T2=T2*T2
       A1=AS1*T1T1
       A2=AS2*T2T2
  5    Z=D/T1
       DD1=Z*Z*0.25
       U1=0.0
       DZ1=Z*0.01
  7    DO 20 I=1,100
       Z1=Z*(1.0+Z*0.5*(1.0+Z*0.33333333*(1.0+Z*0.25*(1.0+Z*0.2))))
       U1=U1   +Z*DZ1/Z1
       Z=Z-DZ1
  20   CONTINUE
        Z=D/T2
       DD2=Z*Z*0.25
       DZ2=Z*0.01
       U2=0.0
       DO 30  I=1,100
       Z2=Z*(1.0+Z*0.5*(1.0+Z*0.33333333*(1.0+Z*0.25*(1.0+Z*0.2))))
       U2=U2+Z*DZ2/Z2
       Z=Z-DZ2
  30   CONTINUE
       W=-A1*(U1+DD1)+A2*(U2+DD2)
       R2=W/(D*D*D)
  6    FORMAT(10XE14.8)
       ER1=EXPF(R1)
```

```
      ER2=EXPF(R2)
      V=(ER1-ER2)/ER1
      V      =ABSF(V)
      D1=D*0.33333333*(4.0-R1/R2)
      PUNCH 40,D,D1,ER1,ER2,V
   40 FORMAT(1H0,2F7.2,2F13.8,F13.9)
      IF(V-0.0001)1,1,42
   42 D=D1
      GO TO 5
      END
```

```
  126.1430000  78.16200000 77.00000   300.000000
   101.8000     101.5100     450.0000
 .71069000 .39161140E-13
```

DEBYE TEMP OLD	DEBYE TEMP NEW	INTENSITY RATO OBSERVED	INTENSITY RATO COMPUTED	(OBS-COMP)/OBS
450.00	428.80	1.61386590	1.52101480	.05753334
428.80	425.77	1.61386590	1.59791340	.00988465
425.77	425.10	1.61386590	1.61024190	.00224553
425.10	424.95	1.61386590	1.61301820	.00052526
424.95	424.91	1.61386590	1.61366600	.00012386
424.91	424.90	1.61386590	1.61381900	.00002906

(d) Numerical Solution for Slope Method

The slope method requires the solution of equation 116 for θ_D. In applying the slope method, it is necessary to determine the integrated intensity of each Bragg reflection in a scan (usually 25° to 55° theta in this work) and the scattering angle associated with each reflection. In this work the weighted mean of the $K_{\alpha 1}$, and $K_{\alpha 2}$ peak intensity values are used. If two adjacent Bragg reflections are too close to separate, the angle to be associated with the total intensity from the two reflections is derived by taking a weighted mean. For example, this arises with the 711-551 and 640 reflections. From appendix V the Bragg angles associated with the 711-551 and 640 reflections are 46.06° and 46.65° theta respectively. The multiplicity factors are 48 and 24. The angle associated with these reflections is then *

$$(48*46.06 + 24*46.65)/72 = 46.26^\circ \text{ theta} \qquad (139)$$

The integrated corrected intensity of each Bragg reflection is divided by the multiplicity factor. Then the slope may be obtained from a graph such as figure 19, but a least square analysis is quicker and more precise; and it also provides the standard deviation in the slope. The least square program that performs this analysis is shown on page

---

* In equation 139, the asterisk* is used as a multiplication symbol to conform with Fortran programming.

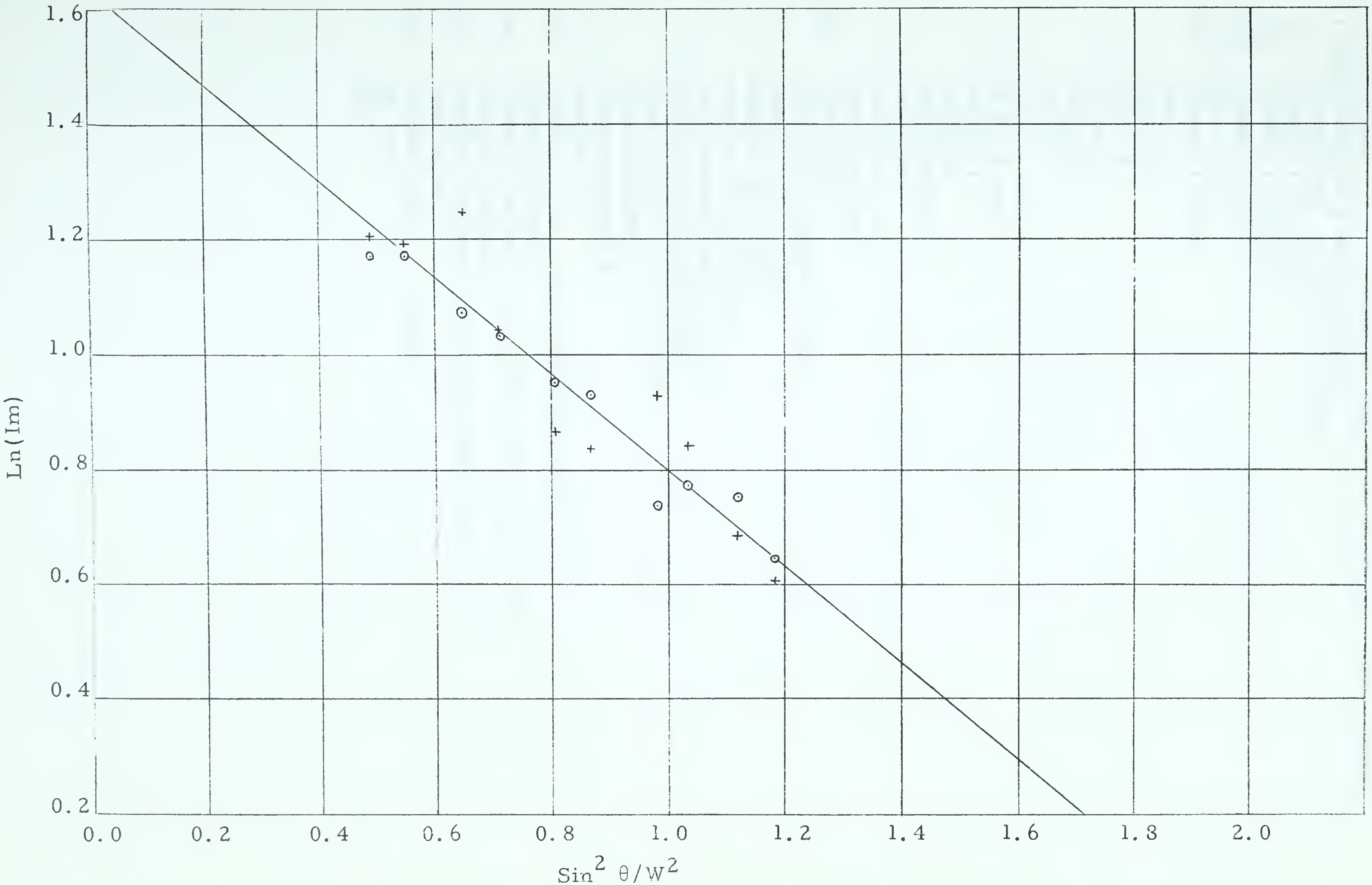

Figure 19 The Ln(Im) vs. $\mathrm{Sin}^2\ \theta/W^2$.

```
..I J.GOLDAK LEAST SQUARES ANALYSIS 922102E  SAVE CARDS
..LOAD FORTRAN EXECUTE DUMP
      DIMENSION IX(100),IY(100)
  5   FORMAT(2F20.10)
  52  FORMAT(1X2E16.9)
 100  FORMAT(7I5)
 1    READ 50,N
 50   FORMAT(1XI4)
      SX=0.0
      SXX=0.0
      SY=0.0
      SYY=0.0
      SXY=0.0
      FN=N
      DO 10 J=1,N
      READ 5,X,Y
      Y=LOGF(Y)
      SX=SX+X
      SXX=SXX+X*X
      SY=SY+Y
      SYY=SYY+Y*Y
      SXY=SXY+X*Y
 10   CONTINUE
      DEN=1.0/(FN*SXX-SX*SX)
      PUNCH 52,SX,SXX
      PUNCH 52,SY,SYY
      PUNCH 52,SXY,DEN
      A=(SY*SXX-SX*SXY)*DEN
      B=(FN*SXY-SY*SX)*DEN
      SD=(SYY-A*SY-B*SXY)/FN
      SB=SD*DEN*FN
      SA=SD*SXX*DEN
      PUNCH 53
 53   FORMAT(50H  LEAST SQUARES ANALYSIS
      PUNCH 54,A,SA
 54   FORMAT(5X2HA=,E16.9,5H(+OR-,E16.9,1H))
      PUNCH 55,B,SB
 55   FORMAT(5X2HB=,E16.9,5H(+OR-,E16.9,1H))
      PUNCH 56
 56   FORMAT(50H   Y=B*X+A
      GO TO 1
      END
```

```
..I J.GOLDAK LEAST SQUARES ANALYSIS 922102E  SAVE CARDS
..LOAD CARDS
    .74068000E+01   .66079341E+01
    .87132537E+01   .90320870E+01
    .67338530E+01   .21688586E+00
  LEAST SQUARES ANALYSIS
     A=    .16700870E+01(+OR-    .35628972E-01)
     B=   -.85293617E+00(+OR-    .48526627E-01)
   Y=B*X+A

    9
         .4832                  3.2487
         .5436                  3.3528
         .6442                  2.5149
        .7061                  4.3901
         .8053                  2.4685
         .8757                  2.5027
        1.0335                  2.1818
        1.1274                  1.9376
        1.1878                  1.9368
```

```
..I   J.GOLDAK DEBYE TEMP FROM X-RAY SLOP 922103 SAVE CARDS
..LOAD FORTRAN EXECUTE DUMP
 100  FORMAT(2F20.10)
      PUNCH 99
 99   FORMAT(1H1/1H5)
  1   READ 100,B,T
      PUNCH 100,B,T
      READ  100, D,A
      PUNCH 100, D,A
      PUNCH 80
  80  FORMAT(1H5,10HDEBYE TEMP,11X14H    SLOPE     ,7X14H(OBS-COMP)/OBS)
      PUNCH 81
  81  FORMAT(3X42HOLD    NEW     OBSERVED     COMPUTED        ,///)
  5   Z=D/T
      DD1=Z*Z*0.25
      U1=0.0
      DZ1=Z*0.01
  7   DO 20 I=1,100
      Z1=Z*(1.0+Z*0.5*(1.0+Z*0.33333333*(1.0+Z*0.25*(1.0+Z*0.2))))
      U1=U1   +Z*DZ1/Z1
      Z=Z-DZ1
  20  CONTINUE
      W= A*(T*T*U1+DD1)/(D*D*D)
  6   FORMAT(10XE14.8)
      V=(W-B)/B
      V     =ABSF(V)
      D1=D*0.33333333*(2.0+W/B )
      PUNCH 40,D,D1,B,W,V
  40  FORMAT(1H0,2F7.2,2F13.8,F13.9)
      IF(V-0.0001)1,1,42
  42  D=D1
      GO TO 5
      END
         .49497           300.
      445.                391.6114
```

.42647000	300.00000000
445.00000000	391.61140000

DEBYE TEMP OLD	NEW	SLOPE OBSERVED	COMPUTED	(OBS-COMP)/OBS
445.00	438.36	.42647000	.40739621	.04472481
438.36	436.88	.42647000	.42214074	.01015138
436.88	436.56	.42647000	.42553706	.00218758
436.56	436.49	.42647000	.42627148	.00046549
436.49	436.48	.42647000	.42642759	.00009944

119. The running time for this program is about thirty seconds. In the output and input data from experiment number 40 shown on page 120, B is the slope and the standard deviation is in brackets.

Having determined the slope it is necessary to solve equation 116 for D. Writing equation 116 in full

$$b = -(12h^2/mkD)D(x) \tag{140}$$

$$b = -(12h^2/mkD)(1/x^2)\left(\int_0^x (z/(\exp z-1))dz+x^2/4\right) \tag{141}$$

$$b = -(12h^2/mkD^3)T^2\left(\int_0 z/(\exp z-1)dz+x^2/4\right) \tag{142}$$

Equation 142 is solved for D by the Fortran program on page 121, with the same iterative technique used for the ratio method. Actually this program uses the slope from the relative scattering factor rather than its square vs. $\sin^2\theta/W^2$.

The data necessary to solve this program are half the measured slope, B, the specimen temperature, the estimated Debye temperature, D, and a constant 391.6114 which contains the factor $12h^2/(mk)$. The computer time required is approximately three minutes. An example of the output from this program is shown on page 122.

In both the ratio and the slope methods, the integral is evaluated by dividing the area into 100 parts. Very little improvement is expected by using smaller divisions because z/(expz-1) in equation 142 varies only slowly (see James 1958 p. 224). However, computer time would increase almost linearly with the increase in the number of divisions -- a fact which would not discourage investigators who use large computers.

SUMMARY OF DEBYE TEMPERATURE DETERMINATIONS

The results of the Debye temperature measurements are summarized below in table 8 for the slope method and on page 125 for the ratio method. The program used to summarize the results from the ratio method, which was written by Dr. K. W. Smillie of the computing centre of the University of Alberta, is the only program used in this thesis that was not written by the author. The Debye temperature determinations from all experiments are listed in appendices III and IV for the ratio and slope methods respectively.

The most probable value of the Debye temperature from the ratio method is 423.0±4K. From the slope method the most probable value is 451.30±9K but because of the small sample size (5 runs) the confidence limits should be treated cautiously.

Table 8 Results from Slope Method

Run	Slope	Temperature	θ_D
113	0.27835	77.	228.93
130	0.29895	77.	222.82
40	0.42647	300.	435.52
41	0.35452	300.	471.77
42	0.41500	300	441.54
112	0.35579	300	471.06
127	0.42867	300	435.52
Average			451.27
Std. Dev.			18.5

```
..I  J.GOLDAK  AVERAGE DEBYE TEMPERATURE  92210  SAVE CARDS
..LOAD CARDS
1
                RUN   0

         5*         X  X
          *         X  XX
          *         X XXX X
          *         X XXX X
          *     XX  XX XXXXXX   XX X
          ******************************
0
          SAMPLE SIZE         28
          MINIMUM          .37597000E+00
          MAXIMUM          .48196000E+00
          RANGE            .10599000E+00
          CLASS WIDTH      .52995000E-02
          MEAN             .42333392E+00
          MEDIAN           .42154570E+00
          MODE             .40511725E+00
          VARIANCE         .53785929E-03
          ST. DEV.         .23191793E-01
          SKEWNESS         .58791777E+00
          KURTOSIS         .83011553E+00
1
                RUN   0

                OBS.  THEOR.  DIFF.
          0      0      .6    -.6
          1      1      .4     .6
          2      1      .6     .4
          3      0      .9    -.9
          4      0     1.2   -1.2
          5      1     1.5    -.5
          6      5     1.9    3.1
          7      0     2.2   -2.2
          8      3     2.4     .6
          9      5     2.6    2.4
         10      4     2.6    1.4
         11      1     2.4   -1.4
         12      3     2.2     .8
         13      1     1.8    -.8
         14      0     1.5   -1.5
         15      0     1.1   -1.1
         16      0      .8    -.8
         17      1      .6     .4
         18      1      .4     .6
         19      0      .2    -.2
         20      1      .1     .9
         21      0      .2    -.2

                28    28.2
```

DISCUSSION OF DEBYE TEMPERATURE DETERMINATIONS

1. LIMITATIONS OF DEBYE'S THEORY

The real spectrum of lattice vibrations in crystals (e.g. Krumhansl, 1959) is much more complex than that suggested by Debye's theory, which assumes an isotropic solid with no dispersion, maintained at constant volume. Further, Debye assumes a cutoff frequency when it is really a cutoff wavelength. In spite of these assumptions, Debye's theory of lattice vibrations is still the most useful. However its limitations must be kept in mind.

2. COMPARISON OF SLOPE AND RATIO METHODS

(a) The Slope Method

The slope method requires a knowledge of the crystal structure, which reduces its usefulness for complex structures. Also a knowledge to the theoretical atomic scattering factor is required, which generally is not considered a serious weakness. However, this method compares data obtained from a relatively large angular range (25° to 55° theta in this thesis) which causes two problems: alignment and extinction errors could be significant over such a range; and the problem of isolating the Bragg scattering is more serious. If the Bragg scattering is not isolated correctly it is likely that the error is angle dependent and will cause errors in the slope. It is desirable to use a specimen with crystallites oriented at random -- this is extremely difficult to achieve and ascertain experimentally. If a sufficently large number of different reflections

are considered, it is possible that this error would not be serious.

The slope method does not require a knowledge of the temperature dependence of the Debye temperature. This is usually considered to be (e.g. Herbstein and Smuts (1963) the most important advantage of this method. It is true that Debye's theory neglects thermal expansion. If Gazzara and Middleton's (1961) equation (which is a gross approximation) is used, the change in the Debye temperature of nickel is 12K, with a temperature change from 77K to 300K.

$$D_{T1} = D_{T2}(1+\alpha\gamma\tau(T1-T2)) \tag{143}$$

where D_{T1} - Debye temperature at T1

D_{T2} - Debye temperature at T2

α - Coefficient of volume expansion, 37.5 E-6 for nickel.

γ - Gruneisen's constant - 1.9 for nickel

τ - "Explicit temperature function" - Gazzara's value of 4.1 for iron is used for nickel.

$$D_{T1} = D_{T2}*1.03$$

The principal disadvantage to the slope method, at least for powder specimens, is difficulty of isolating the Bragg scattering. The two determinations at 77K listed in table 8, which lead to Debye temperatures

of 223 and 229 K compared to an average of 451 for determinations at 300K emphasize this problem.

(b) The Ratio Method

The temperature dependence of the Debye temperature is not accommodated by the ratio method; and this is the principal criticism of the method. However, Gazzara's formula suggests the change in the Debye temperature of nickel caused by a temperature change from 77K to 300K is only 12K. In the author's opinion the uncertainty in the Debye temperature due to the error in separating the Bragg scattering from the background is much more important and more difficult to assess. In the ratio method this error is to some extent compensating. Further, from two scans in this work, one at 77K and one at 300K, nine values of θ_D are determined by the ratio method compared to only two by the slope method.

For the experimental circumstances pertaining to this work, the ratio method is believed to be superior to the slope method. The value of the Debye temperature of nickel determined in this work is taken as 423±4K. The confidence limits are a measure of the precision of the data and the consistency of the method used to isolate the Bragg scattering, but do not necessarily represent the accuracy.

DEBYE TEMPERATURE OF NICKEL DETERMINED BY VARIOUS METHODS

It is useful to compare the Debye temperature determined by various methods given in table 9.

Table 9. Debye Temperatures of Nickel

θ_D	Method	Reference
441. ±15	specific heat	Rayne and Kemp 1956
390	specific heat	Rayne and Kemp 1956
456		Kittel 1956
476	elastic constants	Alers and Neighbors 1959
460	elastic constants	Alers et al 1959
434	Young's modulus	Koster 1954
366	slope method	Iveronova et al 1951
341	ratio method	Ilynia and Kritskaya 1955
420	ratio method	Zhuravlev and Katsnelson 1959
423. ±4	ratio method	this work
410	thermal expansion	Nix and MacNair 1941
413-437	Mossbauer effect	Obenshain and Wegener 1961
AVERAGE 418		

While it is difficult to assess the significance of the average value 418, in table 9, it is satisfying to see the close agreement with the value determined by the work in this thesis. One of the main reasons for the

scatter in the results listed in table 9, is that in each case the Debye temperature is a parameter that provides a best fit between theory and experiment. Without considering each method in detail, it is clear that the accuracy of the Debye temperatures in table 9 is not high.

(a) Effect of Cold Work on the Debye Temperature

The Debye temperature determined from the temperature factor is a parameter such that equation 112 is satisfied. A similar equation is used to determine the Debye temperature from the specific heat. In both cases the integration limits are zero and the cutoff frequency w_m, which imply a range of wavelengths from infinity to $2\pi V/w_m$. However, the maximum wavelength is limited by the dimensions of the crystal. If the crystal is very small the integration should be from some mimimum frequency, say, w_ℓ to w_m. Therefore, it is conceivable that the Debye temperature is a function of size for very small crystals. If the effect of cold work is considered to at least in part reduce effective crystal size, it is possible that cold work will alter the Debye temperature.

There is a second aspect to this problem which is much more difficult to assess. Cold work changes the distribution of interatomic distances in a crystal. If the potential energy is not a symmetric function over the range of interatomic distances involved, the frequency distribution function itself may be changed, which could change the Debye temperature.

Specific heat measurements Martin (1960) down to 0.7 K on copper cold worked at room temperature showed a slight increase (+0.15 percent)

specific heat and hence a decrease in the Debye temperature. However, the cold worked copper may have recovered considerably at room temperature. Further, Druyvesteyn (1962) found the Young's modulus of cold worked copper to decrease as much as 13 percent at low temperatures. He noted that the copper recovered considerably at room temperature. Because the Debye temperature can be related to the Young's modulus, this result suggests that the Debye temperature of cold worked metal should be changed. The different values of thermal expansion of cold worked and annealed speciments listed on page 55 offer some support to this view. However because cold work alters the Bragg profile, the Bragg scattering cannot be isolated from the background with sufficient accuracy to detect a difference in the Debye temperature of cold worked nickel, if such a difference exists.

CONCLUSIONS

1. An x-ray diffraction system -- XRAS -- has been designed and constructed that is capable of measuring intensities with a precision approaching 0.1 percent and lattice parameters with an accuracy of the order of 0.0001A and somewhat higher precision. The operation is automatic and data recorded on IBM cards and processed by a computer. The optical path is contained in a high vacuum (E-6 mm of Hg) chamber and the specimen temperature can be varied from 77 K to 700 K.

2. The Debye temperature of nickel determined in this thesis by the ratio method from 28 experiments is 423. $\pm$ 4K. The error represents the precision of the data and the method of isolating the Bragg scattering rather than the accuracy. The slope method at 300^{o}K yielded a value of 451. K but because of the difficulty of isolating the Bragg scattering from the background, the value is not believed to be accurate.

3. While it is likely that the Debye temperature of nickel is changed by cold work, the change is too small to be detected because of the difficulty in isolating the Bragg scattering from the background.

REFERENCES

Abrahams, S. C., Rev.Sci.Instr. 33,973 (1962)

Alers, G. A., and Neighbours, J. R., Rev.Mod.Phys., 31,675, (1959)

Alers, G. A., Neighbours, J. R., and Sato, H., Bull. Amer.Phys. Soc., 4,131. (1959)

Baun, W. L., and Renton, J. J., J.Sci.Instrum., 40,498-498 (1963)

Brillouin, L., "Wave Propagation in Periodic Structures" (1953)

Born, M., and Huang, K., "Dynamical Theory of Crystal Lattices" (1954)

Compton, A. H., and Allison, S. K., "X-rays in Theory and Experiment" (1935)

Debye, P., Verh. D., Deutsch. Phys. Ges., 15,678,738,857 (1913)

Debye, P., Annalen der Physik, 43,49 (1914)

Druyvesteyn, W. F., and Blaisse, B. S., Physica 28, 695-700, (1962)

Einstein, A., Ann.d. Physik, 22, 180 and 800, (1907)

Forrester, J. D., J.Sci.Instrum. 38,153 (1961)

Freeman, A. S., and Watson, R. E., Acta Cryst., 14,27 (1961)

Gazzara, C. P., and Middleton, R. M., J.Appl.Phys., 32,1546 (1961)

Herbstein, F. H., and Smuts, J., Phil.Mag.,

Hosemann, R., and Baggchi, S. N., "The Direct Analysis of Diffraction by Matter" (1962)

Ilyina, V. A., Kritskaya, V. K., and Kurdyumov, G. V., Physics of Metals and Metallography, 13 (1), 118 (1962)

Ilyina, V. A., and Kritskaya, V. K., Problems of Metallography and the Physics of Metals, Fourth Symposium, p. 294 (English translation by Consultants Bureau, A.E.C. -tr-2924) (1955)

Iveronova, V. I., Kuzmina, Z. I., Futergendler, S. I., and Detlaf, E. I., Izvest Akad. Nauk. S.S.S.R. Ser. Fiz. 15,44 (1951)

James, R. W., "The Optical Principles of the Diffraction of X-rays", (1958)

Keating, D T., Rev. Sci. Instr., 30, 725-727, (1959)

Klein, O. and Nishina, Y., Zeits, F., Phys. 52, 853 (1929)

Kittel, C., "Introduction to Solid State Physics", (1956)

Koster, W., Appl. Sci. Res. A, 4,329 (1954)

Krumhansl, J. A., J. App. Phys. 31, 1, 307-317, (1962)

Lonsdale, K., Reports on Prog. in Phys. 9, 256-293 (1942-43)

Martin, D. L., Can. J. Phys. 38-2, 1390-1391, (1960)

Nix, F. C., and MacNair, D., Phys. Rev., 66, 597 (1941)

Obenshain, E., and Wegener, H., Phys. Rev., 121, 1344 (1961)

Parrish and Lowitzsch, Amer. Mineralogist, 44, 765-787 (1959)

Pearson, W. B., "Handbook of Lattice Spacing and Structures of Metals", (1958)

Rayne, J. A., and Kemp, W. G., Phil. Mag., 1, 918 (1956)

Walker, C. B., Phys. Rev., 103, 547 (1956)

Waller, I., and Hartree, D. R., Proc. Roy. Soc., 124, 119 (1929)

Woo, V. H., Phys. Rev., 27, 119 (1926)

Zhuravlev, N. N., and Katsnelson, A. A., Soviet Physics - Crystallography, 3, 936 (1959)

Data from XRAS for Experiment 100

This appendix is presented as an example of the data by XRAS. Each line of data is recorded on one IBM card by XRAS in the format shown in figure 14 p. 50. The operating conditions for this experiment are as follows: molybdenumtube operated at 40 kv and 15 ma; zirconium filter with 1.0° slit system; vacuum of E-6 mm of Hg; specimen temperature is 300 K; starting angle is 99.00° two theta and the stopping angle is 107.99° two theta.

```
   1         99.00
000077 000000 000093 000010 000079 000020 000089 000030 000076 00004
000077 000050 000072 000060 000081 000070 000073 000080 000091 00009
000082 000100 000097 000110 000077 000120 000071 000130 000070 00014
000077 000150 000069 000160 000087 000170 000067 000180 000087 00019
000083 000200 000093 000210 000088 000220 000076 000230 000060 00024
000089 000250 000080 000260 000086 000270 000073 000280 000066 00029
000088 000300 000079 000310 000082 000320 000057 000330 000088 00034
000111 000350 000083 000360 000086 000370 000079 000380 000072 00039
000067 000400 000076 000410 000082 000420 000077 000430 000076 00044
000077 000450 000071 000460 000070 000470 000076 000480 000079 00049
000086 000500 000076 000510 000088 000520 000086 000530 000086 00054
000070 000550 000076 000560 000058 000570 000070 000580 000072 00059
000072 000600 000067 000610 000076 000620 000073 000630 000069 00064
000066 000650 000062 000660 000069 000670 000077 000680 000067 00069
000082 000700 000076 000710 000069 000720 000052 000730 000090 00074
000106 000750 000086 000760 000083 000770 000076 000780 000080 00079
000088 000800 000092 000810 000076 000820 000069 000830 000086 00084
000059 000850 000076 000860 000081 000870 000086 000880 000071 00089
000060 000900 000069 000910 000073 000920 000076 000930 000086 00094
000067 000950 000067 000960 000082 000970 000077 000980 000069 00099
000076 001000 000079 001010 000062 001020 000077 001030 000087 00104
000073 001050 000088 001060 000077 001070 000089 001080 000062 00109
000077 001100 000066 001110 000076 001120 000082 001130 000081 00114
000067 001150 000088 001160 000066 001170 000071 001180 000071 00119
000076 001200 000086 001210 000071 001220 000071 001230 000078 00124
000080 001250 000077 001260 000077 001270 000069 001280 000071 00129
000072 001300 000076 001310 000082 001320 000068 001330 000106 00134
000079 001350 000071 001360 000088 001370 000076 001380 000080 00139
000087 001400 000076 001410 000076 001420 000088 001430 000067 00144
000078 001450 000088 001460 000070 001470 000077 001480 000082 00149
000089 001500 000066 001510 000100 001520 000066 001530 000088 00154
000077 001550 000073 001560 000083 001570 000073 001580 000083 00159
000096 001600 000079 001610 000072 001620 000079 001630 000081 00164
000080 001650 000076 001660 000109 001670 000089 001680 000091 00169
000079 001700 000088 001710 000076 001720 000076 001730 000100 00174
```

000083	001750	000080	001760	000099	001770	000082	001780	000096	00179
000116	001800	000116	001810	000071	001820	000090	001830	000082	00184
000127	001850	000106	001860	000106	001870	000102	001880	000093	00189
000107	001900	000092	001910	000099	001920	000116	001930	000110	00194
000127	001950	000113	001960	000123	001970	000130	001980	000103	00199
000103	002000	000126	002010	000137	002020	000156	002030	000119	00204
000138	002050	000138	002060	000141	002070	000167	002080	000132	00209
000167	002100	000158	002110	000173	002120	000128	002130	000146	00214
000187	002150	000166	002160	000159	002170	000166	002180	000157	00219
000159	002200	000183	002210	000188	002220	000191	002230	000191	00224
000156	002250	000183	002260	000162	002270	000169	002280	000173	00229
000183	002300	000173	002310	000146	002320	000141	002330	000158	00234
000127	002350	000146	002360	000147	002370	000140	002380	000123	00239
000123	002400	000139	002410	000122	002420	000129	002430	000139	00244
000110	002450	000116	002460	000118	002470	000116	002480	000091	00249
000112	002500	000118	002510	000136	002520	000119	002530	000111	00254
000121	002550	000099	002560	000098	002570	000102	002580	000098	00259
000122	002600	000109	002610	000112	002620	000116	002630	000108	00264
000096	002650	000096	002660	000120	002670	000086	002680	000102	00269
000089	002700	000106	002710	000101	002720	000116	002730	000098	00274
000107	002750	000106	002760	000097	002770	000107	002780	000117	00279
000117	002800	000096	002810	000118	002820	000097	002830	000118	00284
000112	002850	000107	002860	000099	002870	000100	002880	000110	00289
000107	002900	000110	002910	000107	002920	000109	002930	000118	00294
000136	002950	000118	002960	000127	002970	000112	002980	000150	00299
000127	003000	000123	003010	000136	003020	000126	003030	000133	00304
000128	003050	000143	003060	000126	003070	000110	003080	000157	00309
000107	003100	000141	003110	000123	003120	000107	003130	000126	00314
000130	003150	000103	003160	000126	003170	000107	003180	000098	00319
000106	003200	000116	003210	000117	003220	000120	003230	000106	00324
000101	003250	000106	003260	000080	003270	000106	003280	000116	00329
000093	003300	000107	003310	000098	003320	000097	003330	000100	00334
000101	003350	000093	003360	000106	003370	000083	003380	000088	00339
000087	003400	000078	003410	000066	003420	000077	003430	000066	00344
000088	003450	000083	003460	000070	003470	000096	003480	000066	00349
000081	003500	000078	003510	000087	003520	000076	003530	000069	00354
000058	003550	000080	003560	000067	003570	000089	003580	000048	00359
000076	003600	000072	003610	000088	003620	000086	003630	000078	00364
000069	003650	000086	003660	000073	003670	000076	003680	000080	00369
000066	003700	000071	003710	000139	003720	000076	003730	000071	00374
000080	003750	000079	003760	000073	003770	000103	003780	000071	00379
000069	003800	000067	003810	000069	003820	000081	003830	000067	00384
000077	003850	000076	003860	000083	003870	000063	003880	000063	00389
000079	003900	000073	003910	000086	003920	000067	003930	000082	00394
000080	003950	000060	003960	000068	003970	000072	003980	000079	00399
000079	004000	000086	004010	000067	004020	000070	004030	000066	00404
000067	004050	000067	004060	000067	004070	000077	004080	000072	00409
000072	004100	000069	004110	000069	004120	000067	004130	000056	00414
000089	004150	000059	004160	000079	004170	000063	004180	000076	00419
000080	004200	000073	004210	000056	004220	000080	004230	000068	00424
000061	004250	000072	004260	000076	004270	000119	004280	000087	00429
000076	004300	000070	004310	000063	004320	000086	004330	000076	00434
000066	004350	000058	004360	000069	004370	000059	004380	000071	00439
000077	004400	000049	004410	000077	004420	000071	004430	000072	00444
000060	004450	000056	004460	000076	004470	000069	004480	000076	00449
000067	004500	000067	004510	000063	004520	000071	004530	000076	00454

000072	004550	000069	004560	000079	004570	000052	004580	000089	00459
000062	004600	000077	004610	000067	004620	000077	004630	000072	00464
000086	004650	000059	004660	000070	004670	000067	004680	000066	00469
000079	004700	000062	004710	000067	004720	000050	004730	000056	00474
000072	004750	000076	004760	000067	004770	000072	004780	000077	00479
000071	004800	000052	004810	000082	004820	000070	004830	000076	00484
000076	004850	000070	004860	000058	004870	000070	004880	000078	00489
000070	004900	000078	004910	000062	004920	000051	004930	000086	00494
000087	004950	000067	004960	000060	004970	000066	004980	000073	00499
000060	005000	000077	005010	000076	005020	000078	005030	000076	00504
000056	005050	000067	005060	000076	005070	000059	005080	000077	00509
000077	005100	000073	005110	000068	005120	000060	005130	000058	00514
000063	005150	000066	005160	000097	005170	000061	005180	000063	00519
000097	005200	000070	005210	000072	005220	000076	005230	000077	00524
000058	005250	000070	005260	000073	005270	000069	005280	000057	00529
000067	005300	000072	005310	000081	005320	000062	005330	000066	00534
000068	005350	000053	005360	000053	005370	000062	005380	000073	00539
000079	005400	000057	005410	000086	005420	000087	005430	000072	00544
000067	005450	000056	005460	000071	005470	000071	005480	000061	00549
000071	005500	000062	005510	000079	005520	000070	005530	000056	00554
000068	005550	000061	005560	000068	005570	000066	005580	000058	00559
000059	005600	000067	005610	000072	005620	000060	005630	000062	00564
000073	005650	000056	005660	000076	005670	000060	005680	000076	00569
000068	005700	000072	005710	000067	005720	000058	005730	000076	00574
000059	005750	000047	005760	000059	005770	000057	005780	000056	00579
000076	005800	000073	005810	000076	005820	000070	005830	000066	00584
000052	005850	000067	005860	000076	005870	000066	005880	000066	00589
000060	005900	000080	005910	000056	005920	000059	005930	000053	00594
000066	005950	000082	005960	000068	005970	000060	005980	000081	00599
000071	006000	000072	006010	000058	006020	000061	006030	000062	00604
000078	006050	000063	006060	000076	006070	000066	006080	000061	00609
000077	006100	000072	006110	000060	006120	000070	006130	000057	00614
000056	006150	000073	006160	000066	006170	000070	006180	000066	00619
000062	006200	000062	006210	000082	006220	000066	006230	000066	00624
000067	006250	000061	006260	000060	006270	000066	006280	000062	00629
000066	006300	000069	006310	000066	006320	000069	006330	000068	00634
000073	006350	000071	006360	000067	006370	000067	006380	000063	00639
000066	006400	000071	006410	000060	006420	000066	006430	000072	00644
000069	006450	000061	006460	000069	006470	000068	006480	000066	00649
000062	006500	000059	006510	000080	006520	000069	006530	000073	00654
000066	006550	000080	006560	000058	006570	000067	006580	000066	00659
000079	006600	000066	006610	000082	006620	000069	006630	000058	00664
000076	006650	000066	006660	000067	006670	000070	006680	000060	00669
000071	006700	000073	006710	000060	006720	000061	006730	000057	00674
000066	006750	000070	006760	000066	006770	000066	006780	000067	00679
000071	006800	000066	006810	000066	006820	000060	006830	000072	00684
000060	006850	000062	006860	000059	006870	000058	006880	000067	00689
000077	006900	000062	006910	000050	006920	000066	006930	000070	00694
000059	006950	000066	006960	000067	006970	000050	006980	000077	00699
000061	008900	000067	008910	000067	008920	000057	008930	000077	00894
000069	008950	000068	008960	000056	008970	000083	008980	000078	00899

APPENDIX II

The Corrected Intensity from all Experiments

The corrected intensities, which are listed here for all experiments referred to in this thesis, are obtained by dividing the data from XRAS (such as shown in appendix I) by the Lorentz-polarization and theoretical atomic scattering factor squared. The first line for each experiment starts on a new page with "..I" and is followed by a set of numbers which briefly describe the experiment. For example, the first line on page 5 is

..I 40 2801 45.00

This indicates experiment 40, with specimen 2801 and the scan started at 45.00 two theta. The procedure and the Fortran program that perform this correction are described in detail on pages 108 to 111.

..I 40 2801 45 00
..BRANCH 0040R

THETA	INTEGRATED INTENSITY	INTENSITY	RATE OF CHANGE	PROBABLE ERROR	
22.749	5.540	5.540	1.000	.010	92.26
22.999	11.458	5.918	.063	.010	5.95
23.249	17.870	6.412	.077	.010	7.32
23.499	24.313	6.442	.004	.010	.43
23.749	42.449	18.135	.644	.006	98.54
23.999	56.160	13.711	-.322	.007	-41.95
24.249	62.577	6.416	-1.136	.011	-98.91
24.499	68.845	6.268	-.023	.011	-1.99
24.749	75.313	6.468	.030	.011	2.58
24.999	81.901	6.587	.018	.012	1.49
25.249	89.334	7.432	.113	.011	9.75
25.499	98.866	9.531	.220	.010	21.00
25.749	109.551	10.685	.107	.010	10.70
25.999	155.690	46.138	.768	.004	155.31
26.249	208.739	53.049	.130	.004	27.71
26.499	224.624	15.885	-2.339	.008	-267.31
26.749	277.866	53.242	.701	.004	144.07
26.999	323.298	45.432	-.171	.005	-32.00
27.249	337.387	14.088	-2.224	.009	-226.46
27.499	349.767	12.380	-.138	.010	-12.92
27.749	361.811	12.043	-.027	.011	-2.53
27.999	374.017	12.205	.013	.011	1.19
28.249	385.699	11.682	-.044	.011	-3.86
28.499	397.568	11.869	.015	.011	1.34
28.749	410.658	13.089	.093	.011	8.19
28.999	424.688	14.029	.067	.011	5.98
29.249	439.461	14.773	.050	.011	4.53
29.499	478.502	39.040	.621	.006	89.36
29.749	536.516	58.014	.327	.005	56.29
29.999	555.801	19.285	-2.008	.010	-196.07
30.249	570.444	14.642	-.317	.011	-26.56
30.499	585.344	14.900	.017	.012	1.43
30.749	601.324	15.979	.067	.011	5.73
30.999	618.207	16.882	.053	.011	4.59
31.249	636.119	17.911	.057	.011	5.01
31.499	689.333	53.214	.663	.006	98.22
31.749	755.113	65.779	.191	.006	30.98
31.999	779.340	24.227	-1.715	.010	-166.33
32.249	796.762	17.421	-.390	.012	-31.65
32.499	813.587	16.825	-.035	.012	-2.78
32.749	830.247	16.660	-.009	.012	-.76
32.999	846.109	15.861	-.050	.013	-3.72
33.249	862.198	16.089	.014	.013	1.04

33.499	878.379	16.180	.005	.013	.40
33.749	895.292	16.912	.043	.013	3.17
33.999	915.665	20.373	.169	.012	13.45
34.249	933.100	17.434	-.168	.013	-12.18
34.499	951.917	18.817	.073	.013	5.44
34.749	990.587	38.669	.513	.009	53.77
34.999	1021.247	30.660	-.261	.010	-24.07
35.249	1041.626	20.379	-.504	.013	-37.46
35.499	1063.759	22.132	.079	.013	6.06
35.749	1086.636	22.877	.032	.013	2.50
35.999	1111.092	24.455	.064	.012	5.07
36.249	1138.218	27.126	.098	.012	8.05
36.499	1206.998	68.779	.605	.007	77.99
36.749	1293.069	86.071	.200	.007	28.62
36.999	1348.980	55.910	-.539	.008	-61.25
37.249	1425.723	76.743	.271	.007	35.72
37.499	1477.565	51.842	-.480	.009	-51.38
37.749	1505.310	27.745	-.868	.012	-67.25
37.999	1531.850	26.539	-.045	.013	-3.40
38.249	1557.500	25.650	-.034	.013	-2.52
38.499	1584.129	26.628	.036	.013	2.70
38.749	1611.164	27.035	.015	.013	1.10
38.999	1638.449	27.285	.009	.013	.66
39.249	1666.368	27.918	.022	.013	1.65
39.499	1713.756	47.388	.410	.010	38.68
39.749	1763.464	49.708	.046	.010	4.45
39.999	1805.006	41.541	-.196	.011	-17.01
40.249	1834.087	29.080	-.428	.013	-30.77
40.499	1862.774	28.686	-.013	.014	-.97
40.749	1891.878	29.104	.014	.014	1.01
40.999	1921.864	29.986	.029	.014	2.09
41.249	1967.535	45.671	.343	.011	29.92
41.499	2021.233	53.698	.149	.010	14.01
41.749	2071.794	50.560	-.062	.011	-5.60
41.999	2134.467	62.672	.193	.010	19.27
42.249	2183.851	49.383	-.269	.011	-23.65
42.499	2216.734	32.883	-.501	.014	-35.73
42.749	2246.906	30.172	-.089	.014	-6.08
42.999	2276.889	29.982	-.006	.014	-.42
43.249	2307.875	30.986	.032	.014	2.19
43.499	2338.149	30.273	-.023	.015	-1.56
43.749	2369.107	30.958	.022	.014	1.47
43.999	2400.034	30.926	-.001	.015	-.06
44.249	2441.030	40.996	.245	.013	18.66
44.499	2477.983	36.952	-.109	.013	-7.85
44.749	2513.867	35.884	-.029	.014	-2.09
44.999	2548.438	34.571	-.037	.014	-2.60

45.249	2583.389	34.950	.010	.014	.74
45.499	2619.413	36.024	.029	.014	2.06
45.749	2660.045	40.631	.113	.013	8.30
45.999	2750.859	90.814	.552	.009	60.24
46.249	2811.000	60.141	-.510	.011	-45.05
46.499	2886.743	75.742	.205	.010	20.33
46.749	2941.737	54.994	-.377	.011	-31.60
46.999	2993.941	52.204	-.053	.012	-4.34
47.249	3033.264	39.323	-.327	.014	-23.02
47.499	3071.525	38.260	-.027	.014	-1.91
47.749	3110.689	39.164	.023	.014	1.60
47.999	3149.439	38.750	-.010	.014	-.73
48.249	3189.106	39.666	.023	.014	1.60
48.499	3229.938	40.832	.028	.014	2.00
48.749	3280.766	50.828	.196	.012	15.40
48.999	3371.088	90.321	.437	.009	45.51
49.249	3435.795	64.707	-.395	.011	-34.77
49.499	3488.385	52.590	-.230	.012	-18.20
49.749	3532.617	44.232	-.188	.013	-13.65
49.999	3576.156	43.538	-.015	.013	-1.13
50.249	3619.962	43.806	.006	.013	.43
50.499	3674.895	54.932	.202	.012	16.20
50.749	3787.126	112.231	.510	.008	58.25
50.999	3855.607	68.480	-.638	.011	-56.83
51.249	3921.031	65.424	-.046	.011	-4.05
51.499	3965.143	44.111	-.483	.014	-34.38
51.749	4004.243	39.100	-.128	.014	-8.57
51.999	4044.163	39.919	.020	.014	1.38

..I 41 2801

..BRANCH 0040R

THETA	INTEGRATED INTENSITY	INTENSITY	RATE OF CHANGE	PROBABLE ERROR	
22.749	5.667	5.667	1.000	.010	93.31
22.999	11.593	5.926	.043	.010	4.08
23.249	18.028	6.435	.079	.010	7.52
23.499	24.687	6.658	.033	.010	3.17
23.749	42.941	18.254	.635	.006	97.41
23.999	56.854	13.913	-.312	.007	-40.86
24.249	63.449	6.595	-1.109	.011	-97.89
24.499	69.936	6.486	-.016	.011	-1.42
24.749	76.521	6.584	.014	.011	1.25
24.999	83.139	6.617	.004	.012	.41
25.249	90.620	7.481	.115	.011	9.93
25.499	100.385	9.764	.233	.010	22.57
25.749	111.312	10.927	.106	.009	10.66
25.999	159.625	48.312	.773	.004	160.05
26.249	213.390	53.765	.101	.004	21.72
26.499	229.323	15.932	-2.374	.008	-271.72
26.749	362.986	133.663	.880	.003	286.56
26.999	453.631	90.644	-.474	.003	-124.82
27.249	468.164	14.533	-5.236	.009	-541.44
27.499	487.560	19.395	.250	.008	29.39
27.749	500.031	12.470	-.555	.010	-51.25
27.999	512.135	12.104	-.030	.011	-2.70
28.249	524.559	12.423	.025	.011	2.28
28.499	536.735	12.176	-.020	.011	-1.75
28.749	550.488	13.752	.114	.011	10.32
28.999	565.005	14.517	.052	.011	4.78
29.249	580.144	15.138	.041	.010	3.74
29.499	620.415	40.270	.624	.006	91.12
29.749	677.937	57.521	.299	.005	51.39
29.999	697.407	19.470	-1.954	.010	-191.72
30.249	712.436	15.029	-.295	.011	-25.08
30.499	727.176	14.739	-.019	.012	-1.62
30.749	743.774	16.598	.111	.011	9.68
30.999	760.830	17.055	.026	.011	2.31
31.249	778.921	18.091	.057	.011	5.01
31.499	832.056	53.134	.659	.006	97.58
31.749	896.900	64.843	.180	.006	29.07
31.999	920.823	23.923	-1.710	.010	-164.84
32.249	938.175	17.351	-.378	.012	-30.63
32.499	954.823	16.647	-.042	.012	-3.30
32.749	971.114	16.291	-.021	.013	-1.66
32.999	986.867	15.752	-.034	.013	-2.52
33.249	1003.040	16.172	.025	.013	1.91

33.499	1019.089	16.049	-.007	.013	-.55
33.749	1035.784	16.694	.038	.013	2.81
33.999	1052.849	17.065	.021	.013	1.57
34.249	1070.103	17.253	.010	.013	.78
34.499	1088.998	18.895	.086	.013	6.45
34.749	1127.249	38.250	.505	.009	52.71
34.999	1158.572	31.323	-.221	.010	-20.60
35.249	1178.957	20.385	-.536	.013	-39.85
35.499	1200.477	21.520	.052	.013	3.97
35.749	1223.185	22.708	.052	.013	4.00
35.999	1248.004	24.819	.085	.012	6.73
36.249	1274.678	26.673	.069	.012	5.63
36.499	1342.838	68.160	.608	.007	78.03
36.749	1429.149	86.310	.210	.007	30.00
36.999	1484.623	55.474	-.555	.008	-62.87
37.249	1559.396	74.773	.258	.007	33.52
37.499	1611.741	52.344	-.428	.009	-46.06
37.749	1639.507	27.765	-.885	.012	-68.57
37.999	1665.097	25.589	-.085	.013	-6.25
38.249	1690.424	25.326	-.010	.013	-.75
38.499	1716.686	26.262	.035	.013	2.59
38.749	1743.056	26.369	.004	.013	.29
38.999	1769.967	26.911	.020	.013	1.45
39.249	1798.115	28.147	.043	.013	3.21
39.499	1846.311	48.196	.415	.010	39.50
39.749	1895.795	49.483	.026	.010	2.47
39.999	1936.942	41.146	-.202	.011	-17.45
40.249	1966.138	29.196	-.409	.013	-29.45
40.499	1995.210	29.071	-.004	.014	-.30
40.749	2024.380	29.170	.003	.014	.23
40.999	2054.960	30.579	.046	.013	3.31
41.249	2101.404	46.444	.341	.011	30.01
41.499	2155.956	54.552	.148	.010	14.04
41.749	2208.520	52.563	-.037	.010	-3.48
41.999	2269.839	61.318	.142	.010	14.08
42.249	2318.313	48.474	-.264	.011	-23.07
42.499	2350.250	31.937	-.517	.014	-36.33
42.749	2380.442	30.192	-.057	.014	-3.91
42.999	2409.865	29.423	-.026	.015	-1.73
43.249	2439.990	30.125	.023	.014	1.55
43.499	2470.901	30.910	.025	.014	1.70
43.749	2502.798	31.897	.030	.014	2.09
43.999	2533.115	30.316	-.052	.015	-3.42
44.249	2574.072	40.956	.259	.013	19.73
44.499	2610.471	36.399	-.125	.014	-8.91
44.749	2646.250	35.778	-.017	.014	-1.21
44.999	2681.276	35.025	-.021	.014	-1.48

45.249	2715.108	33.832	-.035	.014	-2.38
45.499	2751.409	36.301	.068	.014	4.73
45.749	2792.422	41.012	.114	.013	8.45
45.999	2883.315	90.893	.548	.009	59.86
46.249	2942.185	58.870	-.543	.011	-47.54
46.499	3018.298	76.113	.226	.010	22.41
46.749	3071.673	53.374	-.426	.012	-35.15
46.999	3123.612	51.938	-.027	.012	-2.24
47.249	3162.694	39.082	-.328	.014	-23.05
47.499	3201.827	39.133	.001	.014	.09
47.749	3241.144	39.316	.004	.014	.32
47.999	3279.578	38.434	-.022	.014	-1.57
48.249	3319.594	40.015	.039	.014	2.76
48.499	3360.799	41.205	.028	.014	2.04
48.749	3411.913	51.113	.193	.012	15.22
48.999	3502.845	90.932	.437	.009	45.73
49.249	3569.360	66.514	-.367	.011	-32.70
49.499	3621.990	52.630	-.263	.012	-20.84
49.749	3666.536	44.545	-.181	.013	-13.16
49.999	3710.324	43.787	-.017	.013	-1.24
50.249	3754.013	43.688	-.002	.013	-.16
50.499	3810.481	56.468	.226	.012	18.35
50.749	3925.742	115.261	.510	.008	58.98
50.999	3994.993	69.251	-.664	.011	-59.44
51.249	4063.307	68.313	-.013	.011	-1.21
51.499	4107.966	44.659	-.529	.013	-37.93
51.749	4150.021	42.054	-.061	.014	-4.29
51.999	4191.033	41.012	-.025	.014	-1.74
52.249	4231.836	40.802	-.005	.014	-.35
52.499	4270.889	39.053	-.044	.014	-2.98
52.749	4311.161	40.272	.030	.014	2.04
52.999	4350.518	39.356	-.023	.014	-1.55
53.249	4392.396	41.878	.060	.014	4.15
53.499	4435.157	42.760	.020	.014	1.43
53.749	4480.343	45.186	.053	.013	3.84
53.999	4523.618	43.274	-.044	.014	-3.09

..I 42 2801
..BRANCH 0040R

THETA	INTEGRATED INTENSITY	INTENSITY	RATE OF CHANGE	PROBABLE ERROR	
22.749	5.779	5.779	1.000	.010	94.23
22.999	11.854	6.074	.048	.010	4.58
23.249	18.394	6.539	.071	.010	6.82
23.499	25.147	6.753	.031	.010	3.01
23.749	44.073	18.926	.643	.006	100.42
23.999	57.723	13.649	-.386	.007	-50.14
24.249	64.257	6.533	-1.089	.011	-95.62
24.499	70.695	6.438	-.014	.011	-1.26
24.749	77.306	6.611	.026	.011	2.22
24.999	84.176	6.870	.037	.011	3.17
25.249	91.943	7.766	.115	.011	10.13
25.499	101.624	9.680	.197	.010	19.00
25.749	112.717	11.092	.127	.009	12.85
25.999	164.466	51.749	.785	.004	168.17
26.249	216.513	52.046	.005	.004	1.20
26.499	232.764	16.251	-2.202	.008	-254.55
26.749	290.601	57.836	.719	.004	153.87
26.999	335.683	45.081	-.282	.005	-52.47
27.249	350.017	14.334	-2.145	.009	-220.24
27.499	363.018	13.001	-.102	.010	-9.84
27.749	375.655	12.637	-.028	.010	-2.67
27.999	388.056	12.400	-.019	.011	-1.72
28.249	400.269	12.213	-.015	.011	-1.35
28.499	412.483	12.213	0.000	.011	0.00
28.749	425.953	13.469	.093	.011	8.31
28.999	440.422	14.469	.069	.011	6.27
29.249	455.827	15.404	.060	.010	5.58
29.499	501.006	45.178	.659	.006	101.91
29.749	556.035	55.028	.178	.005	30.00
29.999	574.603	18.568	-1.963	.010	-188.10
30.249	590.002	15.398	-.205	.011	-17.68
30.499	605.412	15.409	0.000	.011	.06
30.749	621.854	16.442	.062	.011	5.40
30.999	639.062	17.208	.044	.011	3.86
31.249	657.045	17.983	.043	.011	3.76
31.499	715.670	58.624	.693	.006	107.73
31.749	777.670	61.999	.054	.006	8.56
31.999	800.659	22.989	-1.696	.010	-160.31
32.249	818.223	17.564	-.308	.012	-25.13
32.499	835.003	16.779	-.046	.012	-3.66
32.749	851.694	16.691	-.005	.012	-.40
32.999	867.543	15.849	-.053	.013	-3.92
33.249	883.606	16.062	.013	.013	.97

33.499	899.649	16.042	-.001	.013	-.09
33.749	916.766	17.117	.062	.013	4.62
33.999	934.242	17.475	.020	.013	1.50
34.249	952.098	17.855	.021	.013	1.55
34.499	971.212	19.114	.065	.013	4.91
34.749	1010.939	39.727	.518	.009	55.09
34.999	1042.008	31.068	-.278	.010	-25.85
35.249	1062.632	20.624	-.506	.013	-37.83
35.499	1084.535	21.903	.058	.013	4.44
35.749	1107.582	23.046	.049	.012	3.82
35.999	1132.791	25.209	.085	.012	6.84
36.249	1160.281	27.490	.082	.012	6.83
36.499	1232.562	72.280	.619	.007	81.81
36.749	1318.059	85.497	.154	.007	21.94
36.999	1372.576	54.516	-.568	.008	-63.72
37.249	1448.843	76.267	.285	.007	37.41
37.499	1501.004	52.161	-.462	.009	-49.59
37.749	1528.880	27.876	-.871	.012	-67.61
37.999	1554.811	25.930	-.075	.013	-5.55
38.249	1580.830	26.018	.003	.013	.24
38.499	1607.135	26.304	.010	.013	.79
38.749	1633.429	26.294	0.000	.013	-.02
38.999	1659.750	26.321	.001	.013	.07
39.249	1687.648	27.897	.056	.013	4.12
39.499	1739.039	51.390	.457	.010	44.82
39.749	1786.420	47.381	-.084	.010	-7.89
39.999	1825.337	38.917	-.217	.011	-18.22
40.249	1853.952	28.614	-.360	.014	-25.65
40.499	1882.298	28.346	-.009	.014	-.66
40.749	1911.295	28.997	.022	.014	1.58
40.999	1941.186	29.891	.029	.014	2.12
41.249	1990.815	49.628	.397	.011	36.12
41.499	2042.521	51.705	.040	.010	3.69
41.749	2091.252	48.730	-.061	.011	-5.41
41.999	2152.074	60.822	.198	.010	19.53
42.249	2200.583	48.509	-.253	.011	-22.11
42.499	2232.443	31.859	-.522	.014	-36.63
42.749	2261.675	29.232	-.089	.014	-5.99
42.999	2291.218	29.543	.010	.015	.70
43.249	2321.601	30.382	.027	.014	1.85
43.499	2351.699	30.098	-.009	.015	-.62
43.749	2381.860	30.160	.002	.015	.13
43.999	2412.304	30.444	.009	.015	.61
44.249	2452.509	40.205	.242	.013	18.27
44.499	2488.580	36.070	-.114	.014	-8.12
44.749	2524.444	35.863	-.005	.014	-.40
44.999	2557.935	33.491	-.070	.014	-4.78

45.249	2591.726	33.791	.008	.014	.59
45.499	2628.612	36.885	.083	.014	5.88
45.749	2668.690	40.078	.079	.013	5.79
45.999	2758.240	89.549	.552	.009	59.81
46.249	2818.155	59.915	-.494	.011	-43.61
46.499	2893.251	75.095	.202	.010	19.86
46.749	2945.317	52.066	-.442	.012	-36.05
46.999	2995.926	50.609	-.028	.012	-2.30
47.249	3035.117	39.190	-.291	.014	-20.44
47.499	3073.609	38.492	-.018	.014	-1.25
47.749	3112.565	38.956	.011	.014	.82
47.999	3150.793	38.228	-.019	.014	-1.30
48.249	3190.202	39.408	.029	.014	2.07
48.499	3230.826	40.624	.029	.014	2.10
48.749	3281.926	51.100	.205	.012	16.09
48.999	3370.933	89.006	.425	.009	44.00
49.249	3437.733	66.800	-.332	.011	-29.67
49.499	3488.967	51.234	-.303	.012	-23.69
49.749	3532.984	44.017	-.163	.013	-11.81
49.999	3575.755	42.770	-.029	.014	-2.06
50.249	3620.016	44.261	.033	.013	2.42
50.499	3676.326	56.310	.213	.012	17.32
50.749	3783.967	107.640	.476	.008	53.29
50.999	3852.910	68.942	-.561	.011	-50.10
51.249	3916.081	63.171	-.091	.011	-7.79
51.499	3958.170	42.089	-.500	.014	-34.82
51.749	3998.989	40.819	-.031	.014	-2.12
51.999	4038.539	39.550	-.032	.014	-2.15
52.249	4078.575	40.035	.012	.014	.82
52.499	4117.832	39.257	-.019	.014	-1.32
52.749	4157.650	39.817	.014	.014	.94
52.999	4196.818	39.168	-.016	.014	-1.10
53.249	4236.451	39.633	.011	.014	.78
53.499	4278.751	42.300	.063	.014	4.37
53.749	4324.303	45.552	.071	.013	5.13
53.999	4367.634	43.330	-.051	.014	-3.59
54.249	4410.667	43.033	-.006	.014	-.48
54.499	4452.548	41.880	-.027	.014	-1.89
54.749	4494.079	41.530	-.008	.014	-.57
54.999	4536.261	42.182	.015	.014	1.06
55.249	4581.148	44.887	.060	.013	4.30
55.499	4645.027	63.879	.297	.011	25.36

..I 104 2803 99.00 77K
..BRANCH 0040R

THETA	INTEGRATED INTENSITY	INTENSITY	RATE OF CHANGE	PROBABLE ERROR	
49.749	34.173	34.173	1.000	.015	63.52
49.999	63.321	29.147	-.172	.017	-10.09
50.249	91.951	28.629	-.018	.017	-1.04
50.499	124.647	32.696	.124	.016	7.67
50.749	188.057	63.409	.484	.011	41.54
50.999	259.334	71.276	.110	.011	10.01
51.249	319.704	60.369	-.180	.011	-15.06
51.499	359.905	40.201	-.501	.014	-34.08
51.749	388.603	28.697	-.400	.017	-22.98
51.999	416.775	28.172	-.018	.017	-1.05
52.249	443.791	27.015	-.042	.018	-2.37
52.499	470.758	26.966	-.001	.018	-.10
52.749	496.932	26.174	-.030	.018	-1.65
52.999	523.091	26.158	0.000	.018	-.03
53.249	549.894	26.803	.024	.018	1.32
53.499	576.278	26.384	-.015	.018	-.87

..I 105 2803 99.00 77K
..BRANCH 0040R

THETA	INTEGRATED INTENSITY	INTENSITY	RATE OF CHANGE	PROBABLE ERROR	
49.749	34.292	34.292	1.000	.015	63.63
49.999	62.913	28.621	-.198	.017	-11.49
50.249	91.504	28.590	-.001	.017	-.06
50.499	123.574	32.069	.108	.016	6.62
50.749	186.745	63.171	.492	.011	42.14
50.999	255.130	68.385	.076	.011	6.77
51.249	315.214	60.084	-.138	.012	-11.49
51.499	354.856	39.641	-.515	.014	-34.79
51.749	383.749	28.893	-.371	.017	-21.40
51.999	410.682	26.932	-.072	.018	-4.04
52.249	438.002	27.320	.014	.017	.79
52.499	464.936	26.934	-.014	.018	-.79
52.749	491.111	26.174	-.029	.018	-1.58
52.999	516.900	25.789	-.014	.018	-.80

..I 100 2803 99.00 300
..BRANCH 0040R

THETA	INTEGRATED INTENSITY	INTENSITY	RATE OF CHANGE	PROBABLE ERROR	
49.749	33.555	33.555	1.000	.015	62.94
49.999	65.974	32.418	-.035	.016	-2.16
50.249	99.231	33.256	.025	.016	1.57
50.499	139.333	40.101	.170	.014	11.66
50.749	203.513	64.180	.375	.011	32.37
50.999	251.592	48.079	-.334	.013	-24.96
51.249	297.973	46.381	-.036	.013	-2.67
51.499	331.530	33.556	-.382	.016	-23.72
51.749	362.945	31.415	-.068	.016	-4.08
51.999	393.730	30.784	-.020	.016	-1.21
52.249	424.404	30.674	-.003	.016	-.21
52.499	453.552	29.148	-.052	.017	-3.01
52.749	483.109	29.557	.013	.017	.80
52.999	512.516	29.406	-.005	.017	-.29

..I 102 2803 99.00 300
..BRANCH 0040R

THETA	INTEGRATED INTENSITY	INTENSITY	RATE OF CHANGE	PROBABLE ERROR	
49.749	32.564	32.564	1.000	.016	62.00
49.999	63.528	30.963	-.051	.016	-3.11
50.249	96.456	32.927	.059	.016	3.70
50.499	137.336	40.880	.194	.014	13.42
50.749	201.859	64.523	.366	.011	31.70
50.999	249.639	47.779	-.350	.013	-26.04
51.249	295.036	45.397	-.052	.013	-3.79
51.499	329.212	34.175	-.328	.015	-20.57
51.749	360.300	31.088	-.099	.016	-5.92
51.999	391.266	30.965	-.003	.016	-.23
52.249	421.267	30.001	-.032	.017	-1.88
52.499	450.865	29.598	-.013	.017	-.79
52.749	480.558	29.693	.003	.017	.18
52.999	509.614	29.055	-.021	.017	-1.26
53.249	540.588	30.973	.061	.016	3.67
53.499	570.847	30.259	-.023	.017	-1.38

..I 101 2803 99.00 300
..BRANCH 0040R

THETA	INTEGRATED INTENSITY	INTENSITY	RATE OF CHANGE	PROBABLE ERROR	
49.749	32.852	32.852	1.000	.016	62.28
49.999	64.652	31.800	-.033	.016	-2.02
50.249	97.844	33.191	.041	.016	2.61
50.499	137.207	39.363	.156	.014	10.61
50.749	201.803	64.596	.390	.011	33.81
50.999	249.263	47.460	-.361	.013	-26.74
51.249	295.778	46.514	-.020	.013	-1.48
51.499	327.777	31.999	-.453	.016	-27.49
51.749	359.030	31.253	-.023	.016	-1.42
51.999	389.962	30.931	-.010	.016	-.61
52.249	419.726	29.764	-.039	.017	-2.28
52.499	450.147	30.420	.021	.016	1.27
52.749	480.708	30.561	.004	.016	.27
52.999	510.660	29.951	-.020	.017	-1.18
53.249	540.524	29.864	-.002	.017	-.17
53.499	570.474	29.950	.002	.017	.16
53.749	601.421	30.947	.032	.016	1.90

..I 103 2803 99.00 300
..BRANCH 0040R

THETA	INTEGRATED INTENSITY	INTENSITY	RATE OF CHANGE	PROBABLE ERROR	
49.749	33.242	33.242	1.000	.015	62.64
49.999	66.177	32.935	-.009	.016	-.58
50.249	99.250	33.073	.004	.016	.25
50.499	139.170	39.920	.171	.014	11.69
50.749	204.616	65.445	.390	.011	33.98
50.999	251.184	46.567	-.405	.013	-29.74
51.249	296.214	45.030	-.034	.013	-2.45
51.499	329.159	32.944	-.366	.016	-22.56
51.749	361.677	32.518	-.013	.016	-.79
51.999	391.115	29.438	-.104	.017	-6.06
52.249	421.340	30.224	.025	.017	1.52
52.499	451.817	30.477	.008	.016	.48
52.749	480.649	28.831	-.057	.017	-3.27
52.999	510.014	29.364	.018	.017	1.04
53.249	539.635	29.621	.008	.017	.50
53.499	571.027	31.391	.056	.016	3.36
53.749	602.797	31.770	.011	.016	.71
53.999	633.790	30.992	-.025	.016	-1.48
54.249	665.495	31.704	.022	.016	1.34

..I 106 2803 99.00 77K
..BRANCH 0040R

THETA	INTEGRATED INTENSITY	INTENSITY	RATE OF CHANGE	PROBABLE ERROR	
49.749	33.166	33.166	1.000	.015	62.57
49.999	61.701	28.534	-.162	.017	-9.39
50.249	90.453	28.752	.007	.017	.43
50.499	122.636	32.182	.106	.016	6.52
50.749	184.714	62.077	.481	.011	40.86
50.999	255.399	70.685	.121	.011	11.00
51.249	314.626	59.227	-.193	.012	-15.97
51.499	353.590	38.963	-.520	.014	-34.78
51.749	382.800	29.210	-.333	.017	-19.31
51.999	411.362	28.561	-.022	.017	-1.29
52.249	437.558	26.195	-.090	.018	-4.93
52.499	464.868	27.310	.040	.017	2.27
52.749	491.107	26.238	-.040	.018	-2.23
52.999	517.372	26.264	0.000	.018	.05
53.249	543.182	25.810	-.017	.018	-.95

..I 107 2803 99.00 77K
..BRANCH 0040R

THETA	INTEGRATED INTENSITY	INTENSITY	RATE OF CHANGE	PROBABLE ERROR	
49.749	34.868	34.868	1.000	.015	64.16
49.999	65.034	30.166	-.155	.016	-9.28
50.249	94.724	29.689	-.016	.016	-.94
50.499	126.176	31.452	.056	.016	3.39
50.749	188.050	61.873	.491	.011	41.65
50.999	258.024	69.974	.115	.011	10.41
51.249	316.585	58.561	-.194	.012	-16.00
51.499	357.938	41.352	-.416	.014	-28.67
51.749	386.637	28.699	-.440	.017	-25.28
51.999	414.459	27.822	-.031	.017	-1.77
52.249	442.769	28.309	.017	.017	.97
52.499	468.896	26.127	-.083	.018	-4.55
52.749	495.941	27.045	.033	.018	1.88
52.999	523.180	27.238	.007	.017	.39
53.249	549.967	26.786	-.016	.018	-.93
53.499	577.020	27.053	.009	.018	.54
53.749	606.242	29.221	.074	.017	4.27
53.999	635.697	29.455	.007	.017	.45
54.249	664.403	28.705	-.026	.017	-1.49
54.499	693.339	28.936	.007	.017	.45
54.749	721.469	28.130	-.028	.017	-1.61
54.999	750.363	28.893	.026	.017	1.51
55.249	780.517	30.154	.041	.017	2.45
55.499	813.322	32.805	.080	.016	4.94
55.749	859.817	46.494	.294	.013	21.44
55.999	897.645	37.828	-.229	.015	-15.06

..I 108 2803 99.00 300K
..BRANCH 0040R

THETA	INTEGRATED INTENSITY	INTENSITY	RATE OF CHANGE	PROBABLE ERROR	
49.749	32.666	32.666	1.000	.016	62.10
49.999	64.720	32.053	-.019	.016	-1.17
50.249	97.298	32.578	.016	.016	.99
50.499	135.643	38.344	.150	.014	10.05
50.749	201.523	65.880	.417	.011	36.54
50.999	250.534	49.011	-.344	.013	-25.90
51.249	298.113	47.578	-.030	.013	-2.22
51.499	331.567	33.453	-.422	.016	-26.16
51.749	362.833	31.265	-.069	.016	-4.18
51.999	393.529	30.695	-.018	.016	-1.10
52.249	423.983	30.454	-.007	.016	-.46
52.499	454.699	30.716	.008	.016	.50
52.749	484.938	30.238	-.015	.017	-.92
52.999	514.711	29.772	-.015	.017	-.91

..I 109 2803 99.00 300K
..BRANCH 0040R

THETA	INTEGRATED INTENSITY	INTENSITY	RATE OF CHANGE	PROBABLE ERROR	
49.749	32.962	32.962	1.000	.016	62.38
49.999	65.665	32.703	-.007	.016	-.49
50.249	98.548	32.882	.005	.016	.33
50.499	137.892	39.343	.164	.014	11.11
50.749	204.203	66.311	.406	.011	35.67
50.999	251.323	47.120	-.407	.013	-30.05
51.249	299.076	47.753	.013	.013	.98
51.499	332.575	33.498	-.425	.016	-26.39
51.749	364.191	31.615	-.059	.016	-3.58
51.999	394.820	30.628	-.032	.016	-1.90
52.249	424.800	29.980	-.021	.017	-1.26
52.499	454.627	29.826	-.005	.017	-.30
52.749	484.708	30.081	.008	.017	.49
52.999	513.856	29.147	-.032	.017	-1.84
53.249	543.836	29.980	.027	.017	1.62
53.499	574.482	30.646	.021	.016	1.28
53.749	606.722	32.239	.049	.016	2.98

..I 110 2803 99.00 300K
..BRANCH 0040R

THETA	INTEGRATED INTENSITY	INTENSITY	RATE OF CHANGE	PROBABLE ERROR	
49.749	31.929	31.929	1.000	.016	61.40
49.999	62.921	30.992	-.030	.016	-1.82
50.249	95.927	33.005	.060	.016	3.78
50.499	135.039	39.112	.156	.014	10.53
50.749	200.849	65.809	.405	.011	35.44
50.999	246.857	46.008	-.430	.013	-31.38
51.249	293.125	46.267	.005	.013	.40
51.499	326.550	33.425	-.384	.016	-23.80
51.749	358.784	32.234	-.036	.016	-2.24
51.999	388.815	30.030	-.073	.017	-4.29
52.249	419.719	30.903	.028	.016	1.67
52.499	449.422	29.702	-.040	.017	-2.35
52.749	480.468	31.046	.043	.016	2.57
52.999	509.299	28.830	-.076	.017	-4.40
53.249	539.540	30.241	.046	.017	2.73
53.499	569.934	30.393	.005	.017	.29
53.749	601.228	31.294	.028	.016	1.71
53.999	632.015	30.786	-.016	.016	-.97
54.249	663.779	31.764	.030	.016	1.84
54.499	694.573	30.794	-.031	.016	-1.86
54.749	725.421	30.848	.001	.016	.10
54.999	756.484	31.062	.006	.016	.41
55.249	788.748	32.263	.037	.016	2.25
55.499	829.512	40.764	.208	.014	14.21

..I 111 2803 99.00 300K
..BRANCH 0040R

THETA	INTEGRATED INTENSITY	INTENSITY	RATE OF CHANGE	PROBABLE ERROR	
49.749	32.437	32.437	1.000	.016	61.88
49.999	65.306	32.868	.013	.016	.81
50.249	99.327	34.021	.033	.015	2.13
50.499	140.114	40.786	.165	.014	11.43
50.749	206.636	66.522	.386	.011	33.98
50.999	254.632	47.995	-.385	.013	-28.74
51.249	300.413	45.781	-.048	.013	-3.51
51.499	334.975	34.561	-.324	.015	-20.45
51.749	367.106	32.130	-.075	.016	-4.59
51.999	397.258	30.152	-.065	.017	-3.85
52.249	428.776	31.518	.043	.016	2.59
52.499	459.204	30.427	-.035	.016	-2.11
52.749	489.379	30.174	-.008	.017	-.49
52.999	520.030	30.651	.015	.016	.91
53.249	551.062	31.031	.012	.016	.72
53.499	582.413	31.351	.010	.016	.60
53.749	614.853	32.439	.033	.016	2.03
53.999	646.239	31.386	-.033	.016	-2.00
54.249	678.203	31.963	.018	.016	1.08
54.499	709.536	31.333	-.020	.016	-1.20

..I 112 2803 99.00 300K
..BRANCH 0040R

THETA	INTEGRATED INTENSITY	INTENSITY	RATE OF CHANGE	PROBABLE ERROR	
25.249	6.229	6.229	1.000	.012	78.58
25.499	14.155	7.925	.213	.011	18.61
25.749	22.747	8.592	.077	.011	6.89
25.999	45.544	22.797	.623	.007	88.52
26.249	97.537	51.992	.561	.004	118.25
26.499	111.948	14.411	-2.607	.009	-283.79
26.749	142.369	30.420	.526	.006	81.68
26.999	185.431	43.061	.293	.005	53.21
27.249	198.466	13.034	-2.303	.010	-225.56
27.499	208.755	10.289	-.266	.011	-22.78
27.749	218.835	10.079	-.020	.012	-1.73
27.999	229.134	10.298	.021	.012	1.75
28.249	239.200	10.066	-.023	.012	-1.84
28.499	249.137	9.937	-.012	.012	-1.01
28.749	259.752	10.614	.063	.012	5.04
28.999	270.885	11.133	.046	.012	3.71
29.249	282.444	11.558	.036	.012	2.92
29.499	300.061	17.617	.343	.010	33.21
29.749	340.317	40.256	.562	.006	80.62
29.999	358.285	17.968	-1.240	.010	-116.89
30.249	370.157	11.871	-.513	.013	-38.74
30.499	381.996	11.839	-.002	.013	-.19
30.749	394.257	12.260	.034	.013	2.55
30.999	406.814	12.556	.023	.013	1.74
31.249	419.995	13.181	.047	.013	3.54
31.499	442.037	22.042	.402	.010	38.30
31.749	480.376	38.339	.425	.008	52.63
31.999	500.386	20.009	-.916	.011	-80.73
32.249	514.409	14.022	-.426	.013	-31.04
32.499	527.535	13.125	-.068	.014	-4.73
32.749	540.787	13.252	.009	.014	.65
32.999	553.639	12.851	-.031	.015	-2.07
33.249	566.681	13.041	.014	.015	.96
33.499	579.540	12.859	-.014	.015	-.91
33.749	593.894	14.353	.104	.014	7.01
33.999	608.658	14.763	.027	.014	1.87
34.249	623.760	15.102	.022	.014	1.50
34.499	640.051	16.290	.072	.014	5.02
34.749	679.370	39.319	.585	.009	61.86
34.999	714.811	35.441	-.109	.010	-10.84
35.249	735.056	20.245	-.750	.013	-55.55
35.499	753.103	18.046	-.121	.014	-8.41
35.749	771.051	17.947	-.005	.014	-.37

35.999	790.977	19.926	.099	.014	7.04
36.249	812.442	21.465	.071	.013	5.21
36.499	850.369	37.926	.434	.010	41.50
36.749	922.198	71.828	.471	.007	61.42
36.999	970.490	48.292	-.487	.009	-51.43
37.249	1014.644	44.154	-.093	.010	-9.35
37.499	1048.829	34.185	-.291	.011	-25.33
37.749	1071.602	22.772	-.501	.014	-35.15
37.999	1091.987	20.385	-.117	.015	-7.68
38.249	1112.838	20.850	.022	.015	1.46
38.499	1133.701	20.862	0.000	.015	.03
38.749	1154.273	20.571	-.014	.015	-.90
38.999	1175.640	21.367	.037	.015	2.40
39.249	1196.859	21.218	-.007	.015	-.44
39.499	1224.589	27.730	.234	.013	16.91
39.749	1259.160	34.571	.197	.012	15.76
39.999	1290.317	31.156	-.109	.013	-8.21
40.249	1313.108	22.791	-.367	.015	-23.33
40.499	1335.132	22.023	-.034	.016	-2.16
40.749	1357.619	22.486	.020	.016	1.27
40.999	1380.070	22.450	-.001	.016	-.09
41.249	1407.817	27.747	.190	.014	12.96
41.499	1444.658	36.841	.246	.012	19.16
41.749	1477.563	32.904	-.119	.013	-8.71
41.999	1518.939	41.375	.204	.012	16.59
42.249	1552.393	33.454	-.236	.013	-17.13
42.499	1578.553	26.159	-.278	.015	-17.71
42.749	1602.581	24.027	-.088	.016	-5.36
42.999	1626.506	23.925	-.004	.016	-.25
43.249	1649.857	23.350	-.024	.017	-1.44
43.499	1673.048	23.191	-.006	.017	-.39
43.749	1696.852	23.803	.025	.017	1.50
43.999	1720.829	23.977	.007	.017	.42
44.249	1747.349	26.519	.095	.016	5.86
44.499	1774.626	27.276	.027	.016	1.71
44.749	1801.905	27.278	0.000	.016	0.00
44.999	1828.170	26.265	-.038	.016	-2.30
45.249	1855.654	27.483	.044	.016	2.69
45.499	1884.347	28.692	.042	.016	2.60
45.749	1915.709	31.362	.085	.015	5.47
45.999	1977.606	61.897	.493	.011	44.40
46.249	2028.415	50.808	-.218	.012	-17.71
46.499	2087.717	59.301	.143	.011	12.50
46.749	2138.264	50.547	-.173	.012	-13.90
46.999	2182.589	44.325	-.140	.013	-10.51
47.249	2216.509	33.919	-.306	.015	-20.02
47.499	2247.108	30.599	-.108	.016	-6.70

47.749	2277.278	30.170	-.014	.016	-.87
47.999	2307.994	30.715	.017	.016	1.09
48.249	2339.057	31.062	.011	.016	.68
48.499	2370.476	31.419	.011	.016	.70
48.749	2407.328	36.851	.147	.014	9.82
48.999	2468.273	60.944	.395	.011	33.80
49.249	2514.753	46.480	-.311	.013	-23.17
49.499	2556.985	42.231	-.100	.014	-7.12
49.749	2589.687	32.702	-.291	.016	-18.10
49.999	2622.277	32.590	-.003	.016	-.21
50.249	2654.279	32.001	-.018	.016	-1.12
50.499	2692.498	38.219	.162	.014	10.85
50.749	2757.955	65.456	.416	.011	36.26
50.999	2806.175	48.220	-.357	.013	-26.68
51.249	2854.589	48.413	.003	.013	.29
51.499	2889.461	34.871	-.388	.015	-24.57
51.749	2922.397	32.936	-.058	.016	-3.61
51.999	2954.760	32.363	-.017	.016	-1.07
52.249	2990.967	36.206	.106	.015	6.82
52.499	3021.050	30.082	-.203	.017	-11.92
52.749	3051.836	30.786	.022	.016	1.35
52.999	3082.607	30.771	0.000	.016	-.02
53.249	3113.200	30.592	-.005	.016	-.34
53.499	3145.005	31.805	.038	.016	2.29
53.749	3178.180	33.174	.041	.016	2.53
53.999	3209.123	30.943	-.072	.016	-4.27
54.249	3241.215	32.091	.035	.016	2.15
54.499	3272.831	31.615	-.015	.016	-.90
54.749	3303.536	30.705	-.029	.016	-1.75
54.999	3334.703	31.166	.014	.016	.88
55.249	3369.576	34.873	.106	.015	6.69
55.499	3409.705	40.128	.130	.014	8.85
55.749	3449.132	39.427	-.017	.014	-1.19
55.999	3491.841	42.708	.076	.014	5.36
56.249	3540.107	48.266	.115	.013	8.56
56.499	3578.443	38.336	-.259	.015	-17.17
56.749	3619.009	40.565	.054	.014	3.75
56.999	3653.963	34.954	-.160	.015	-10.19
57.249	3687.083	33.119	-.055	.016	-3.42
57.499	3721.035	33.952	.024	.015	1.53
57.749	3754.223	33.187	-.023	.016	-1.43
57.999	3788.406	34.183	.029	.015	1.83
58.249	3823.338	34.932	.021	.015	1.37
58.499	3862.250	38.912	.102	.014	6.91
58.749	3913.808	51.557	.245	.012	19.12
58.999	3956.040	42.231	-.220	.014	-15.61

..I 113 2803 50.00 77K
..BRANCH 0040R

THETA	INTEGRATED INTENSITY	INTENSITY	RATE OF CHANGE	PROBABLE ERROR	
25.249	4.774	4.774	1.000	.014	68.79
25.499	11.196	6.421	.256	.012	20.07
25.749	18.381	7.185	.106	.012	8.63
25.999	30.104	11.722	.387	.009	39.43
26.249	90.269	60.164	.805	.004	182.40
26.499	111.564	21.294	-1.825	.007	-241.47
26.749	128.336	16.772	-.269	.008	-31.07
26.999	184.886	56.550	.703	.004	146.12
27.249	201.658	16.771	-2.371	.009	-263.42
27.499	210.453	8.795	-.906	.012	-71.60
27.749	219.331	8.877	.009	.012	.71
27.999	228.033	8.702	-.020	.013	-1.51
28.249	236.360	8.326	-.045	.013	-3.28
28.499	245.041	8.681	.040	.013	2.98
28.749	253.968	8.926	.027	.013	1.99
28.999	263.735	9.767	.086	.013	6.41
29.249	273.782	10.047	.027	.013	2.07
29.499	286.238	12.455	.193	.012	15.70
29.749	329.486	43.248	.711	.006	105.80
29.999	354.803	25.316	-.708	.008	-79.23
30.249	365.273	10.469	-1.418	.014	-100.45
30.499	375.247	9.973	-.049	.014	-3.38
30.749	386.268	11.021	.095	.014	6.70
30.999	397.619	11.351	.029	.014	2.04
31.249	408.984	11.364	.001	.014	.08
31.499	423.798	14.814	.232	.012	18.19
31.749	467.596	43.797	.661	.007	87.57
31.999	495.156	27.560	-.589	.009	-60.94
32.249	508.451	13.294	-1.073	.014	-75.96
32.499	519.949	11.498	-.156	.015	-10.13
32.749	531.049	11.099	-.035	.015	-2.25
32.999	542.241	11.192	.008	.016	.51
33.249	552.930	10.688	-.047	.016	-2.82
33.499	564.280	11.350	.058	.016	3.54
33.749	575.799	11.518	.014	.016	.88
33.999	588.678	12.878	.105	.015	6.65
34.249	601.715	13.036	.012	.016	.75
34.499	615.674	13.959	.066	.015	4.21
34.749	641.257	25.582	.454	.011	38.71
34.999	689.933	48.676	.474	.008	55.09
35.249	717.703	27.769	-.752	.011	-65.26
35.499	732.483	14.779	-.878	.015	-54.93
35.749	747.982	15.499	.046	.015	2.93

35.999	764.436	16.453	.058	.015	3.73
36.249	783.037	18.601	.115	.014	7.81
36.499	807.724	24.687	.246	.012	19.02
36.749	899.872	92.147	.732	.006	107.92
36.999	962.395	62.522	-.473	.008	-56.90
37.249	1003.772	41.376	-.511	.010	-49.38
37.499	1044.851	41.079	-.007	.010	-.68
37.749	1071.755	26.903	-.526	.013	-40.17
37.999	1090.137	18.382	-.463	.016	-28.90
38.249	1107.609	17.471	-.052	.016	-3.13
38.499	1125.207	17.598	.007	.016	.42
38.749	1143.287	18.080	.026	.016	1.59
38.999	1161.048	17.760	-.017	.017	-1.05
39.249	1179.618	18.570	.043	.016	2.59
39.499	1200.819	21.201	.124	.015	7.81
39.749	1241.110	40.290	.473	.011	40.73
39.999	1273.640	32.530	-.238	.013	-18.27
40.249	1296.027	22.387	-.453	.015	-28.54
40.499	1315.182	19.155	-.168	.017	-9.75
40.749	1334.482	19.300	.007	.017	.43
40.999	1354.125	19.643	.017	.017	1.00
41.249	1375.202	21.076	.068	.016	4.02
41.499	1415.638	40.435	.478	.012	38.94
41.749	1449.359	33.721	-.199	.013	-14.68
41.999	1490.274	40.915	.175	.012	14.17
42.249	1527.337	37.062	-.103	.013	-7.91
42.499	1560.303	32.965	-.124	.014	-8.86
42.749	1581.595	21.291	-.548	.017	-31.20
42.999	1602.044	20.449	-.041	.018	-2.28
43.249	1622.286	20.242	-.010	.018	-.56
43.499	1642.324	20.038	-.010	.018	-.55
43.749	1663.031	20.706	.032	.018	1.76
43.999	1683.720	20.688	0.000	.018	-.04
44.249	1705.525	21.805	.051	.018	2.83
44.499	1732.323	26.797	.186	.016	11.37
44.749	1756.750	24.427	-.097	.017	-5.62
44.999	1780.563	23.812	-.025	.017	-1.47
45.249	1803.617	23.053	-.032	.017	-1.83
45.499	1827.566	23.949	.037	.017	2.11
45.749	1853.170	25.603	.064	.017	3.75
45.999	1894.182	41.012	.375	.013	27.52
46.249	1974.100	79.917	.486	.009	49.57
46.499	2036.954	62.854	-.271	.011	-24.41
46.749	2110.357	73.402	.143	.010	13.90
46.999	2155.692	45.335	-.619	.013	-46.90
47.249	2196.194	40.502	-.119	.014	-8.51
47.499	2249.661	53.466	.242	.012	19.79

47.749	2275.694	26.033	-1.053	.017	-59.82
47.999	2301.489	25.794	-.009	.017	-.52
48.249	2326.798	25.308	-.019	.017	-1.06
48.499	2352.140	25.342	.001	.018	.07
48.749	2380.769	28.629	.114	.017	6.74
48.999	2438.019	57.249	.499	.012	41.42
49.249	2498.283	60.264	.050	.011	4.24
49.499	2552.909	54.625	-.103	.012	-8.31
49.749	2587.088	34.179	-.598	.015	-38.00
49.999	2616.372	29.283	-.167	.017	-9.80
50.249	2644.071	27.699	-.057	.017	-3.25
50.499	2675.403	31.332	.115	.016	7.00
50.749	2735.991	60.588	.482	.011	40.48
50.999	2807.693	71.702	.155	.010	14.11
51.249	2866.339	58.645	-.222	.012	-18.29
51.499	2906.795	40.456	-.449	.014	-30.64
51.749	2935.102	28.307	-.429	.017	-24.44
51.999	2962.633	27.530	-.028	.017	-1.58
52.249	2989.188	26.554	-.036	.018	-2.02
52.499	3015.405	26.217	-.012	.018	-.70
52.749	3041.221	25.816	-.015	.018	-.84
52.999	3067.227	26.006	.007	.018	.39
53.249	3093.097	25.869	-.005	.018	-.28
53.499	3119.736	26.639	.028	.018	1.59
53.749	3148.356	28.619	.069	.017	3.94
53.999	3177.586	29.230	.020	.017	1.20
54.249	3206.474	28.888	-.011	.017	-.67
54.499	3234.523	28.048	-.029	.017	-1.69
54.749	3262.355	27.832	-.007	.017	-.43
54.999	3290.287	27.932	.003	.017	.20
55.249	3318.948	28.661	.025	.017	1.45
55.499	3350.679	31.730	.096	.016	5.81
55.749	3396.796	46.117	.311	.013	22.63
55.999	3433.230	36.433	-.265	.015	-17.15
56.249	3487.903	54.672	.333	.012	26.39
56.499	3539.306	51.402	-.063	.013	-4.88
56.749	3579.194	39.888	-.288	.014	-19.55
56.999	3619.451	40.256	.009	.014	.62
57.249	3650.635	31.184	-.290	.016	-17.46
57.499	3679.359	28.724	-.085	.017	-4.94
57.749	3708.020	28.661	-.002	.017	-.12
57.999	3736.453	28.433	-.008	.017	-.46
58.249	3766.200	29.746	.044	.016	2.60
58.499	3797.990	31.790	.064	.016	3.92
58.749	3840.970	42.980	.260	.014	18.53
58.999	3902.381	61.410	.300	.011	25.58
59.249	3943.990	41.608	-.475	.014	-33.47
59.499	3992.385	48.395	.140	.013	10.66

59.749	4029.200	36.815	-.314	.015	-20.90
59.999	4060.906	31.705	-.161	.016	-9.96
60.249	4092.145	31.238	-.014	.016	-.91
60.499	4125.761	33.615	.070	.015	4.52
60.749	4175.889	50.128	.329	.012	25.81
60.999	4258.542	82.652	.393	.009	39.70
61.249	4308.122	49.579	-.667	.012	-52.28
61.499	4375.210	67.088	.260	.010	23.86
61.749	4438.403	63.193	-.061	.011	-5.48
61.999	4477.835	39.432	-.602	.014	-42.50
62.249	4518.458	40.622	.029	.013	2.10
62.499	4552.911	34.452	-.179	.015	-11.88
62.749	4582.865	29.954	-.150	.016	-9.32
62.999	4612.479	29.613	-.011	.016	-.71
63.249	4641.990	29.510	-.003	.016	-.21
63.499	4671.706	29.715	.006	.015	.43
63.749	4701.212	29.506	-.007	.015	-.44
63.999	4731.650	30.437	.030	.015	1.94
64.249	4766.279	34.629	.121	.014	8.25
64.499	4808.999	42.719	.189	.013	14.41
64.749	4844.974	35.974	-.187	.014	-13.14
64.999	4878.617	33.643	-.069	.014	-4.71
65.249	4914.932	36.314	.073	.014	5.22
65.499	4947.189	32.257	-.125	.014	-8.45
65.749	4976.521	29.332	-.099	.015	-6.41
65.999	5006.404	29.882	.018	.015	1.20
66.249	5037.323	30.919	.033	.014	2.23
66.499	5073.571	36.247	.146	.013	10.66
66.749	5126.626	53.055	.316	.011	27.92
66.999	5177.679	51.053	-.039	.011	-3.40
67.249	5218.399	40.719	-.253	.012	-19.78
67.499	5272.342	53.943	.245	.011	22.10
67.749	5334.082	61.740	.126	.010	12.24

..I127 2804 50.00 300
..BRANCH 0040R

THETA	INTEGRATED INTENSITY	INTENSITY	RATE OF CHANGE	PROBABLE ERROR	
25.249	5.153	5.153	1.000	.013	71.47
25.499	11.388	6.235	.173	.012	13.39
25.749	18.398	7.009	.110	.012	8.86
25.999	32.399	14.000	.499	.008	55.59
26.249	81.365	48.965	.714	.004	145.94
26.499	91.279	9.914	-3.938	.011	-355.55
26.749	115.311	24.031	.587	.007	81.04
26.999	160.397	45.085	.466	.005	86.62
27.249	169.815	9.418	-3.787	.012	-315.20
27.499	178.412	8.597	-.095	.012	-7.44
27.749	186.673	8.260	-.040	.013	-3.06
27.999	195.472	8.798	.061	.013	4.65
28.249	203.715	8.243	-.067	.013	-4.87
28.499	211.987	8.271	.003	.014	.24
28.749	220.911	8.924	.073	.013	5.30
28.999	230.427	9.515	.062	.013	4.57
29.249	240.085	9.658	.014	.013	1.07
29.499	252.316	12.230	.210	.012	16.91
29.749	293.157	40.840	.700	.006	101.16
29.999	308.672	15.515	-1.632	.011	-142.94
30.249	318.800	10.128	-.531	.014	-37.06
30.499	328.610	9.809	-.032	.014	-2.19
30.749	339.598	10.987	.107	.014	7.54
30.999	350.359	10.761	-.021	.014	-1.44
31.249	361.545	11.186	.037	.014	2.61
31.499	376.206	14.660	.237	.012	18.41
31.749	417.841	41.634	.647	.007	83.59
31.999	436.525	18.683	-1.228	.011	-104.61
32.249	448.281	11.756	-.589	.015	-39.22
32.499	458.994	10.712	-.097	.015	-6.09
32.749	470.260	11.265	.049	.015	3.10
32.999	481.308	11.048	-.019	.016	-1.21
33.249	491.892	10.583	-.043	.016	-2.61
33.499	503.070	11.178	.053	.016	3.20
33.749	514.639	11.568	.033	.016	2.04
33.999	528.722	14.082	.178	.015	11.75
34.249	541.165	12.443	-.131	.016	-8.04
34.499	553.784	12.618	.013	.016	.84
34.749	583.030	29.246	.568	.010	51.79
34.999	606.266	23.235	-.258	.012	-20.75
35.249	620.420	14.154	-.641	.016	-39.70
35.499	634.755	14.334	.012	.016	.77
35.749	649.870	15.114	.051	.016	3.22

35.999	665.775	15.905	.049	.015	3.15
36.249	682.805	17.029	.066	.015	4.27
36.499	705.528	22.723	.250	.013	18.54
36.749	771.941	66.412	.657	.007	82.32
36.999	814.609	42.667	-.556	.010	-55.20
37.249	852.923	38.314	-.113	.010	-10.56
37.499	882.440	29.516	-.298	.012	-24.06
37.749	900.272	17.831	-.655	.016	-40.67
37.999	917.368	17.096	-.043	.016	-2.58
38.249	934.365	16.997	-.005	.016	-.34
38.499	951.808	17.442	.025	.016	1.51
38.749	969.158	17.349	-.005	.017	-.31
38.999	986.592	17.433	.004	.017	.27
39.249	1004.510	17.918	.027	.017	1.58
39.499	1025.249	20.738	.135	.016	8.47
39.749	1060.371	35.121	.409	.012	32.87
39.999	1088.337	27.966	-.255	.014	-18.17
40.249	1106.847	18.510	-.510	.017	-29.26
40.499	1125.963	19.115	.031	.017	1.82
40.749	1144.785	18.822	-.015	.017	-.88
40.999	1163.247	18.461	-.019	.017	-1.08
41.249	1183.432	20.185	.085	.017	4.94
41.499	1216.904	33.471	.396	.013	29.37
41.749	1244.254	27.350	-.223	.015	-14.86
41.999	1282.893	38.639	.292	.012	22.88
42.249	1312.137	29.244	-.321	.014	-21.73
42.499	1332.518	20.381	-.434	.017	-24.38
42.749	1352.110	19.591	-.040	.018	-2.19
42.999	1371.309	19.198	-.020	.018	-1.09
43.249	1390.402	19.092	-.005	.018	-.29
43.499	1409.871	19.469	.019	.018	1.03
43.749	1429.792	19.920	.022	.018	1.21
43.999	1449.164	19.371	-.028	.019	-1.48
44.249	1470.981	21.817	.112	.018	6.21
44.499	1492.537	21.555	-.012	.018	-.66
44.749	1514.479	21.941	.017	.018	.96
44.999	1535.812	21.333	-.028	.018	-1.53
45.249	1557.391	21.579	.011	.018	.61
45.499	1579.462	22.070	.022	.018	1.20
45.749	1602.962	23.499	.060	.017	3.38
45.999	1656.777	53.815	.563	.011	47.28
46.249	1685.175	28.397	-.895	.016	-54.33
46.499	1730.071	44.896	.367	.013	27.92
46.749	1774.926	44.855	0.000	.013	-.06
46.999	1811.465	36.539	-.227	.014	-15.47
47.249	1836.718	25.252	-.446	.017	-25.17
47.499	1861.956	25.237	0.000	.017	-.03

47.749	1886.372	24.416	-.033	.018	-1.84
47.999	1911.219	24.846	.017	.018	.95
48.249	1935.669	24.449	-.016	.018	-.88
48.499	1960.740	25.071	.024	.018	1.36
48.749	1988.356	27.616	.092	.017	5.31
48.999	2046.456	58.100	.524	.011	43.80
49.249	2079.761	33.304	-.744	.015	-46.92
49.499	2118.476	38.715	.139	.014	9.47
49.749	2146.016	27.540	-.405	.017	-23.14
49.999	2172.512	26.495	-.039	.017	-2.19
50.249	2198.871	26.358	-.005	.018	-.28
50.499	2226.800	27.929	.056	.017	3.20
50.749	2293.772	66.971	.582	.011	51.38
50.999	2324.615	30.843	-1.171	.016	-69.93
51.249	2370.959	46.344	.334	.013	24.43
51.499	2398.219	27.260	-.700	.017	-39.16
51.749	2424.203	25.984	-.049	.018	-2.67
51.999	2450.498	26.294	.011	.018	.64
52.249	2475.544	25.046	-.049	.018	-2.66
52.499	2500.055	24.510	-.021	.018	-1.15
52.749	2525.101	25.046	.021	.018	1.14
52.999	2550.168	25.067	0.000	.018	.04
53.249	2574.507	24.339	-.029	.019	-1.57
53.499	2599.690	25.182	.033	.018	1.79
53.749	2626.297	26.607	.053	.018	2.94

..I 130 2804 50.00 77
..BRANCH 0040R

THETA	INTEGRATED INTENSITY	INTENSITY	RATE OF CHANGE	PROBABLE ERROR	
25.249	4.449	4.449	1.000	.015	66.40
25.499	10.357	5.908	.246	.013	18.54
25.749	16.442	6.084	.029	.013	2.17
25.999	24.119	7.677	.207	.012	17.10
26.249	74.790	50.671	.848	.004	176.40
26.499	94.473	19.683	-1.574	.007	-200.23
26.749	105.513	11.040	-.782	.010	-73.20
26.999	166.515	61.001	.819	.004	176.71
27.249	180.771	14.255	-3.279	.009	-335.77
27.499	188.589	7.818	-.823	.013	-61.29
27.749	196.217	7.627	-.025	.013	-1.81
27.999	204.455	8.237	.074	.013	5.45
28.249	212.259	7.804	-.055	.014	-3.90
28.499	220.015	7.756	-.006	.014	-.42
28.749	228.091	8.076	.039	.014	2.73
28.999	237.019	8.927	.095	.014	6.79
29.249	246.207	9.187	.028	.014	2.01
29.499	256.165	9.958	.077	.013	5.62
29.749	297.910	41.745	.761	.006	111.17
29.999	323.378	25.467	-.639	.008	-71.71
30.249	332.799	9.420	-1.703	.014	-114.45
30.499	341.800	9.001	-.046	.015	-3.01
30.749	351.717	9.917	.092	.014	6.17
30.999	362.145	10.427	.048	.014	3.30
31.249	372.536	10.391	-.003	.015	-.22
31.499	384.108	11.571	.101	.014	7.04
31.749	430.856	46.748	.752	.007	102.88
31.999	459.094	28.237	-.655	.009	-68.63
32.249	470.541	11.447	-1.466	.015	-96.34
32.499	480.879	10.337	-.107	.016	-6.60
32.749	491.663	10.783	.041	.016	2.56
32.999	502.064	10.401	-.036	.016	-2.20
33.249	512.417	10.352	-.004	.016	-.27
33.499	523.223	10.806	.041	.016	2.49
33.749	533.630	10.406	-.038	.017	-2.20
33.999	544.925	11.294	.078	.016	4.63
34.249	556.328	11.402	.009	.017	.55
34.499	568.431	12.103	.057	.016	3.43
34.749	582.851	14.419	.160	.015	10.27
34.999	619.242	36.390	.603	.009	60.62
35.249	642.340	23.097	-.575	.012	-45.49
35.499	655.120	12.779	-.807	.017	-46.92
35.749	669.364	14.244	.102	.016	6.23

35.999	683.761	14.396	.010	.016	.63
36.249	700.051	16.290	.116	.015	7.36
36.499	716.954	16.902	.036	.015	2.31
36.749	803.174	86.220	.803	.007	114.63
36.999	856.029	52.854	-.631	.009	-69.70
37.249	888.641	32.612	-.620	.011	-53.24
37.499	926.742	38.100	.144	.010	13.21
37.749	953.100	26.358	-.445	.013	-33.62
37.999	968.710	15.609	-.688	.017	-39.56
38.249	984.150	15.440	-.010	.017	-.61
38.499	1000.112	15.961	.032	.017	1.85
38.749	1015.925	15.812	-.009	.017	-.52
38.999	1031.794	15.869	.003	.017	.19
39.249	1047.882	16.087	.013	.018	.74
39.499	1064.774	16.892	.047	.017	2.67
39.749	1107.934	43.160	.608	.011	54.16
39.999	1139.111	31.176	-.384	.013	-28.82
40.249	1156.997	17.886	-.743	.017	-41.85
40.499	1173.690	16.692	-.071	.018	-3.85
40.749	1190.348	16.657	-.002	.018	-.11
40.999	1207.233	16.885	.013	.018	.72
41.249	1224.450	17.216	.019	.018	1.02
41.499	1263.609	39.159	.560	.012	44.86
41.749	1292.477	28.868	-.356	.014	-24.31
41.999	1325.565	33.087	.127	.013	9.24
42.249	1359.382	33.817	.021	.013	1.56
42.499	1391.225	31.842	-.062	.014	-4.34
42.749	1409.275	18.050	-.764	.019	-40.03
42.999	1426.618	17.342	-.040	.019	-2.08
43.249	1444.152	17.534	.010	.019	.55
43.499	1461.170	17.017	-.030	.020	-1.51
43.749	1479.245	18.075	.058	.019	2.98
43.999	1496.935	17.690	-.021	.019	-1.09
44.249	1514.830	17.895	.011	.019	.57
44.499	1536.645	21.814	.179	.018	9.90
44.749	1558.196	21.551	-.012	.018	-.66
44.999	1577.690	19.494	-.105	.019	-5.43
45.249	1597.874	20.184	.034	.019	1.78
45.499	1617.880	20.005	-.008	.019	-.46
45.749	1638.101	20.221	.010	.019	.55
45.999	1662.525	24.424	.172	.017	9.73
46.249	1736.088	73.562	.667	.010	65.26
46.499	1786.387	50.299	-.462	.012	-37.20
46.749	1849.669	63.281	.205	.011	18.43
46.999	1877.270	27.601	-1.292	.016	-76.41
47.249	1916.755	39.485	.300	.014	21.19
47.499	1939.100	22.344	-.767	.018	-40.49

47.749	1961.167	22.067	-.012	.019	-.65
47.999	1983.230	22.062	0.000	.019	-.01
48.249	2005.136	21.905	-.007	.019	-.37
48.499	2027.327	22.191	.012	.019	.66

..I 130A 2804 90.00 77
..BRANCH 0040R

THETA	INTEGRATED INTENSITY	INTENSITY	RATE OF CHANGE	PROBABLE ERROR	
45.249	21.220	21.220	1.000	.018	53.45
45.499	41.555	20.335	-.043	.019	-2.26
45.749	63.255	21.700	.062	.018	3.36
45.999	88.341	25.085	.134	.017	7.73
46.249	165.685	77.344	.675	.009	67.68
46.499	217.164	51.478	-.502	.012	-40.89
46.749	282.563	65.398	.212	.010	19.44
46.999	311.168	28.605	-1.286	.016	-77.40
47.249	351.840	40.671	.296	.013	21.20
47.499	375.108	23.268	-.747	.018	-40.28
47.749	396.658	21.549	-.079	.019	-4.11
47.999	419.497	22.839	.056	.018	2.99
48.249	441.164	21.666	-.054	.019	-2.78
48.499	463.576	22.412	.033	.019	1.73
48.749	486.852	23.275	.037	.018	1.96
48.999	531.295	44.442	.476	.013	34.77
49.249	589.850	58.555	.241	.011	20.14
49.499	641.200	51.350	-.140	.012	-10.95
49.749	667.568	26.368	-.947	.017	-52.86
49.999	692.650	25.081	-.051	.018	-2.78
50.249	717.518	24.867	-.008	.018	-.46
50.499	742.473	24.954	.003	.018	.18
50.749	780.742	38.269	.347	.015	23.18
50.999	869.027	88.285	.566	.009	57.22
51.249	929.606	60.578	-.457	.011	-38.20
51.499	959.332	29.726	-1.037	.017	-60.63
51.749	982.938	23.605	-.259	.019	-13.51
51.999	1006.317	23.379	-.009	.019	-.49
52.249	1029.279	22.962	-.018	.019	-.93
52.499	1051.237	21.957	-.045	.019	-2.28
52.749	1074.293	23.056	.047	.019	2.44
52.999	1097.689	23.396	.014	.019	.75
53.249	1120.756	23.066	-.014	.019	-.73
53.499	1144.025	23.269	.008	.019	.44
53.749	1168.159	24.133	.035	.019	1.87
53.999	1195.570	27.411	.119	.017	6.67
54.249	1220.365	24.795	-.105	.018	-5.59
54.499	1245.190	24.825	.001	.018	.06
54.749	1268.938	23.747	-.045	.019	-2.35
54.999	1292.877	23.939	.008	.019	.41
55.249	1317.199	24.322	.015	.019	.82
55.499	1342.689	25.489	.045	.018	2.46
55.749	1388.270	45.580	.440	.013	31.79

55.999	1414.176	25.906	-.759	.018	-41.33
56.249	1459.021	44.845	.422	.013	30.26
56.499	1514.599	55.578	.193	.012	15.42
56.749	1543.385	28.786	-.930	.017	-53.55
56.999	1584.595	41.210	.301	.014	20.78

..I 134 2804 50.00 300K
..BRANCH 0040R

THETA	INTEGRATED INTENSITY	INTENSITY	RATE OF CHANGE	PROBABLE ERROR	
25.249	5.641	5.641	1.000	.013	74.77
25.499	12.638	6.996	.193	.012	15.83
25.749	20.319	7.680	.089	.011	7.48
25.999	42.878	22.558	.659	.007	93.21
26.249	85.220	42.341	.467	.005	88.79
26.499	96.441	11.221	-2.773	.010	-266.32
26.749	127.171	30.730	.634	.006	99.03
26.999	161.957	34.786	.116	.006	18.99
27.249	172.450	10.493	-2.315	.011	-203.38
27.499	181.203	8.752	-.198	.012	-15.66
27.749	190.133	8.929	.019	.012	1.54
27.999	198.936	8.802	-.014	.013	-1.09
28.249	207.622	8.685	-.013	.013	-1.00
28.499	216.306	8.683	0.000	.013	-.01
28.749	225.354	9.048	.040	.013	2.94
28.999	235.273	9.918	.087	.013	6.58
29.249	245.409	10.136	.021	.013	1.60
29.499	263.245	17.835	.431	.010	41.94
29.749	302.009	38.764	.539	.007	75.95
29.999	316.509	14.499	-1.673	.011	-141.66
30.249	326.863	10.353	-.400	.014	-28.21
30.499	337.292	10.429	.007	.014	.50
30.749	348.375	11.082	.058	.014	4.16
30.999	359.710	11.335	.022	.014	1.57
31.249	371.284	11.573	.020	.014	1.44
31.499	394.939	23.654	.510	.010	50.41
31.749	432.267	37.328	.366	.008	44.75
31.999	448.833	16.565	-1.253	.012	-100.51
32.249	460.788	11.955	-.385	.014	-25.89
32.499	472.277	11.489	-.040	.015	-2.62
32.749	483.601	11.324	-.014	.015	-.92
32.999	494.844	11.242	-.007	.016	-.45
33.249	506.340	11.496	.022	.016	1.37
33.499	517.444	11.104	-.035	.016	-2.12
33.749	529.310	11.865	.064	.016	3.93
33.999	541.638	12.328	.037	.016	2.31
34.249	554.015	12.377	.003	.016	.24
34.499	567.276	13.260	.066	.016	4.13
34.749	593.998	26.721	.503	.011	43.86
34.999	617.199	23.201	-.151	.012	-12.16
35.249	631.852	14.653	-.583	.015	-36.73
35.499	646.983	15.131	.031	.015	1.99
35.749	662.461	15.477	.022	.015	1.41

35.999	678.954	16.493	.061	.015	3.97
36.249	697.519	18.564	.111	.014	7.55
36.499	732.974	35.455	.476	.010	44.05
36.749	795.277	62.302	.430	.008	52.23
36.999	836.773	41.496	-.501	.010	-49.05
37.249	878.868	42.094	.014	.010	1.38
37.499	910.055	31.187	-.349	.012	-29.02
37.749	929.023	18.968	-.644	.015	-41.24
37.999	946.484	17.460	-.086	.016	-5.24
38.249	963.951	17.467	0.000	.016	.02
38.499	981.781	17.829	.020	.016	1.22
38.749	999.429	17.648	-.010	.016	-.60
38.999	1017.486	18.056	.022	.016	1.33
39.249	1035.602	18.115	.003	.017	.19
39.499	1062.225	26.623	.319	.014	22.55
39.749	1093.836	31.611	.157	.013	12.01
39.999	1120.119	26.283	-.202	.014	-13.95
40.249	1139.066	18.946	-.387	.017	-22.44
40.499	1158.081	19.015	.003	.017	.20
40.749	1177.200	19.118	.005	.017	.31
40.999	1197.286	20.086	.048	.017	2.80
41.249	1221.487	24.201	.170	.015	10.78
41.499	1253.669	32.182	.247	.013	17.99
41.749	1283.530	29.860	-.077	.014	-5.39
41.999	1320.542	37.011	.193	.013	14.81
42.249	1351.195	30.653	-.207	.014	-14.36
42.499	1372.966	21.771	-.407	.017	-23.63
42.749	1392.620	19.653	-.107	.018	-5.89
42.999	1412.412	19.792	.006	.018	.38
43.249	1431.772	19.360	-.022	.018	-1.19
43.499	1451.312	19.539	.009	.018	.49
43.749	1471.205	19.893	.017	.018	.95
43.999	1491.201	19.995	.005	.018	.27
44.249	1513.370	22.169	.098	.017	5.48
44.499	1535.797	22.427	.011	.017	.64
44.749	1557.752	21.955	-.021	.018	-1.18
44.999	1579.174	21.421	-.024	.018	-1.34
45.249	1601.660	22.486	.047	.018	2.60
45.499	1624.780	23.120	.027	.018	1.52
45.749	1651.513	26.732	.135	.016	8.03
45.999	1701.832	50.318	.468	.012	38.04
46.249	1739.889	38.057	-.322	.014	-22.63
46.499	1785.933	46.043	.173	.012	13.34
46.749	1823.525	37.591	-.224	.014	-15.57
46.999	1857.795	34.270	-.096	.015	-6.38
47.249	1883.603	25.807	-.327	.017	-18.67
47.499	1909.029	25.426	-.014	.017	-.84

47.749	1934.772	25.742	.012	.017	.69
47.999	1960.296	25.524	-.008	.017	-.47
48.249	1985.988	25.691	.006	.017	.36
48.499	2011.712	25.724	.001	.017	.07
48.749	2042.897	31.185	.175	.016	10.74
48.999	2096.992	54.095	.423	.012	34.11
49.249	2136.089	39.096	-.383	.014	-26.19
49.499	2171.424	35.334	-.106	.015	-6.89
49.749	2200.256	28.832	-.225	.017	-13.15
49.999	2227.529	27.272	-.057	.017	-3.23
50.249	2255.330	27.801	.019	.017	1.08
50.499	2290.750	35.419	.215	.015	13.81
50.749	2352.916	62.166	.430	.011	36.53
50.999	2394.247	41.330	-.504	.014	-34.84
51.249	2434.604	40.357	-.024	.014	-1.64
51.499	2462.291	27.687	-.457	.017	-25.80
51.749	2489.283	26.991	-.025	.017	-1.43
51.999	2515.919	26.635	-.013	.018	-.73
52.249	2541.590	25.671	-.037	.018	-2.03
52.499	2566.930	25.340	-.013	.018	-.70
52.749	2591.588	24.658	-.027	.018	-1.46
52.999	2617.725	26.136	.056	.018	3.08
53.249	2643.138	25.413	-.028	.018	-1.52
53.499	2669.624	26.486	.040	.018	2.22
53.749	2697.599	27.975	.053	.017	2.99
53.999	2723.503	25.903	-.079	.018	-4.33
54.249	2751.024	27.520	.058	.017	3.28
54.499	2777.079	26.055	-.056	.018	-3.05
54.749	2803.609	26.529	.017	.018	.98
54.999	2831.161	27.551	.037	.017	2.07
55.249	2858.738	27.577	0.000	.017	.05
55.499	2893.565	34.827	.208	.015	13.11

APPENDIX III

Results of Debye Temperature Determinations by the Ratio Method

The data listed here are printed by the Fortran program shown on page 115. The numerical analysis is described on pages 112 to 116. Each page contains the results of one determination of the Debye temperature. The first three lines on each page are the input data. For the results shown on page 46 the input data have the following meanings:

607.7 -- integrated intensity at T1

355.6 -- integrated intensity at T2

77.0 -- T1

300.0 -- T2

101.80 -- Bragg angle at T1

101.51 -- Bragg angle at T2

450.0 -- Estimated Debye temperature

0.71069 -- x-ray wavelength

0.3916114E-13 -- a constant containing the factor $(12h^2/mk)$

```
607.7000000 355.60000000 77.00000   300.000000
 101.8000      101.5100     450.0000
.71069000 .39161140E-13
```

DEBYE TEMP OLD	NEW	INTENSITY RATO OBSERVED	COMPUTED	(OBS-COMP)/OBS
450.00	408.33	1.70894250	1.52101480	.10996724
408.33	405.29	1.70894250	1.68905240	.01163883
405.29	404.60	1.70894250	1.70430650	.00271278
404.60	404.43	1.70894250	1.70782870	.00065174
404.43	404.39	1.70894250	1.70867430	.00015693
404.39	404.39	1.70894250	1.70887690	.00003838

```
 570.7000000 366.20000000 77.00000   300.000000
  101.8000      101.5100     450.0000
.71069000 .39161140E-13
```

DEBYE TEMP OLD	DEBYE TEMP NEW	INTENSITY RATO OBSERVED	INTENSITY RATO COMPUTED	(OBS-COMP)/OBS
450.00	441.30	1.55843790	1.52101480	.02401321
441.30	439.63	1.55843790	1.55070880	.00495951
439.63	439.26	1.55843790	1.55668340	.00112580
439.26	439.18	1.55843790	1.55803350	.00025949
439.18	439.16	1.55843790	1.55834370	.00006044

```
 577.1000000 358.80000000 77.00000   300.000000
  101.8000      101.5100     450.0000
.71069000 .39161140E-13
```

DEBYE TEMP OLD	DEBYE TEMP NEW	INTENSITY RATO OBSERVED	INTENSITY RATO COMPUTED	(OBS-COMP)/OBS
450.00	430.01	1.60841680	1.52101480	.05434039
430.01	427.06	1.60841680	1.59309190	.00952794
427.06	426.41	1.60841680	1.60493790	.00216293
426.41	426.26	1.60841680	1.60760440	.00050509
426.26	426.23	1.60841680	1.60822480	.00011937
426.23	426.22	1.60841680	1.60837190	.00002791

```
606.9000000 357.70000000 77.00000   300.000000
  101.8000      101.5100     450.0000
.71069000 .39161140E-13
```

DEBYE TEMP OLD	NEW	INTENSITY RATO OBSERVED	COMPUTED	(OBS-COMP)/OBS
450.00	410.90	1.69667300	1.52101480	.10353096
410.90	407.73	1.69667300	1.67649890	.01189038
407.73	407.02	1.69667300	1.69199250	.00275863
407.02	406.85	1.69667300	1.69555290	.00066017
406.85	406.81	1.69667300	1.69640420	.00015842
406.81	406.80	1.69667300	1.69660740	.00003866

```
572.4000000 354.10000000 77.00000   300.000000
 101.8000      101.5100     450.0000
.71069000 .39161140E-13
```

DEBYE TEMP OLD	NEW	INTENSITY RATO OBSERVED	COMPUTED	(OBS-COMP)/OBS
450.00	428.22	1.61649240	1.52101480	.05906467
428.22	425.15	1.61649240	1.60025190	.01004675
425.15	424.48	1.61649240	1.61280150	.00228327
424.48	424.32	1.61649240	1.61562800	.00053473
424.32	424.28	1.61649240	1.61628950	.00012551
424.28	424.27	1.61649240	1.61644370	.00003012

```
 602.5000000 385.10000000 77.00000   300.000000
  101.8000      101.5100     450.0000
.71069000 .39161140E-13
```

DEBYE TEMP OLD	DEBYE TEMP NEW	INTENSITY RATO OBSERVED	INTENSITY RATO COMPUTED	(OBS-COMP)/OBS
450.00	439.91	1.56452850	1.52101480	.02781266
439.91	438.03	1.56452850	1.55570220	.00564150
438.03	437.61	1.56452850	1.56252590	.00128000
437.61	437.51	1.56452850	1.56406570	.00029580
437.51	437.49	1.56452850	1.56442130	.00006851

```
616.1000000 379.10000000 77.00000   300.000000
  101.8000      101.5100      450.0000
.71069000 .39161140E-13
```

DEBYE TEMP OLD	NEW	INTENSITY RATO OBSERVED	COMPUTED	(OBS-COMP)/OBS
450.00	426.31	1.62516470	1.52101480	.06408575
426.31	423.14	1.62516470	1.60804150	.01053628
423.14	422.44	1.62516470	1.62126880	.00239723
422.44	422.27	1.62516470	1.62424970	.00056301
422.27	422.23	1.62516470	1.62494940	.00013247
422.23	422.23	1.62516470	1.62511360	.00003144

```
 126.1430000  78.16200000 77.00000   300.000000
  101.8000      101.5100     450.0000
.71069000 .39161140E-13
```

DEBYE TEMP OLD	DEBYE TEMP NEW	INTENSITY RATO OBSERVED	INTENSITY RATO COMPUTED	(OBS-COMP)/OBS
450.00	428.80	1.61386590	1.52101480	.05753334
428.80	425.77	1.61386590	1.59791340	.00988465
425.77	425.10	1.61386590	1.61024190	.00224553
425.10	424.95	1.61386590	1.61301820	.00052526
424.95	424.91	1.61386590	1.61366600	.00012386
424.91	424.90	1.61386590	1.61381900	.00002906

```
642.4000000 439.90000000 77.00000   300.000000
  101.8000     101.5100     450.0000
.71069000 .39161140E-13
```

DEBYE TEMP OLD	NEW	INTENSITY RATO OBSERVED	COMPUTED	(OBS-COMP)/OBS
450.00	464.56	1.46033170	1.52101480	.04155432
464.56	468.87	1.46033170	1.47624400	.01089636
468.87	469.91	1.46033170	1.46406420	.00255592
469.91	470.15	1.46033170	1.46117420	.00057692
470.15	470.20	1.46033170	1.46051950	.00012860
470.20	470.22	1.46033170	1.46037400	.00002896

```
627.1000000 400.00000000 77.00000   300.000000
  101.8000      101.5100     450.0000
.71069000 .39161140E-13
```

DEBYE TEMP OLD	NEW	INTENSITY RATO OBSERVED	COMPUTED	(OBS-COMP)/OBS
450.00	439.17	1.56774990	1.52101480	.02981030
439.17	437.19	1.56774990	1.55836140	.00598851
437.19	436.75	1.56774990	1.56562100	.00135793
436.75	436.64	1.56774990	1.56725690	.00031446
436.64	436.62	1.56774990	1.56763550	.00007297

```
   2.2873000   1.86680000 77.00000   300.000000
   59.3500       59.2200     450.0000
.71069000 .39161140E-13
```

DEBYE TEMP OLD	NEW	INTENSITY RATO OBSERVED	COMPUTED	(OBS-COMP)/OBS
450.00	421.50	1.22525160	1.18615810	.03190650
421.50	418.18	1.22525160	1.21951340	.00468328
418.18	417.44	1.22525160	1.22394400	.00106720
417.44	417.27	1.22525160	1.22494280	.00025202
417.27	417.23	1.22525160	1.22517810	.00005998

```
   63.3400       63.2100      450.0000
   1.9903000    1.49020000 77.00000    300.000000
 .71069000 .39161140E-13
```

DEBYE TEMP OLD	DEBYE TEMP NEW	INTENSITY RATO OBSERVED	INTENSITY RATO COMPUTED	(OBS-COMP)/OBS
450.00	374.04	1.33559240	1.21179040	.09269444
374.04	375.48	1.33559240	1.34011930	.00338943
375.48	375.85	1.33559240	1.33674960	.00086643
375.85	375.95	1.33559240	1.33588400	.00021833
375.95	375.97	1.33559240	1.33566590	.00005503

```
   5.2422000    3.78470000 77.00000   300.000000
   69.5600       69.5300     450.0000
 .71069000 .39161140E-13
```

DEBYE TEMP OLD	DEBYE TEMP NEW	INTENSITY RATO OBSERVED	INTENSITY RATO COMPUTED	(OBS-COMP)/OBS
450.00	385.59	1.38510300	1.25597820	.09322396
385.59	384.99	1.38510300	1.38300820	.00151237
384.99	384.84	1.38510300	1.38458640	.00037296
384.84	384.81	1.38510300	1.38497470	.00009262

```
   3.6491000   2.72640000 77.00000   300.000000
   73.3400       73.2400     450.0000
.71069000 .39161140E-13
```

DEBYE TEMP OLD	NEW	INTENSITY RATO OBSERVED	COMPUTED	(OBS-COMP)/OBS
450.00	424.48	1.33843150	1.28290390	.04148706
424.48	421.23	1.33843150	1.32968670	.00653361
421.23	420.51	1.33843150	1.33643910	.00148860
420.51	420.34	1.33843150	1.33796240	.00035048
420.34	420.30	1.33843150	1.33832040	.00008300

```
   1.7577000    1.26190000 77.00000   300.000000
   79.5100       79.2400     450.0000
.71069000 .39161140E-13
```

DEBYE TEMP OLD	DEBYE TEMP NEW	INTENSITY RATO OBSERVED	INTENSITY RATO COMPUTED	(OBS-COMP)/OBS
450.00	424.98	1.39289940	1.32845550	.04626601
424.98	421.76	1.39289940	1.38268760	.00733132
421.76	421.05	1.39289940	1.39058020	.00166501
421.05	420.88	1.39289940	1.39235510	.00039076
420.88	420.84	1.39289940	1.39277090	.00009225

```
   1.9071000    1.33440000 77.00000    300.000000
   83.6000        83.3800     450.0000
.71069000 .39161140E-13
```

DEBYE TEMP OLD	DEBYE TEMP NEW	INTENSITY RATO OBSERVED	INTENSITY RATO COMPUTED	(OBS-COMP)/OBS
450.00	426.80	1.42918150	1.36242990	.04670617
426.80	423.65	1.42918150	1.41819010	.00769069
423.65	422.96	1.42918150	1.42668450	.00174715
422.96	422.80	1.42918150	1.42859630	.00040946
422.80	422.76	1.42918150	1.42904330	.00009669

```
   1.1209000      .86950000 77.00000   300.000000
   88.9400        88.6200      450.0000
 .71069000 .39161140E-13
```

DEBYE TEMP OLD	NEW	INTENSITY RATO OBSERVED	COMPUTED	(OBS-COMP)/OBS
450.00	488.21	1.28913150	1.40606730	.09070897
488.21	504.29	1.28913150	1.32551700	.02822481
504.29	508.88	1.28913150	1.29835760	.00715683
508.88	509.94	1.28913150	1.29119100	.00159758
509.94	510.16	1.28913150	1.28957160	.00034139
510.16	510.21	1.28913150	1.28922450	.00007214

```
   2.1774000   1.35900000 77.00000   300.000000
   98.2500       97.9800     450.0000
.71069000 .39161140E-13
```

DEBYE TEMP OLD	DEBYE TEMP NEW	INTENSITY RATO OBSERVED	INTENSITY RATO COMPUTED	(OBS-COMP)/OBS
450.00	422.41	1.60220740	1.48908610	.07060340
422.41	419.11	1.60220740	1.58498060	.01075191
419.11	418.37	1.60220740	1.59827490	.00245442
418.37	418.20	1.60220740	1.60127980	.00057895
418.20	418.16	1.60220740	1.60198740	.00013731
418.16	418.15	1.60220740	1.60215460	.00003295

```
   1.8127000    1.22700000 77.00000   300.000000
  101.8000      101.5100     450.0000
.71069000 .39161140E-13
```

DEBYE TEMP OLD	NEW	INTENSITY RATO OBSERVED	COMPUTED	(OBS-COMP)/OBS
450.00	460.41	1.47734300	1.52101480	.02956104
460.41	463.29	1.47734300	1.48839390	.00748025
463.29	463.98	1.47734300	1.47991120	.00173839
463.98	464.13	1.47734300	1.47792530	.00039415
464.13	464.17	1.47734300	1.47747390	.00008860

```
  55.0760000  48.78900000 77.00000   300.000000
   53.7000       53.6000      450.0000
.71069000 .39161140E-13
```

DEBYE TEMP OLD	DEBYE TEMP NEW	INTENSITY RATO OBSERVED	INTENSITY RATO COMPUTED	(OBS-COMP)/OBS
450.00	472.15	1.12886090	1.15282770	.02123095
472.15	479.55	1.12886090	1.13563340	.00599941
479.55	481.43	1.12886090	1.13049070	.00144375
481.43	481.86	1.12886090	1.12922730	.00032457
481.86	481.96	1.12886090	1.12894190	.00007175

```
 53.4430000  43.53500000 77.00000   300.000000
  59.3400       59.2200      450.0000
.71069000 .39161140E-13
```

DEBYE TEMP OLD	NEW	INTENSITY RATO OBSERVED	COMPUTED	(OBS-COMP)/OBS
450.00	419.87	1.22758680	1.18620390	.03371077
419.87	416.53	1.22758680	1.22172520	.00477489
416.53	415.78	1.22758680	1.22624790	.00109067
415.78	415.61	1.22758680	1.22727040	.00025774
415.61	415.57	1.22758680	1.22751150	.00006133

```
  63.5000000  50.74000000 77.00000   300.000000
   63.3400       63.2100     450.0000
.71069000 .39161140E-13
```

DEBYE TEMP OLD	NEW	INTENSITY RATO OBSERVED	COMPUTED	(OBS-COMP)/OBS
450.00	424.83	1.25147800	1.21179040	.03171258
424.83	421.60	1.25147800	1.24522540	.00499617
421.60	420.88	1.25147800	1.25005580	.00113641
420.88	420.71	1.25147800	1.25114400	.00026688
420.71	420.67	1.25147800	1.25139880	.00006328

```
 37.4510000  27.79500000 77.00000   300.000000
  69.5600       69.5300     450.0000
.71069000 .39161140E-13
```

DEBYE TEMP OLD	DEBYE TEMP NEW	INTENSITY RATO OBSERVED	INTENSITY RATO COMPUTED	(OBS-COMP)/OBS
450.00	403.75	1.34740050	1.25597820	.06785087
403.75	400.99	1.34740050	1.33935520	.00597097
400.99	400.36	1.34740050	1.34550680	.00140544
400.36	400.21	1.34740050	1.34694220	.00034013
400.21	400.17	1.34740050	1.34728890	.00008282

```
 172.4960000 125.61600000 77.00000   300.000000
    73.3400        73.2400     450.0000
.71069000 .39161140E-13
```

DEBYE TEMP OLD	NEW	INTENSITY RATO OBSERVED	COMPUTED	(OBS-COMP)/OBS
450.00	409.04	1.37320070	1.28290390	.06575644
409.04	405.95	1.37320070	1.36356630	.00701601
405.95	405.24	1.37320070	1.37095870	.00163268
405.24	405.08	1.37320070	1.37266290	.00039163
405.08	405.04	1.37320070	1.37307060	.00009474

```
  45.1040000  33.13100000 77.00000   300.000000
   79.5100       79.2400      450.0000
 .71069000 .39161140E-13
```

DEBYE TEMP OLD	NEW	INTENSITY RATO OBSERVED	COMPUTED	(OBS-COMP)/OBS
450.00	437.06	1.36138340	1.32845550	.02418708
437.06	434.81	1.36138340	1.35500000	.00468890
434.81	434.31	1.36138340	1.35993980	.00106039
434.31	434.19	1.36138340	1.36104910	.00024555
434.19	434.17	1.36138340	1.36130610	.00005678

```
 155.8020000  97.39900000 77.00000   300.000000
   92.7700       92.5200     450.0000
 .71069000 .39161140E-13
```

DEBYE TEMP OLD	NEW	INTENSITY RATO OBSERVED	COMPUTED	(OBS-COMP)/OBS
450.00	406.93	1.59962610	1.44047980	.09948968
406.93	403.97	1.59962610	1.58368900	.00996301
403.97	403.30	1.59962610	1.59590420	.00232673
403.30	403.14	1.59962610	1.59873040	.00055994
403.14	403.10	1.59962610	1.59940900	.00013571
403.10	403.09	1.59962610	1.59957330	.00003300

```
   1.8150000   1.20140000 77.00000   300.000000
   98.2500        97.9800     450.0000
.71069000 .39161140E-13
```

DEBYE TEMP OLD	NEW	INTENSITY RATO OBSERVED	COMPUTED	(OBS-COMP)/OBS
450.00	444.56	1.51073730	1.48908610	.01433154
444.56	443.44	1.51073730	1.50608380	.00308028
443.44	443.19	1.51073730	1.50967900	.00070051
443.19	443.13	1.51073730	1.51049390	.00016111
443.13	443.12	1.51073730	1.51068170	.00003680

```
   1.6186000    1.00640000 77.00000    300.000000
  101.8000      101.5100     450.0000
.71069000 .39161140E-13


DEBYE TEMP           INTENSITY RATO         (OBS-COMP)/OBS
  OLD    NEW      OBSERVED     COMPUTED



 450.00 430.04   1.60830670   1.52101480    .05427565

 430.04 427.09   1.60830670   1.59299490    .00952044

 427.09 426.44   1.60830670   1.60483110    .00216103

 426.44 426.29   1.60830670   1.60749460    .00050494

 426.29 426.25   1.60830670   1.60811490    .00011925

 426.25 426.24   1.60830670   1.60826180    .00002791
SUBROUTINE ERROR NUMBER H1.  $$$$$$$$$$$$$$$$$$$$$$$$$$$$$$$$$$$$
```

APPENDIX IV

Results of Debye Temperature Determination by the Slope Method

The data listed here are printed by the Fortran program shown on page 121 . The numerical analysis is described on pages 117 to 123 . Each page contains the results of one determination of the Debye temperature. The first two lines on each page are the input data. For the results shown on page 75 the input data have the following meanings:

0.42647 -- the slope

300.0 -- specimen temperature

445.0 -- estimated Debye temperature

391.6114 -- a constant containing the factor $(12h^2/mk)$.

.42647000	300.00000000
445.00000000	391.61140000

DEBYE TEMP		SLOPE		(OBS-COMP)/OBS
OLD	NEW	OBSERVED	COMPUTED	
445.00	438.36	.42647000	.40739621	.04472481
438.36	436.88	.42647000	.42214074	.01015138
436.88	436.56	.42647000	.42553706	.00218758
436.56	436.49	.42647000	.42627148	.00046549
436.49	436.48	.42647000	.42642759	.00009944

.35452000	300.00000000
445.00000000	391.61140000

DEBYE TEMP		SLOPE		(OBS-COMP)/OBS
OLD	NEW	OBSERVED	COMPUTED	
445.00	467.12	.35452000	.40739621	.14914873
467.12	470.84	.35452000	.36300272	.02392733
470.84	471.58	.35452000	.35618211	.00468833
471.58	471.73	.35452000	.35485606	.00094792
471.73	471.76	.35452000	.35458791	.00019155
471.76	471.77	.35452000	.35453386	.00003909

.41500000	300.00000000
445.00000000	391.61140000

DEBYE TEMP		SLOPE		(OBS-COMP)/OBS
OLD	NEW	OBSERVED	COMPUTED	
445.00	442.28	.41500000	.40739621	.01832238
442.28	441.69	.41500000	.41335054	.00397460
441.69	441.57	.41500000	.41465012	.00084308
441.57	441.54	.41500000	.41492569	.00017906
441.54	441.54	.41500000	.41498432	.00003778

.27835000	77.00000000
445.00000000	391.61140000

DEBYE TEMP OLD	NEW	SLOPE OBSERVED	COMPUTED	(OBS-COMP)/OBS
445.00	320.07	.27835000	.04393030	.84217603
320.07	256.28	.27835000	.11193495	.59786258
256.28	234.03	.27835000	.20584774	.26047156
234.03	229.60	.27835000	.26252149	.05686549
229.60	229.01	.27835000	.27620043	.00772254
229.01	228.94	.27835000	.27809373	.00092067
228.94	228.93	.27835000	.27831934	.00011014
228.93	228.93	.27835000	.27834645	.00001275

.35579000	300.00000000
445.00000000	391.61140000

DEBYE TEMP OLD	DEBYE TEMP NEW	SLOPE OBSERVED	SLOPE COMPUTED	(OBS-COMP)/OBS
445.00	466.51	.35579000	.40739621	.14504682
466.51	470.16	.35579000	.36413397	.02345195
470.16	470.88	.35579000	.35742720	.00460159
470.88	471.02	.35579000	.35612132	.00093122
471.02	471.05	.35579000	.35585695	.00018817
471.05	471.06	.35579000	.35580377	.00003870

.42867000	300.00000000
445.00000000	391.61140000

DEBYE TEMP		SLOPE		(OBS-COMP)/OBS
OLD	NEW	OBSERVED	COMPUTED	
445.00	437.63	.42867000	.40739621	.04962742
437.63	435.98	.42867000	.42380130	.01135768
435.98	435.62	.42867000	.42761749	.00245529
435.62	435.54	.42867000	.42844542	.00052389
435.54	435.53	.42867000	.42862190	.00011220
435.53	435.52	.42867000	.42866017	.00002293

.29895000	77.00000000
445.00000000	391.61140000

DEBYE TEMP OLD	NEW	SLOPE OBSERVED	COMPUTED	(OBS-COMP)/OBS
445.00	318.46	.29895000	.04393030	.85305134
318.46	252.61	.29895000	.11352001	.62027091
252.61	228.69	.29895000	.21400388	.28414825
228.69	223.63	.29895000	.27911932	.06633443
223.63	222.92	.29895000	.29611654	.00947803
222.92	222.84	.29895000	.29859961	.00117206
222.84	222.83	.29895000	.29890678	.00014457
222.83	222.82	.29895000	.29894478	.00001746

Some Parameters for Bragg Reflections from Nickel with MoK

In this appendix the lattice parameter of nickel used is 3.5237Å. The hkl are the Miller indices and θ is the Bragg angle. For each value of hkl, the parameters are listed for three wavelengths. The number in column three specifies the wavelength; a '1' denotes the MoK_{α_1} = 0.70926Å; a '2' denotes the MoK_{α_2} = 0.713543Å; and a '3' denotes the mean MoK_{α} = 0.71069Å.

hkl	θ	W	sinθ	$\sin^2\theta$	$\frac{\sin\theta}{W}$	$\frac{\sin^2\theta}{W^2}$	$\frac{4\pi\sin^2\theta}{W^2}$	Lorentz Polarization	Nelson Riley
111	10.03	1	.1743	.0303	.2457	.0604	.759	.0158	5.5481
111	10.10	2	.1753	.0307	.2457	.0604	.759	.0160	5.5126
111	10.05	3	.1746	.0305	.2457	.0604	.759	.0159	5.5361
200	11.61	1	.2012	.0405	.2837	.0805	1.012	.0215	4.7505
200	11.68	2	.2024	.0410	.2837	.0805	1.012	.0217	4.7194
200	11.63	3	.2016	.0406	.2837	.0805	1.012	.0216	4.7400
220	16.53	1	.2846	.0810	.4013	.1610	2.024	.0456	3.2060
220	16.64	2	.2863	.0820	.4013	.1610	2.024	.0462	3.1831
220	16.57	3	.2852	.0813	.4013	.1610	2.024	.0458	3.1982
311	19.49	1	.3337	.1114	.4706	.2214	2.783	.0654	2.6365
311	19.62	2	.3358	.1127	.4706	.2214	2.783	.0663	2.6164
311	19.54	3	.3344	.1118	.4706	.2214	2.783	.0657	2.6297
222	20.40	1	.3486	.1215	.4915	.2416	3.036	.0724	2.4932
222	20.53	2	.3507	.1230	.4915	.2416	3.036	.0734	2.4738
222	20.44	3	.3493	.1220	.4915	.2416	3.036	.0727	2.4867
400	23.73	1	.4025	.1620	.5675	.3221	4.048	.1018	2.0519
400	23.89	2	.4049	.1640	.5675	.3221	4.048	.1033	2.0345
400	23.78	3	.4033	.1627	.5675	.3221	4.048	.1023	2.0460
331	26.02	1	.4386	.1924	.6185	.3825	4.807	.1254	1.8095
331	26.18	2	.4413	.1947	.6185	.3825	4.807	.1273	1.7930

331	26.07	3	.4395	.1932	.6185	.3825	4.807	.1260	1.8039
420	26.74	1	.4500	.2025	.6345	.4026	5.060	.1336	1.7399
420	26.92	2	.4527	.2050	.6345	.4026	5.060	.1356	1.7237
420	26.80	3	.4509	.2033	.6345	.4026	5.060	.1342	1.7344
422	29.54	1	.4930	.2430	.6951	.4832	6.072	.1673	1.5016
422	29.73	2	.4960	.2460	.6951	.4832	6.072	.1698	1.4863
422	29.60	3	.4940	.2440	.6951	.4832	6.072	.1681	1.4964
511	31.53	1	.5229	.2734	.7373	.5436	6.831	.1934	1.3547
511	31.74	2	.5261	.2767	.7373	.5436	6.831	.1962	1.3400
511	31.60	3	.5240	.2745	.7373	.5436	6.831	.1943	1.3497
333	31.53	1	.5229	.2734	.7373	.5436	6.831	.1934	1.3547
333	31.74	2	.5261	.2767	.7373	.5436	6.831	.1962	1.3400
333	31.60	3	.5240	.2745	.7373	.5436	6.831	.1943	1.3497
440	34.70	1	.5693	.3241	.8026	.6443	8.096	.2371	1.1515
440	34.94	2	.5727	.3280	.8026	.6443	8.096	.2404	1.1375
440	34.78	3	.5704	.3254	.8026	.6443	8.096	.2382	1.1468
531	36.54	1	.5954	.3545	.8394	.7047	8.855	.2625	1.0481
531	36.79	2	.5989	.3587	.8394	.7047	8.855	.2660	1.0344
531	36.62	3	.5966	.3559	.8394	.7047	8.855	.2637	1.0435
600	37.14	1	.6038	.3646	.8513	.7248	9.108	.2707	1.0161
600	37.40	2	.6074	.3690	.8513	.7248	9.108	.2743	1.0025
600	37.23	3	.6050	.3661	.8513	.7248	9.108	.2719	1.0115
620	39.53	1	.6365	.4051	.8974	.8053	10.120	.3016	.8983
620	39.81	2	.6403	.4100	.8974	.8053	10.120	.3050	.8850
620	39.62	3	.6378	.4067	.8974	.8053	10.120	.3027	.8938
533	41.29	1	.6599	.4355	.9304	.8657	10.879	.3218	.8192
533	41.60	2	.6639	.4408	.9304	.8657	10.879	.3250	.8062
533	41.39	3	.6612	.4373	.9304	.8657	10.879	.3229	.8148
622	41.88	1	.6675	.4456	.9412	.8859	11.132	.3279	.7943
622	42.19	2	.6716	.4510	.9412	.8859	11.132	.3310	.7814
622	41.98	3	.6689	.4474	.9412	.8859	11.132	.3289	.7899
444	44.20	1	.6972	.4861	.9830	.9664	12.144	.3482	.7014
444	44.54	2	.7014	.4920	.9830	.9664	12.144	.3506	.6887
444	44.32	3	.6986	.4881	.9830	.9664	12.144	.3490	.6971

711	45.94	1	.7187	.5165	1.0133	1.0268	12.903	.3587	.6377
711	46.30	2	.7230	.5228	1.0133	1.0268	12.903	.3604	.6251
711	46.06	3	.7201	.5186	1.0133	1.0268	12.903	.3593	.6334
551	45.94	1	.7187	.5165	1.0133	1.0268	12.903	.3587	.6377
551	46.30	2	.7230	.5228	1.0133	1.0268	12.903	.3604	.6251
551	46.06	3	.7201	.5186	1.0133	1.0268	12.903	.3593	.6334
640	46.53	1	.7257	.5266	1.0232	1.0469	13.156	.3613	.6174
640	46.89	2	.7301	.5330	1.0232	1.0469	13.156	.3626	.6050
640	46.65	3	.7272	.5288	1.0232	1.0469	13.156	.3617	.6132
642	48.86	1	.7531	.5672	1.0618	1.1275	14.169	.3665	.5410
642	49.25	2	.7576	.5740	1.0618	1.1275	14.169	.3666	.5287
642	48.99	3	.7546	.5695	1.0618	1.1275	14.169	.3665	.5369
553	50.62	1	.7730	.5975	1.0899	1.1879	14.928	.3651	.4879
553	51.05	2	.7777	.6048	1.0899	1.1879	14.928	.3642	.4758
553	50.76	3	.7746	.6000	1.0899	1.1879	14.928	.3648	.4838
731	50.62	1	.7730	.5975	1.0899	1.1879	14.928	.3651	.4879
731	51.05	2	.7777	.6048	1.0899	1.1879	14.928	.3642	.4758
731	50.76	3	.7746	.6000	1.0899	1.1879	14.928	.3648	.4838
800	53.62	1	.8051	.6482	1.1351	1.2886	16.193	.3534	.4063
800	54.09	2	.8099	.6560	1.1351	1.2886	16.193	.3505	.3944
800	53.78	3	.8067	.6508	1.1351	1.2886	16.193	.3524	.4023
733	55.46	1	.8237	.6786	1.1614	1.3490	16.952	.3411	.3610
733	55.97	2	.8287	.6868	1.1614	1.3490	16.952	.3372	.3492
733	55.63	3	.8254	.6813	1.1614	1.3490	16.952	.3398	.3570
820	56.08	1	.8299	.6887	1.1701	1.3691	17.205	.3363	.3464
820	56.60	2	.8349	.6970	1.1701	1.3691	17.205	.3320	.3347
820	56.26	3	.8315	.6915	1.1701	1.3691	17.205	.3349	.3425
644	56.08	1	.8299	.6887	1.1701	1.3691	17.205	.3363	.3464
644	56.60	2	.8349	.6970	1.1701	1.3691	17.205	.3320	.3347
644	56.26	3	.8315	.6915	1.1701	1.3691	17.205	.3349	.3425
822	58.64	1	.8539	.7292	1.2040	1.4496	18.217	.3135	.2907
822	59.21	2	.8591	.7380	1.2040	1.4496	18.217	.3079	.2791
822	58.83	3	.8557	.7322	1.2040	1.4496	18.217	.3116	.2868

660	58.64 1	.8539	.7292	1.2040	1.4496	18.217	.3135	.2907
660	59.21 2	.8591	.7380	1.2040	1.4496	18.217	.3079	.2791
660	58.83 3	.8557	.7322	1.2040	1.4496	18.217	.3116	.2868
751	60.64 1	.8715	.7596	1.2288	1.5100	18.976	.2933	.2514
751	61.26 2	.8768	.7688	1.2288	1.5100	18.976	.2867	.2399
751	60.85 3	.8733	.7627	1.2288	1.5100	18.976	.2911	.2475
555	60.64 1	.8715	.7596	1.2288	1.5100	18.976	.2933	.2514
555	61.26 2	.8768	.7688	1.2288	1.5100	18.976	.2867	.2399
555	60.85 3	.8733	.7627	1.2288	1.5100	18.976	.2911	.2475
662	61.32 1	.8773	.7697	1.2370	1.5302	19.229	.2860	.2387
662	61.96 2	.8826	.7790	1.2370	1.5302	19.229	.2791	.2272
662	61.54 3	.8791	.7729	1.2370	1.5302	19.229	.2837	.2348
840	64.17 1	.9001	.8102	1.2691	1.6107	20.241	.2547	.1900
840	64.90 2	.9055	.8201	1.2691	1.6107	20.241	.2467	.1787
840	64.42 3	.9019	.8135	1.2691	1.6107	20.241	.2521	.1862